



**UNIVERSIDADE ESTADUAL DE CAMPINAS
INSTITUTO DE QUÍMICA**

MATHEUS BATISTA CORDEIRO DE SOUZA

**DEVELOPMENT OF P-BLOCK ADATOM-MODIFIED PLATINUM
ELECTROCATALYSTS FOR THE ELECTROCHEMICAL CONVERSION OF
GLYCEROL IN ALKALINE MEDIUM**

**DESENVOLVIMENTO DE ELETROCATALISADORES DE PLATINA
MODIFICADOS POR ADÁTOMOS DO BLOCO P PARA A CONVERSÃO
ELETROQUÍMICA DE GLICEROL EM MEIO ALCALINO**

**CAMPINAS
2022**

MATHEUS BATISTA CORDEIRO DE SOUZA

**DEVELOPMENT OF P-BLOCK ADATOM-MODIFIED PLATINUM
ELECTROCATALYSTS FOR THE ELECTROCHEMICAL CONVERSION OF
GLYCEROL IN ALKALINE MEDIUM**

**DESENVOLVIMENTO DE ELETROCATALISADORES DE PLATINA
MODIFICADOS POR ADÁTOMOS DO BLOCO P PARA A CONVERSÃO
ELETROQUÍMICA DE GLICEROL EM MEIO ALCALINO**

Tese de Doutorado apresentada ao Instituto de Química da Universidade Estadual de Campinas como parte dos requisitos exigidos para a obtenção do título de Doutor em Ciências.

Doctor's Thesis presented to the Institute of Chemistry of the University of Campinas as part of the requirements to obtain the title of Doctor in Sciences.

Supervisor: Dr. Pablo Sebastián Fernández

O arquivo digital corresponde à versão final da Tese defendida pelo aluno Matheus Batista Cordeiro de Souza e orientada pelo Prof. Dr. Pablo Sebastián Fernández.

Ficha catalográfica
Universidade Estadual de Campinas
Biblioteca do Instituto de Química
Simone Luiz Alves - CRB 8/9094

So89d Souza, Matheus Batista Cordeiro de, 1992-
Development of p-block adatom-modified platinum electrocatalysts for the electrochemical conversion of glycerol in alkaline medium / Matheus Batista Cordeiro de Souza. – Campinas, SP : [s.n.], 2022.

Orientador: Pablo Sebastian Fernandez.
Tese (doutorado) – Universidade Estadual de Campinas, Instituto de Química.

1. Glicerol. 2. Platina. 3. Eletro-oxidação. 4. Células a combustível. 5. Eletrólise. I. Fernandez, Pablo Sebastian, 1983-. II. Universidade Estadual de Campinas. Instituto de Química. III. Título.

Informações Complementares

Título em outro idioma: Desenvolvimento de eletrocatalisadores de platina modificados por adátomos do bloco p para a conversão eletroquímica de glicerol em meio alcalino

Palavras-chave em inglês:

Glycerol

Platinum

Electrooxidation

Fuel cells

Electrolysis

Área de concentração: Físico-Química

Titulação: Doutor em Ciências

Banca examinadora:

Pablo Sebastian Fernandez [Orientador]

Claudia Longo

William Reis de Araujo

Camilo Andrea Angelucci

José Joaquín Linares León

Data de defesa: 25-10-2022

Programa de Pós-Graduação: Química

Identificação e informações acadêmicas do(a) aluno(a)

- ORCID do autor: <https://orcid.org/0000-0003-4785-3839>

- Currículo Lattes do autor: <http://lattes.cnpq.br/9622344882181310>

BANCA EXAMINADORA

Prof. Dr. Pablo Sebastián Fernández (Orientador)

Profa. Dra. Claudia Longo (Universidade Estadual de Campinas)

Prof. Dr. William Reis de Araujo (Universidade Estadual de Campinas)

Prof. Dr. Camilo Andrea Angelucci (Universidade Federal do ABC)

Prof. Dr. José Joaquín Linares León (Universidade de Brasília)

A Ata da defesa assinada pelos membros da Comissão Examinadora, consta no SIGA/Sistema de Fluxo de Dissertação/Tese e na Secretaria do Programa da Unidade.

Este exemplar corresponde à redação final da Tese de Doutorado defendida pelo aluno **Matheus Batista Cordeiro de Souza**, aprovada pela Comissão Julgadora em 25 de outubro de 2022.

Agradecimentos

À Fundação de Amparo à Pesquisa do Estado de São Paulo (FAPESP), processo nº 2019/00305-2 pelo financiamento do projeto de pesquisa, tornando possível a produção desta tese.

Ao Conselho Nacional de Desenvolvimento Científico e Tecnológico (CNPq), processo nº 142478/2018-0 pela concessão da bolsa de estudos nos primeiros anos do curso de doutorado.

This study was financed in part by the Coordenação de Aperfeiçoamento de Pessoal de Nível Superior - Brasil (CAPES) - Finance Code 001.

Resumo

Alternativas à atual dependência por combustíveis fósseis são constantemente visadas, pois representam a única maneira de minimizar os impactos causados pelo aquecimento global. O gás hidrogênio de alta pureza é unanimemente considerado como a mais importante fonte de energia renovável para o futuro próximo, e pode ser obtido de forma sustentável a partir da eletrólise da água. Dos vários problemas que cerceiam o assunto, a substituição da reação anódica (evolução de oxigênio) pela oxidação de biomassa, como a oxidação de glicerol, não só reduziria o custo energético para operar esses dispositivos, mas também possibilitaria a geração de produtos de maior valor agregado a partir da conversão da biomassa. O glicerol é obtido em abundância como coproduto de síntese durante a produção de biodiesel, um combustível renovável de amplo uso no setor de transporte, e o próprio glicerol também pode ser utilizado como fonte de energia a partir da sua oxidação direta, com a possibilidade de gerar hidrogênio verde, além da sua conversão em outras moléculas de maior interesse econômico. Nesse contexto, o presente trabalho tem por objetivo desenvolver catalisadores a partir de platina para a oxidação eletroquímica do glicerol em meio alcalino, e posteriormente transferir o conhecimento adquirido para dispositivos eletroquímicos. A partir de uma investigação eletroquímica inicial, os eletrodos de platina foram modificados por nove elementos distintos do bloco "p", e foi observado que três deles aumentaram a atividade do eletrodo, com respeito ao eletrodo de platina não modificado: chumbo, bismuto e tálio. A adição desses elementos resultou em maiores correntes anódicas durante um período de tempo mais longo. Usando FTIR *in situ*, nós mostramos que a presença desses adátomos reduziu a quebra de ligações C-C durante a oxidação, e preveniram a adsorção de CO no eletrodo, um intermediário responsável por envenenar o catalisador. Os produtos de oxidação solúveis foram identificados através de cromatografia líquida, e apesar de não haver mudanças na seletividade com a modificação, houve um aumento significativo no rendimento da reação. Por último, conseguimos transferir o conhecimento acumulado para uma célula a combustível microfluídica, onde modificamos o anodo, nanopartículas de Pt/C suportadas em papel carbono, com bismuto. Foi observado um aumento significativo na voltagem de circuito aberto e potência extraída do dispositivo, e uma mistura de glicolato e formato foi identificada a partir do eletrólito de exaustão do dispositivo, confirmando a possibilidade de cogeração de energia com produtos de alto valor agregado.

Abstract

Alternatives to the current dependency on fossil fuels are constantly sought after, as it is the only way to minimize the current impact of global warming effect. High-purity hydrogen gas is unanimously considered an important renewable energy source in the foreseeable future, and it can be sustainably synthesized from water electrolysis. Of the many issues surrounding water electrolysis, substituting the anode reaction (oxygen evolution) for biomass oxidation, like the glycerol oxidation, not only would decrease the energy cost needed to operate these devices, but would also enable the generation of value-added products from the biomass conversion. Glycerol is readily obtained as a byproduct from the biodiesel synthesis, another renewable fuel source widely used in the transportation sector, and glycerol itself can also be used as an energy source by its direct oxidation, with the added possibility of generating green hydrogen, in addition to its conversion into other value-added molecules. In this context, this work aims to develop platinum-based catalysts for the electrochemical oxidation of glycerol in alkaline media, and later apply the acquired knowledge to electrochemical devices. In an initial electrochemical investigation, we modified the electrodes with nine different elements from the p-block and identified three elements that improved the electrode activity when compared to the clean platinum electrode: lead, bismuth, and thallium. The addition of these elements resulted in higher anodic currents for a longer period. Using *in situ* FTIR, we showed that the presence of adatoms reduced the cleavage of C-C bonds during the oxidation, and prevented the adsorption of CO, a poisonous intermediate. Soluble oxidation products were identified using liquid chromatography, and while the selectivity of the reaction did not change, there was a significant increase in the reaction yield. Lastly, we were able to transfer the resulting knowledge to a glycerol-based microfluidic fuel cell, where we modified the anode, Pt/C nanoparticles supported on carbon paper, with bismuth. We saw a significant increase in the open circuit voltage and power extracted from the device after modification, and a mixture of glycolate and formate was generated in the exhaust electrolyte, confirming the possibility of the cogeneration of energy with value-added chemicals.

Table of Contents

1. General Introduction	9
1.1. Renewable energy sources.....	9
1.2. Glycerol oxidation and its products	11
1.3. Catalyst choice for the oxidation reaction.....	15
1.4. Main objectives	18
2. Electrochemical Systems	20
2.1. Electrochemical cell and techniques.....	20
2.2. Methodology	22
2.3. Electrochemical modification by Bismuth and Lead	28
2.4. Electrochemical modification by other elements.....	38
3. Spectroscopy applied to electrochemical systems.....	45
3.1. Spectroscopy applied to electrochemical research.....	45
3.2. Experimental setup for <i>in situ</i> Fourier Transform Infrared Spectroscopy.....	47
3.3. <i>In situ</i> FTIR results.....	49
3.4. Experimental setup for <i>in situ</i> X-Ray Absorption Spectroscopy	53
3.5. <i>In situ</i> XAS results	56
4. Product identification with liquid chromatography	60
4.1. Basics of liquid chromatography.....	60
4.2. Experimental setup for on-line sample collection and HPLC separation method.....	60
4.3. Results for HPLC with on-line sample collection	63
5. Pt-Bi catalyst applied to glycerol-based microfluidic fuel cells.....	70
5.1. Introduction to electrochemical devices	70
5.2. Fuel cell fabrication and nanoparticle synthesis	71
5.3. Anode modification results.....	75
5.4. Cell operational results	77
6. Proposal for reaction pathways and suggested mechanism.....	85
7. Conclusions and perspectives.....	92
8. References	94
9. Appendix	113

1. General Introduction

1.1. Renewable energy sources

Energy demands across the globe are increasing, and almost all countries rely on fossil fuels to supply this demand. With over two-thirds of the worldwide energy supply coming from fossil fuels, especially in the transport sector, the buildup of CO₂ on the Earth's atmosphere throughout the years has crossed a point of no return, where it is no longer possible to avoid an increase to the average global temperature, and now all efforts can only minimize this effect.¹ Switching the energy matrix towards sustainable and renewable energy sources is essential. Among the many alternative fuel sources, high-purity hydrogen is considered the most important of them, wherein all future predictions about an economy around renewable energies point to it as the main energy source in many different sectors.^{2,3}

Almost all of the hydrogen produced nowadays is labeled as 'grey hydrogen', for being produced from fossil fuels. In 2020, hydrogen production from water electrolysis and fossil fuels with carbon capture, utilization, and storage accounted for less than 1% of the total production.³ Its sustainable production, from renewable resources, is not a novelty, as water electrolysis was discovered more than 200 years ago, with industrial alkaline water electrolysis plants being commissioned since the early 20th century.⁴ Water electrolysis is the electrochemical process in which water is split into high-purity H₂ and O₂ with no generation of greenhouse gases in the process. When this process is powered up by renewable electricity, the hydrogen is labeled as 'green', as the process is almost entirely renewable, with a minimal carbon footprint.

The three main technologies available for water electrolysis, besides the aforementioned alkaline water electrolysis, are using polymer electrolyte membranes or solid oxide electrolysis.^{4,5} An alkaline water electrolyzer is a device where both electrodes, usually from nickel due to its low cost, are submerged into a highly alkaline solution, separated by a diaphragm. A polymer electrolyte membrane (PEM) water electrolyzer is built similarly, however, the membrane allows the passage of protons, and they are capable of operating for much longer than alkaline electrolyzers, with the drawback of requiring expensive catalysts, such as platinum and iridium.⁶ Recently, the development of anion-exchange membrane (AEM) water electrolyzers has been growing, an alternate technology where hydroxyl anions flow through the polymeric

membrane, instead of protons. The main advantage is that in an alkaline environment it is possible to maintain the high current density shown for the acidic electrolyzer, while also having milder conditions, such as non-corrosive electrolyte, cheap and abundant catalyst materials.⁷ Research on these devices often tends to focus on developing catalysts based on cheaper, more abundant materials (Mn, Fe, Co, and Ni) and their respective oxides, as well as on improving the device architecture, to minimize internal resistances that may arise from the electrolyte, contact and those due to the presence of side reactions.⁴

Another barrier that green hydrogen production has to overcome is thermodynamics. Under standard conditions, a potential of 1.23 V is required to break water into H₂ and O₂, however, typically much higher voltages are necessary due to energy barriers arising from resistances due to kinetics, mass transport, and parasitic reactions. In addition to this, the gaseous mixture of hydrogen and oxygen may be explosive in the operating conditions of alkaline water electrolyzers.⁸ These safety and thermodynamic concerns are solvable by substituting the anode reaction for the oxidation of biomass, which produces liquid products and is thermodynamically much more favorable. The biomass used may come from waste products⁹, chitin⁸, glucose, amine, and alcohols such as methanol, ethanol, glycerol, and others.^{10–12} This approach allows the cogeneration of high-purity H₂ on the cathode with liquid products of interest on the anode side of the same device.

Among the aforementioned biomass sources, glycerol is of major interest, as it is cheap and readily available. It is obtained as a byproduct of biodiesel synthesis through a transesterification reaction (**figure a**), at a 10 wt%.¹³ Thanks to its three hydroxyl groups, it can be used as a platform chemical to synthesize more complex and valuable compounds, and also as a renewable energy source in fuel cells, since a single glycerol molecule releases 14 electrons in its complete oxidation to H₂O and CO₂.^{10,14–18} Therefore, the relevance of the electrochemical conversion of glycerol is twofold, namely: i) it would improve the relevance of biodiesel, since both products of the reaction in **fig. a** would be commercially desirable, and ii) as a possible substitute for the anode side of PEM and/or AEM water electrolyzers, since the thermodynamic barrier of the reaction is near zero, despite it having slow oxidation kinetics (and is still a faster process than oxygen evolution).¹⁹

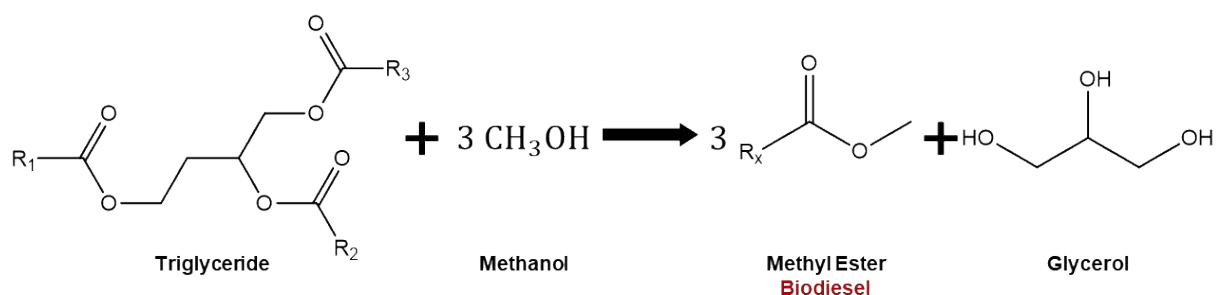


Figure 1: Biodiesel production through a transesterification reaction.

1.2. Glycerol oxidation and its products

Glycerol is a polyol compound, made up of three carbons each with a hydroxyl group to it. It is an odorless, viscous liquid, with a sweet taste and is non-toxic to humans. Crude glycerol from biodiesel synthesis can be distilled into glycerin (technical grade), a reagent widely used in many industrial applications.¹³ However, this usage accounts for less than 20% of all crude glycerol production, prompting the necessity of creating other valorization routes for glycerol, in line with the current sustainability trend present in the chemical industry. **Figure 2** shows some of the possible pathways for glycerol valorization in the chemical industry, including some of the value-added chemicals obtained from them. Owing to its three hydroxyl groups, glycerol can be functionalized using several reaction pathways, turning it into a platform chemical in the industry.

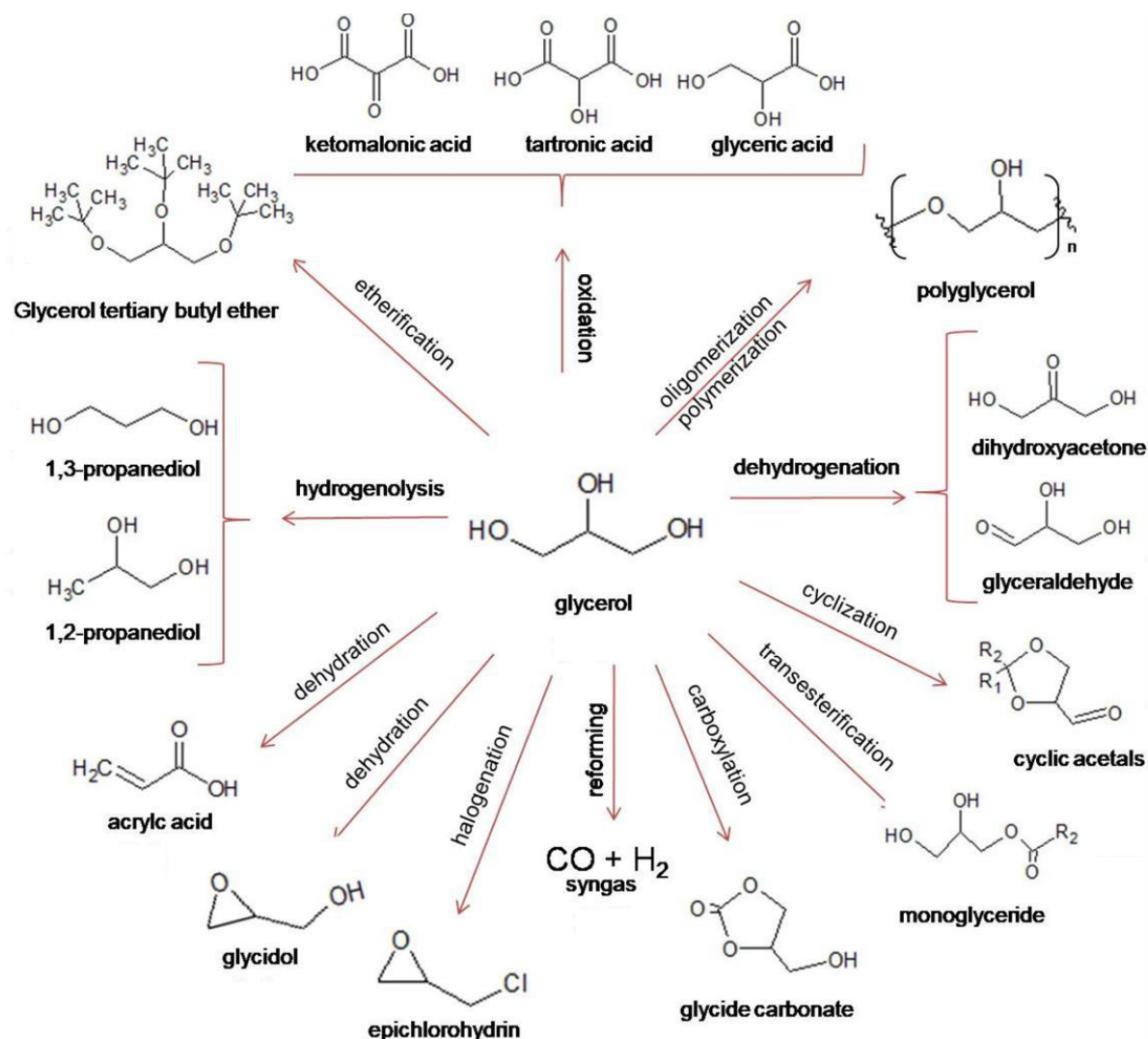


Figure 2: Possible pathways for the valorization of glycerol into value-added chemicals. Adapted from ref.[13].

We are concerned primarily with the oxidation route for glycerol valorization, in particular, its electrochemical conversion (or electrooxidation). Using this route, glycerol can be converted into many different molecules (**figure 3**), several of which have a high economic value added to them. These products have a variety of different applications, and the purpose of this section is to present them to the reader.

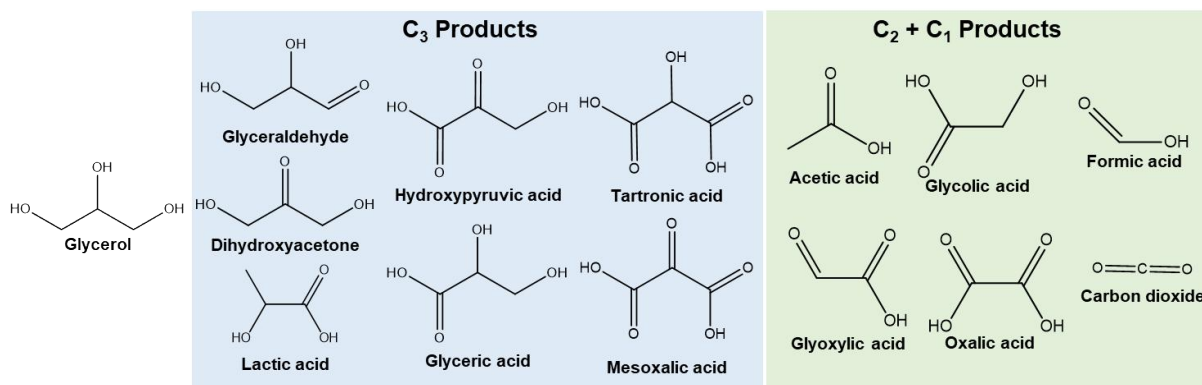


Figure 3: Molecular structure of compounds obtainable from glycerol oxidation.

From the C₃ products, dihydroxyacetone is obtained after oxidizing the secondary hydroxyl group in glycerol, and it is economically the most interesting of these products, as it is widely used in the cosmetics industry, mainly in sunless tanners.²⁰ Commercially, dihydroxyacetone is obtained using a fermentation process^{20,21}, while its chemical synthesis from glycerol can be done using either catalytic^{22–24} or microbiological²¹ oxidation. On the other hand, glycerinaldehyde is obtained after oxidizing a primary hydroxyl group in glycerol and can be used in the preparation of polyesters, as a cellulose modifier, among others.²⁵ It is mainly obtained from the chemical oxidation of glycerol in alkali-free media.^{23,24}

Glyceric acid has few industrial applications, being mostly used as an intermediate for further oxidation products, such as tartronic and mesoxalic acids.^{20,26} It has the highest reported mass yield among the possible oxidation products from glycerol, obtainable both in alkali and acidic conditions, however, this route for glyceric acid production competes with its biosynthesis production using bacteria.^{20,26–28} Tartronic acid is another chemical with a high value-added, as it is used in the pharmaceutical industry in the treatment of osteoporosis, as an oxygen absorber in the food industry, and as an anti-corrosive agent to protect equipment operating at high temperatures. Commercially, it is produced from the chemical oxidation of maleic acid, with its production from the selective oxidation of glycerol being considered a better alternative.²⁰ It can be obtained in high yield when glyceric acid is used as the starting reagent²⁹, however, starting from glycerol it is only obtained as a minor product in alkali solution.^{14,18,30} Mesoxalic acid is the final C₃ oxidation product that can be obtained, afterward, the only possible pathway is C-C bond scission. It is industrially produced from three distinct chemical routes,²⁰ with its production from glycerol coming from

further oxidizing tartronic acid, and thus far all published reports have shown a yield lower than 50%.^{10,31}

The last C₃ products that can be derived from glycerol are lactic and hydroxypyruvic acid. Hydroxypyruvic acid can be obtained from the catalytic oxidation of glyceric acid at low pH (< 6), because if it were to be produced from glycerol oxidation it would have low yield and selectivity.^{23,29,32} In alkali solutions, glycerol can be used to obtain hydroxypyruvic acid using platinum-based electrocatalysts.³³ To the extent of our knowledge, we found no information concerning its commercial production and industrial applications. Lastly, lactic acid is widely used in industrial applications, from being a building block for the synthesis of polylactic acid, in pharmaceutical and food industries, and it is widely regarded as an important platform molecule in the production of biobased chemicals. It is industrially produced from either a chemical or fermentation route.^{34,35} Starting from glycerol, lactic acid can only be obtained in an alkali environment, after a series of base-catalyzed rearrangements stemming from either glyceraldehyde or dihydroxyacetone.³⁴

Of the C₂ products, acetic acid is the most widely available and commonly used in the chemical and food sectors. Its industrial synthesis is over 90% following a chemical route, with only 10% of it from fermentative processes.³⁶ From glycerol, this molecule has been detected mainly from gold-based catalysts in alkali media, as a minor product with a low yield.^{34,37} Glycolic acid is another important compound in many industrial sectors, used as a food preservative in the food industry, and as a dyeing and tanning agent in the textiles industry, and it is produced mainly from petrochemical resources, in addition to enzymatic processes.³⁵ It is usually obtained as a minor product, present in a mixture of several compounds, regardless of the solution pH. High selectivity for glycolate production depends on applying high potentials to the electrocatalyst being used, as it is dependent on breaking a C-C bond, which happens more easily on noble metal catalysts.^{10,34,38}

The other C₂ products are glyoxylic and oxalic acid. Glyoxylic acid is mainly produced from the nitric acid oxidation of glyoxal, and it is mainly used as a reagent in fine organic synthesis.³⁹ It has been detected in a mixture of oxidation products from the electrochemical conversion of glycerol, both in acidic and alkali media, however, no reports on yield or selectivity have been made.¹⁷ Oxalic acid is another widely used compound, mainly in the agricultural and pharmaceutical sectors, and it is only obtainable from several possible chemical routes.⁴⁰ Starting from glycerol, oxalic acid

can be obtained after oxidation and C-C bond breaking of glyceric acid, and it is also obtained in a mixture with other products, as no selective oxidation has been reported as of yet.^{17,24} For the C₁ products, there are only carbon dioxide and formic acid. Formic acid is another commodity widely used in many industries, from agriculture to textiles, in addition to being considered a promising chemical for hydrogen storage in a hydrogen-based economy. Nowadays it is mostly mass-produced from carbon monoxide reforming⁴⁰, and coming from glycerol, it is one of the last steps in its oxidation pathway, and similarly to glycolic acid, it can be selectively produced when high potentials are applied to the electrode.^{14,17,28,30}

Lastly, the main bottleneck of the glycerol oxidation route is the separation process between reactants and products. Distillation is not feasible, as the products often have similar boiling points or lose stability near them, degrading into other substances.²⁷ Separating these mixtures is only feasible using liquid chromatography and is often accompanied by other constraints, in balancing out the stationary phase (ion-exchange resins) and a sustainable eluent (without organic acids).⁴¹⁻⁴³ In this regard, the electrochemical route has a main advantage over the chemical oxidation, in that it can be used as a direct energy (electricity) source in glycerol-based fuel cells, or coupled with another relevant cathodic reaction in electrolyzers, such as the CO₂ reduction or water electrolysis, for green H₂ production.^{11,44,45}

1.3. Catalyst choice for the oxidation reaction

Many different types of catalysts have been explored for the chemical or electrochemical oxidation of glycerol, with varying nature and associated costs. Roughly, these catalysts can be divided by the presence or not of platinum-group metals (PGM), namely: platinum, palladium, rhodium, iridium, ruthenium, and osmium.^{10,14-18} These elements are scarcely found on the Earth's surface and are used in many other applications, especially electronics, hence there is a constant, increasing demand for them. High demand, combined with low availability, results in high market prices, and high catalyst costs, an undesirable situation for large-scale industrial practices.

These PGMs have a prominent position in catalysis, as their electronic structure allows for optimal bond strength with many species, such as -O₂, -N₂, -H, -CO, and others.⁴⁶ From a purely thermodynamic point of view, they can be considered

“ideal” catalysts, owing to their combination of low activation energy combined with moderate adsorption energies, where species are adsorbed neither too strongly nor too weakly, such as the adsorption of hydrogen on platinum, which has near-zero activation energy. Other interesting properties of the PGM-based catalyst are their resistance to thermal degradation and corrosion, in addition to their stability. Hence, studying mono- or bimetallic catalysts containing PGMs can provide a deeper understanding of the general phenomena of catalysis, as one can investigate how deviations (e.g., alloying a PGM with a cheaper, Earth-abundant metal) from these “ideal surfaces” impact the reaction being studied. This is best seen in computational studies, particularly those that employ density functional theory (DFT), where complex chemical reactions are broken down into a series of elementary steps, to the point where one or two variables, called descriptors, can be used to determine the rate of a reaction.^{46–48} By combining experimental and theoretical data, computational models for the reaction can be developed, which allow for a catalyst screening to be performed, so that an optimal catalyst for the reaction being studied can be found. Lastly, it is important to note that optimal catalysts for practical applications need to find a balance between performance (activity, selectivity, and stability) and fabrication costs.

Hybrid catalysts, composed of precious and PGM-free components, contribute by not only decreasing the usage of these scarce elements but also their presence often improves the performance of these PGM-based catalysts, improving their activity and selectivity. Such cases will be exemplified in the following paragraphs.

Concerning the chemical oxidation of glycerol, its study began in the 1990s with the works of Kimura *et al.*²³ and Gallezot *et al.*^{24,31}, using PGM elements (Pt, Pd, and Ru) and rhenium supported on activated charcoal. Kimura²³ first observed, in 1993, that Pt alone showed activity for the oxidation of the secondary hydroxyl, yielding dihydroxyacetone, and the selectivity could be increased by modifying the Pt/C catalyst with bismuth (from 10% selectivity on 5% Pt/C to 80% after adding 1% Bi, at 20% yield). The works by Gallezot further optimized the reaction condition and catalyst, attaining a 37% yield to dihydroxyacetone at 75% glycerol conversion, with a higher Bi concentration (Bi/Pt molar ratio = 0.37). From their pioneering work, many others came. Hirasawa *et al.*⁴⁹ also selectively obtained dihydroxyacetone, with a selectivity of over 80% on Pd-Ag/C catalysts, despite a low conversion of 20%. For the production of glyceric acid, Carretin *et al.*⁵⁰ reported 100% selectivity with 1% Au supported on either charcoal or graphite, with a 56% conversion, while Chornaja *et al.*⁵¹ achieved

74% selectivity at 100% conversion using 2.5% Pd/Al₂O₃. Lastly, Lakshmanan *et al.*⁵² obtained 83% selectivity to lactic acid using 1% Au/CeO₂, at 98% conversion.

Regarding the electrochemical route for glycerol oxidation, the earliest known report comes from 1980⁵³, and then gained traction between the middle 2000s and early 2010s, all using PGM electrocatalysts.^{28,54–57} A special note has to be made about the work of Simões *et al.*⁵⁷, as they used a PdNi hybrid catalyst, which improved the activity of the clean Pd electrode (in this context, catalyst activity is measured as the registered anodic current density). Similar to the findings of Kimura *et al.*²³, Kwon *et al.*²² observed that modifying Pt/C electrodes with Bi resulted in a change to the reaction selectivity, favoring the formation of dihydroxyacetone, achieving 100% selectivity in a Bi-saturated H₂SO₄ electrolyte. The major difference between those works is that in heterogeneous catalysis, precise temperature and atmosphere control is necessary, in addition to the constant stirring of the reaction mixture, whereas electrocatalysis works with much milder conditions, at room temperature, ambient pressure, and with a stagnant solution. In other words, Kwon *et al.*²² was able to reproduce the findings of Kimura *et al.*²³ in a significantly different, more mild, reaction environment, which is extremely desirable for large-scale applications. They continued this investigation, using other p-block elements to modify the Pt/C electrodes⁵⁸, and found that Sb-Pt/C also resulted in high selectivity towards dihydroxyacetone, while Kimura *et al.*²³ reported that this catalyst did not change the selectivity during the chemical oxidation.

Another important observation to be made about the work of Kwon *et al.*⁵⁸ is that slight changes to the surface of Pt electrocatalysts (electrodes) resulted in appreciable changes to their activity towards glycerol oxidation. This phenomenon, where small amounts of a metal adsorbate (adatoms) cause appreciable changes to the activity of Pt electrodes, was first reported by Clavilier *et al.*^{59–62}. They modified the electrodes by submerging them in a solution containing ions of the chosen metal (originally, Bi and Pb), causing their spontaneous deposition on the electrodes, a phenomenon now known as irreversible adsorption. Up to this date, the mechanism in which this happens is still not fully understood.^{63,64} It is important to highlight that these changes in activity happen because electrocatalysis is inherently a surface phenomenon. Electrocatalysts are often bulk materials and have a much lower surface area than conventional heterogeneous catalysts, which are materials supported on a porous matrix. Thus, small changes to the surface of electrocatalysts have a significant

impact on their activity, while changes to heterogeneous catalysts require alloying with multiple components. There are instances in which porous electrodes are used, but this will be addressed in a later chapter.^{45,65}

Besides the aforementioned PdNi electrode developed by Simões *et al.*⁵⁷, there are other instances in which bimetallic alloys are used as electrodes, with an improvement to the catalyst activity when compared to the electrode made up of a precious element. Some of the elements that have been used are Sn, Cu, Co, and Fe, in addition to Ni.¹⁶ Multi-component catalysts have also been used, but those are less common because, with 3 or more elements on a single alloy, there are many more variables at play, which end up being detrimental to the computational screening process. An important observation has to be made on nickel-based electrodes because their hydroxides are capable of oxidizing glycerol in alkaline media.^{16,30} Nickel is an abundant low-cost element, thus it has been gaining widespread attention, for a Ni-based catalyst could represent a low-cost solution to the development of electrochemical devices operating on glycerol oxidation.

Nickel electrodes require an alkaline environment to oxidize glycerol because they are attacked by H⁺ ions and decompose at low pHs. A major drawback of Ni-based electrodes is that they need high applied potentials to begin oxidation. Some of the solutions developed so far include chemical⁶⁶ or thermal treatment⁶⁷, aging⁶⁸, and forming multi-component alloys with other abundant elements, such as Co^{67,69}, Cu⁶⁹, Bi⁶⁸, among others.^{16,44}

1.4. Main objectives

Based on the discussion so far, the main objective of this doctoral thesis was to investigate if it is possible to modify the reaction pathways of the glycerol oxidation reaction on platinum electrodes by modifying the electrode surface by deposition of p-block elements in alkaline media.

The specific objectives are:

- Modification of the Pt electrodes with two methodologies: deposition outside of the electrochemical cell (irreversible adsorption, spontaneous), and inside the cell (saturating the electrolyte with ions of the chosen element). The goal of this step is to determine if these two methodologies provide the same result, or if one is superior to the other.

- Screening of the various Pt-Adatom systems, to determine which element(s) improve the activity of the electrode towards the reaction, and also to see how they are affecting the electrochemical behavior of the electrodes in the supporting electrolyte.
- Investigate possible changes to the reaction pathways and product selectivity: (I) *in situ* FTIR to identify the reaction products and intermediates that are being generated by the Pt-Adatom systems that improved activity; (II) HPLC with on-line sample collection, to determine product distribution as a function of electrode potential; and (III) X-ray absorption spectroscopy under electrochemical conditions, to investigate how the adatoms are affecting the oxidation state of the Pt electrodes;
- Apply the knowledge acquired with conventional three-electrode cells to electrochemical devices. In this step, the anode of a glycerol-fed fuel cell is modified with our Pt-Adatom catalysts, to concomitantly generate energy and value-added chemicals.

2. Electrochemical Systems

This chapter aims to describe the electrochemical apparatus and the methodology used in our investigation. Here we describe how the electrodes are modified and how we study their activity and stability. The main analytical technique used to study the electrocatalysts was cyclic voltammetry. Anodic currents give a measure of electrocatalyst activity, and other parameters used to compare the different catalysts were the maximum anodic current (peak current, j_{peak}) and the potential where the anodic reaction begins (onset potential, E_{onset}). The arbitrary choice of j_{peak} as a descriptor was one of the possible ways to compare how the anodic currents in the different electrodes behave with potential cycling.

2.1. Electrochemical cell and techniques

The electrochemical cells used were composed of three electrodes: a working electrode (WE), a counter electrode (CE), and a reference electrode (RE). The shape and material of the cell were dependent on the type of application. A schematic of this cell is shown in **fig. 4**.

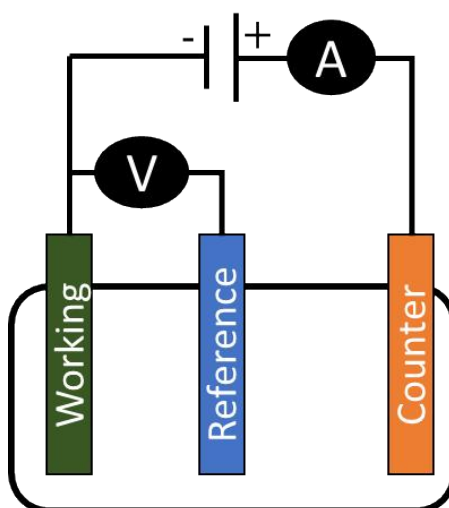


Figure 4: Scheme of a three-electrode electrochemical cell, showing the WE, RE, and CE. The potential of the working electrode is controlled with respect to the reference electrode, while current is allowed to flow between the working and counter electrode.

The WE is the electrode in which the electrochemical reaction of interest takes place, the object of study. The potential applied to the WE is with respect to the RE, an electrode with a fixed composition throughout the electrochemical process

happening in the cell. Since its composition remains unchanged, the standard reduction potential (E°) of the reaction happening on this electrode does not change. All values of E° are measured against one primary electrode, the standard hydrogen electrode (SHE), made by dipping a platinized platinum electrode into an acidic solution and bubbling pure H_2 gas through it.⁷⁰ In this electrode, the redox reaction is $2 H^+ + 2 e^- \rightarrow H_{2(g)}$, with the activity and partial pressure of H^+ and H_2 at unity, respectively. This means that the SHE works as a universal scale, and all electrode potentials can be compared against it, while the RE works as a “local scale”. The potential measured against different types of RE may be compared by knowing where they are positioned with respect to the SHE scale (**fig. 5**). Lastly, the current flows between the WE and CE electrodes (also called an auxiliary electrode), and usually, it is made of a material that will not produce any substances that might interfere with the electrochemical reactions being studied.

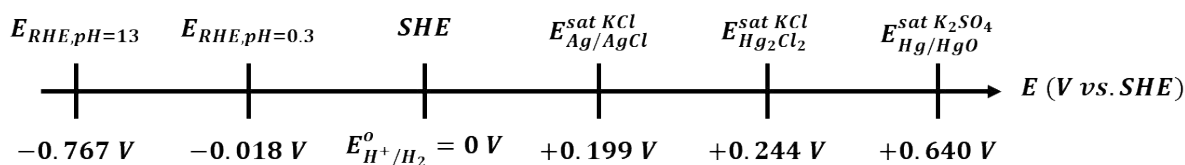


Figure 5: Comparison between E° of various reference electrodes. Using E° values provided by ref.⁷⁰.

The main electrochemical techniques employed throughout this work were cyclic voltammetry (CV) and chronoamperometry (CA), as displayed in **figure 6**. Cyclic voltammetry is a technique where the potential applied to the WE is varied linearly (usually) between two vertex points, an upper and lower potential limit. The change in potential with respect to time is called the sweep or scan rate, and the result is a curve of current versus applied potential, called a voltammogram. This technique is commonly used to investigate oxidation and reduction of molecules, and it is vital to obtaining information from chemical reactions that begin with an electron transfer, which is the case for most catalytic reactions.⁷¹ Chronoamperometry, on the other hand, is a static technique in which the potential on the WE is fixed and the current is registered with respect to time, with $t = 0$ being the instant in which the potential is applied. This technique is mostly used in electrolysis experiments, where reaction products, both aqueous and gaseous, are collected as a function of applied potential

and reaction time, and later identified and quantified using chromatography. Another application of chronoamperometry is when performing *in situ* spectroscopical experiments, resulting in a series of spectra registered as a function of the applied potential on the WE.

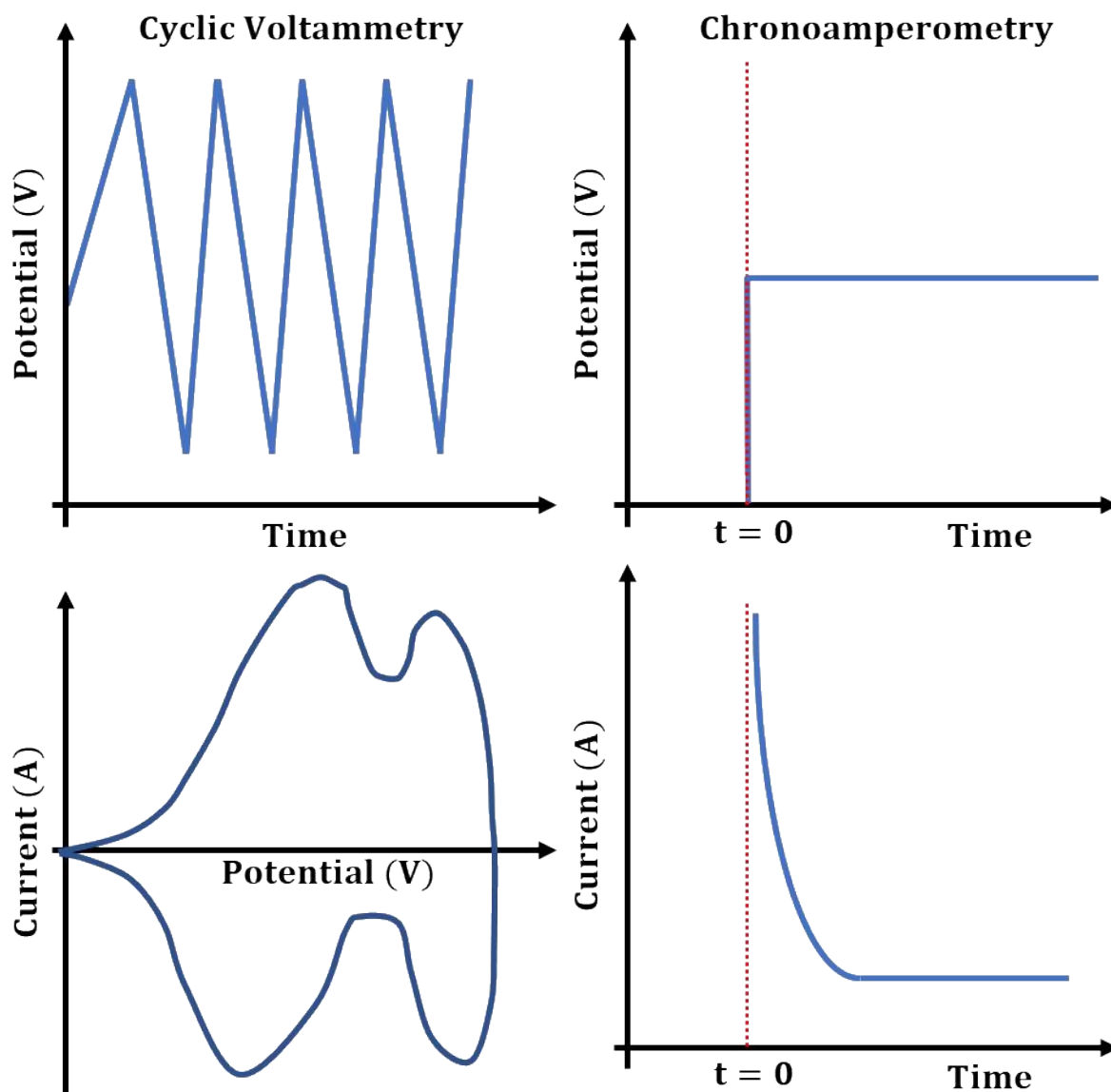


Figure 6: Scheme of the cyclic voltammetry and chronoamperometry techniques (top) with their respective answers (bottom).

2.2. Methodology

This section will mainly concern the methods for cleaning the electrochemical cells and electrodes used throughout this work. Unless stated otherwise, all electrochemical cells used were made of glass.

All glassware used on electrochemical measurements, as well as the cells

themselves, were cleaned by overnight immersion in an alkaline KMnO_4 solution, by placing them inside 2 L beakers. This step was followed by rinsing with ultrapure water and then rinsing using a dilute solution of $\text{H}_2\text{SO}_4 + \text{H}_2\text{O}_2$, to remove the oxides formed during the KMnO_4 bath. Afterward, the beaker containing the glassware was filled with ultrapure water and heated to a boil, and the water was discarded into the sink. The boiling process is then repeated a minimum of three times, and only then the glassware was used. After the measurements are finished and the solutions used adequately discarded, the glassware and cells are rinsed and filled with ultrapure water, and then stored in cabinets.

The WEs used in the non-coupled electrochemical experiments were either polycrystalline platinum (Pt_p) wires with a spherical end or Pt single crystals of the main crystallographic orientations, i.e. (111), (110), and (100). The CEs were Pt_p sheets, and RHE electrodes were made by welding a Pt-Rh(10%) mesh to a Pt_p wire. All platinum materials were acquired from Impalla Metals Brasil[®], except for the single crystals. Control of applied potential and registering of electric current was done by using a potentiostat/galvanostat, and in this work, we used potentiostats from both Metrohm[®] and Ametek Scientific Instruments[®].

The WEs and CEs were initially cleaned by submerging them in aqua regia (1:3 $\text{HNO}_3 + \text{HCl}$) for 30s, rinsed with ultrapure water, and flame annealed using a butane flame until bright red, followed by rapid quenching. This step was only executed on electrodes that had direct contact with p-block ions in solution, for they tend to strongly adsorb on Pt, thus requiring a harsh cleaning methodology. For the platinum single crystals, they were cleaned by forming a meniscus with the aqua regia solution for 5s and rinsed with ultrapure water. Afterward, they were cleaned by the methodology established by Clavilier⁷², where they were heated in a butane flame for 30s and cooled in a reductive atmosphere of Ar/H_2 ($\sim 2:1$). Once cooled, the surface of the single crystal was protected by a droplet of ultrapure water and then transferred to the electrochemical cell.

All electrolyte solutions were prepared using ultrapure water (18.2 $\text{M}\Omega/\text{cm}$, 25 °C, Millipore) on the day they were used, and the chemicals were used without any purification or pretreatment. The chemicals used were: Sulfuric acid (ISO grade, Merck Emsure), hydrogen peroxide (30% wt, LS Chemicals), nitric acid (p. a. ACS, LS Chemicals), hydrochloric acid (p. a. ACS, Vetec Chemistry), potassium permanganate (PA ACS grade, Vetec Química), sodium hydroxide (semiconductor grade, 99.99%

trace metal basis, Sigma-Aldrich), glycerol (ACS grade, Sigma-Aldrich), lead(II) nitrate (99.999% trace metals basis, Sigma-Aldrich), bismuth(III) oxide (ReagentPlus, Sigma-Aldrich), thallium (I) sulfate (99.99% trace metal basis, Sigma-Aldrich), antimony oxide (99.999% trace metal basis, Sigma-Aldrich), indium (III) nitrate hydrate (99.99% trace metal basis, Sigma-Aldrich), tin (II) sulfate ($\geq 95.0\%$, Sigma-Aldrich), germanium (IV) oxide (99.999% trace metal basis, Sigma-Aldrich), selenium (IV) oxide (99.9% trace metal basis, Sigma-Aldrich) and sodium sulfide nonahydrate (P.A. ACS, Vetec).

The final step in checking the cleanliness of the electrodes and electrochemical cell is by performing a CV of the WE on the supporting electrolyte. The supporting electrolyte is a solution that contains only an electrolyte, a species added to decrease the solution resistance by working as an ionic conductor. Common choices of electrolytes are HClO_4 , NaOH , and H_2SO_4 , of which the latter two were used in this work. A voltammogram of the WE on the supporting electrolyte alone is called a blank voltammogram and shows the reversible (symmetrical) response of the electrode on the electrolyte of choice. The behavior of Pt electrodes is well-documented⁷²⁻⁷⁴, so any discrepancies indicate the presence of contaminants in the system. **Fig. 7** shows the blank voltammograms of the electrodes used in our work, while **fig. 8** shows one of those voltammograms highlighting the zones for hydrogen adsorption/desorption (also called hydrogen underpotential deposition, or H_{UPD}) and the platinum oxide formation.

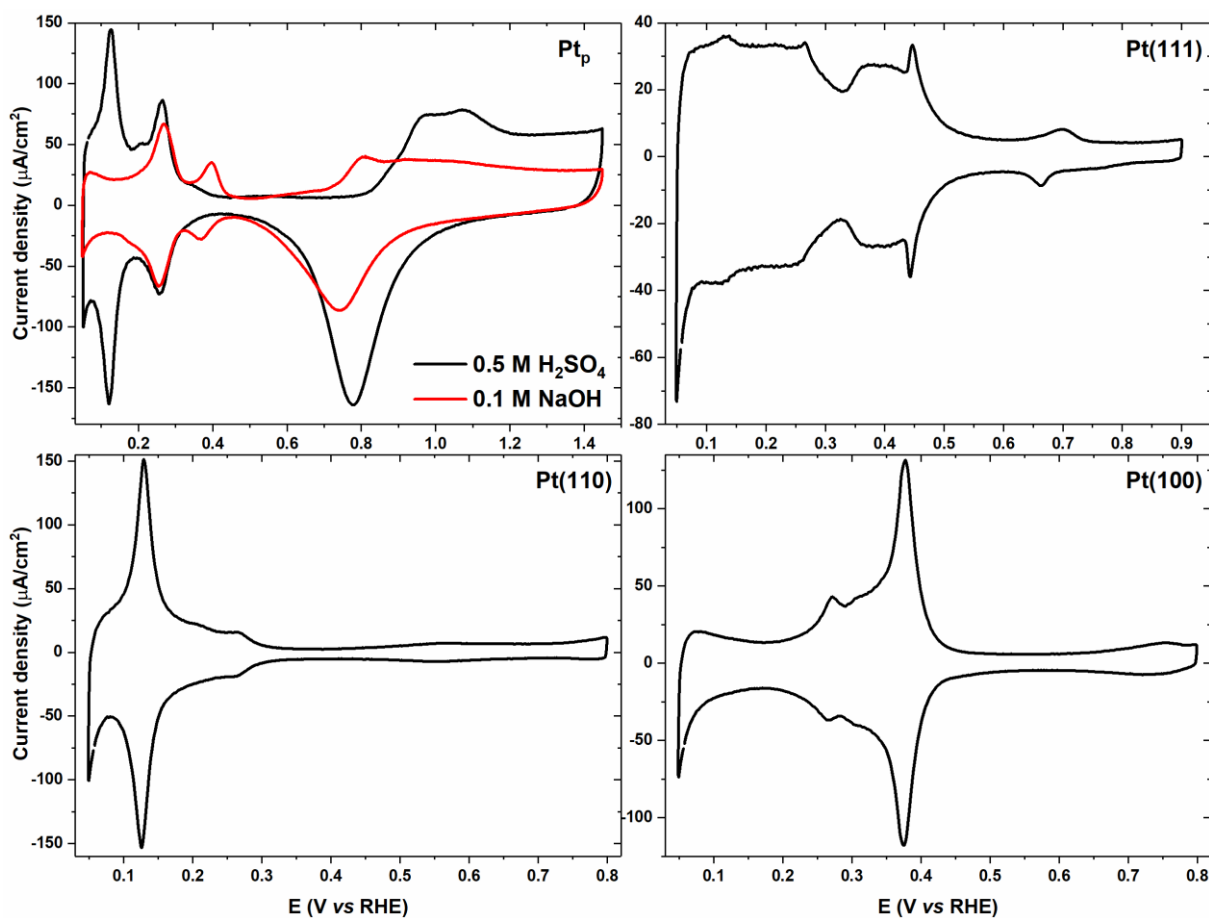


Figure 7: Blank voltammograms of polycrystalline and single crystal platinum electrodes, recorded in 0.5 M H₂SO₄ (black) and 0.1 M NaOH (red) with a sweep rate of 50 mV/s. Pt_p voltammograms for H₂SO₄ and NaOH were done in different electrodes.

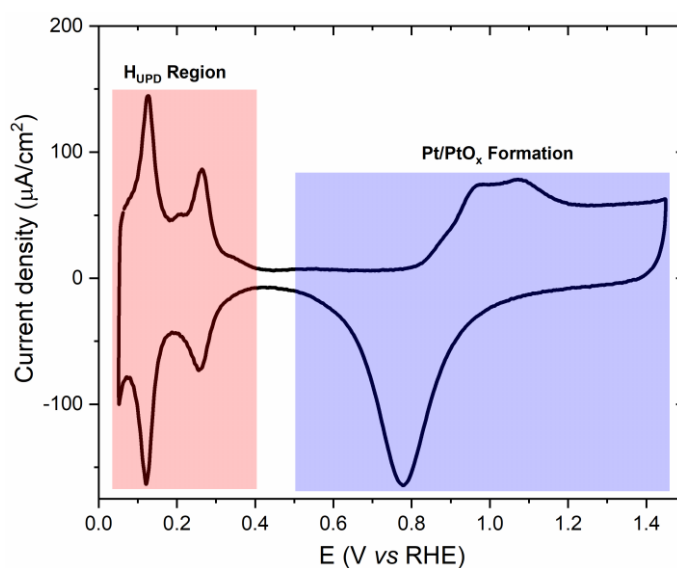


Figure 8: Blank voltammogram of Pt_p in 0.5 M H₂SO₄ highlighting the H_{upD} and Pt/PtO_x formation regions.

Besides showing the cleanliness of the electrochemical system, the blank voltammograms of Pt are used to calculate the electrochemically active surface area (ECSA) of the WE. The ECSA is a vital property to describe and compare different electrocatalysts since the rate of an electrocatalytic reaction is proportional to its active surface area. For Pt electrodes, this is obtained by measuring the charge involved in the H_{UPD} region (red highlighted in **fig. 8**), and dividing it by the charge for total site density, which for Pt_p is $210 \mu C/cm^2$.^{73,75}

Once cleaned, the electrodes can be modified by the p-block elements. The electrodes were modified using two methodologies: *ex situ*, where the WE was modified outside of the electrochemical cell, and *in situ*, where a known quantity of ions was added to the electrolyte solution containing glycerol so that oxidation and adatom deposition happens simultaneously on the same cell. A total of nine elements of the p-block were chosen to modify Pt in our work: Bi, Pb, Tl, Ge, Sb, Se, S, In, and Sn.

This investigation began with the *ex situ* modification, a process commonly named irreversible adsorption^{59,62,76,77} by electrochemists. This process consists of the spontaneous deposition of the desired element (in our case, the p-block elements) on the electrode, by immersing it in a solution containing ions of said element. While it is called “irreversible adsorption”, it is possible to electrochemically remove these adatoms from the electrode surface, by applying high potentials on the WE, to cause oxygen evolution and subsequent adatom desorption, however, such potentials are enough to cause irreparable damage to the organized surface of single crystals. Thus, it is considered to be irreversible because, in regular working conditions (potential windows), the adatoms do not leave the Pt surface.

The amount of adatoms deposited on the electrode surface, i.e., the electrode coverage (θ), depends on both, the adatom concentration and the time it remained submerged. Salts of the aforementioned elements were all dissolved in ultrapure water, except for Bi_2O_3 , which was dissolved in 0.5 M H_2SO_4 . Despite it being a common process, and particularly useful in the characterization of stepped platinum single crystals^{76,78,79}, the mechanism by which this occurs is still unknown.⁶⁴ After deposition, the WE is submerged in a beaker containing ultrapure water, to remove the excess of the adatom solution, and transferred to an electrochemical cell containing 0.1 M NaOH where θ is determined by looking at the decrease in the H_{UPD} region, as shown in **fig. 9**.

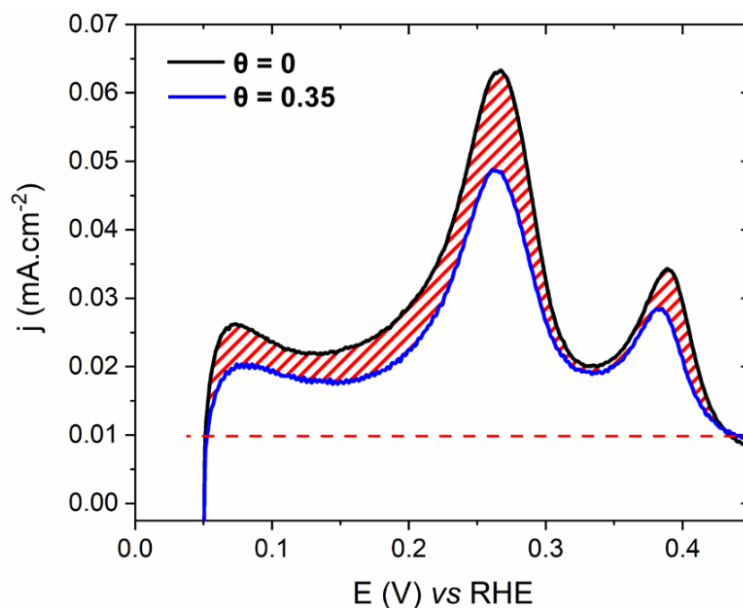


Figure 9: Scheme of θ determination on Pt_p in a 0.1 M NaOH solution with a sweep rate of 10 mV/s, by comparing the H_{UPD} region on the WE before (black) and after (blue) adatom deposition, since the Pt sites covered by adatoms are inaccessible to the H^+ ions involved the adsorption/desorption process. Adapted from ref.[80].

We measure θ according to **fig. 9** by measuring the charge involved in the H_{UPD} region before and after modification as follows:

$$\theta = 1 - \frac{Q_{\text{Hydrogen UPD,modified}}}{Q_{\text{Hydrogen UPD,clean}}}$$

We define coverage in terms of the availability of Pt sites for the hydrogen adsorption/desorption process, however, it may also be defined by the number of platinum sites occupied by foreign atoms.⁸¹ In practice, this would mean that θ , as according to our definition, would have to be divided by the number of electrons transferred during the deposition of the foreign atom. The result is that, using our definition, $\theta = 1$ means full electrode coverage regardless of the adatom being deposited, and by adding this correction each Pt-adatom system would have a different θ for full coverage. Regardless, the choice of the method used to measure the coverage is not important for our work, where we only use this value to follow trends in our measurements.

Lastly, the *in situ* modification is achieved by simply adding a known amount

of the dissolved salts of the foreign element to the electrolyte containing glycerol.^{22,58} The end result is that both the deposition and oxidation reaction are taking place simultaneously and, if glycerol is removed, i.e. the Pt_p electrode is cycled in a 0.1 M NaOH solution with the p-block ions alone, θ can be measured as a function of the number of cycles.

2.3. Electrochemical modification by Bismuth and Lead

The modification of Pt_p electrodes began with the irreversible adsorption of Bi and Pb adatoms. These results are summarized in **fig. 10**, where we observe that the catalyst activity increases concomitantly with θ until full coverage, an observation in line with what was observed for those systems in acidic media.^{22,58} However this modification lacks stability, which is seen by observing how j_{peak} changes with the number of cycles (**fig. 11**), where the system rapidly loses stability. For Pt-Bi, by the 10th cycle, the system shows j_{peak} comparable to that of clean electrodes regardless of the θ , while for Pt-Pb this was observed for all $\theta < 0.8$. For Pt-Pb, a shoulder can be seen on the voltammogram centered around 0.6 V when $\theta > 0.85$, indicating that a new oxidation mechanism is present.

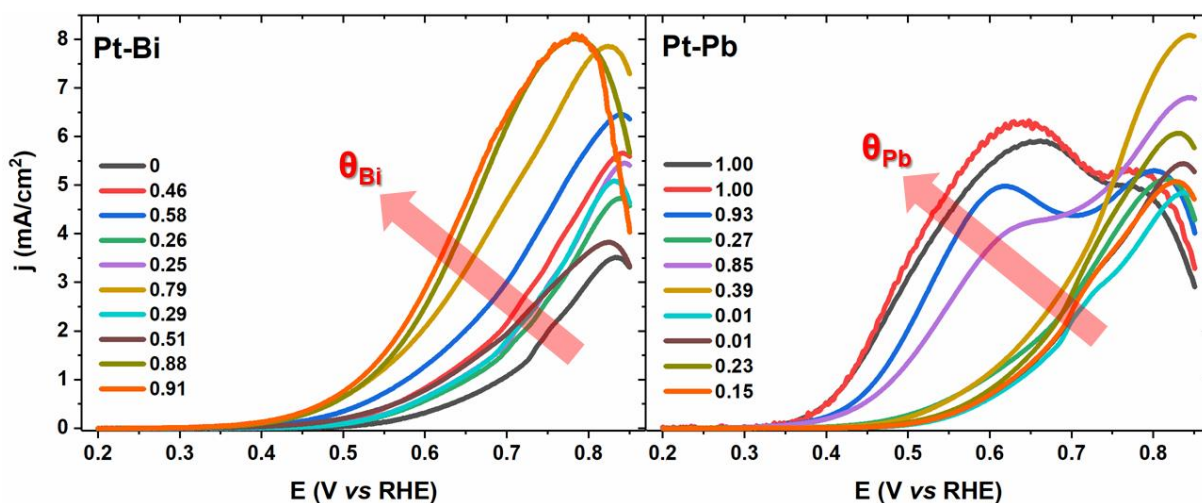


Figure 10: 1st positive scan of the glycerol oxidation on Pt_p modified by Bi and Pb. Inserts show the electrode θ . The electrolyte was 0.1 M NaOH + 0.1 M glycerol with a sweep rate of 10 mV/s. Adapted from refs. [82,83].

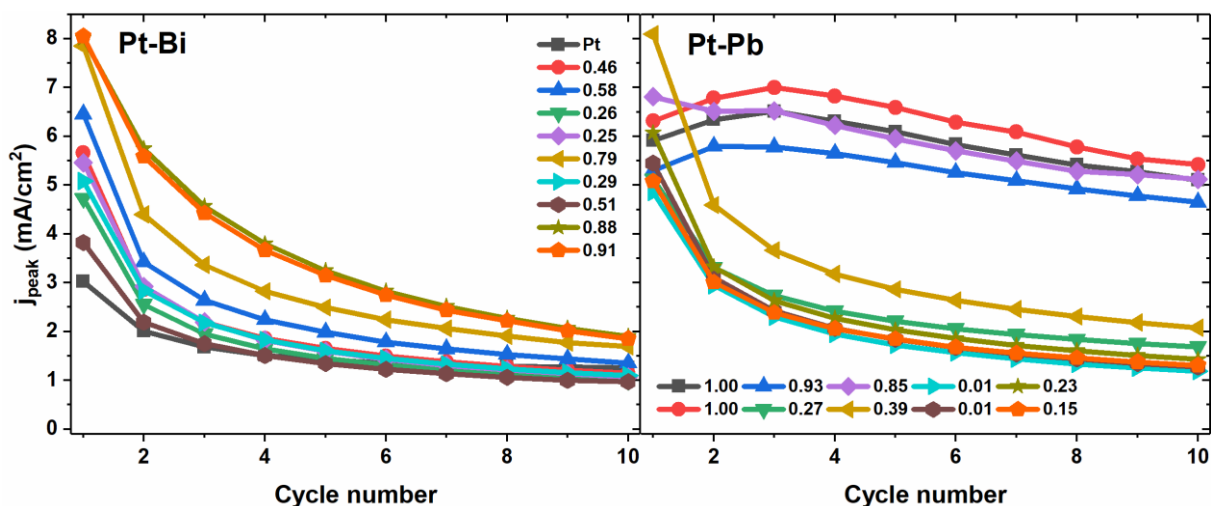


Figure 11: Change in j_{peak} with cycle number, for the measurements shown previously in **fig. 10**. Adapted from refs. [82,83].

This loss of activity can be rationalized in terms of: i) the electrode is being poisoned by reaction intermediates, which can be attributed to a combination of adsorbed CO and glycerol derivatives^{84–87}, and/or ii) the adatoms are leaving the Pt surface when the potential is cycled, thus the electrode slowly reverses back to the activity originally shown in a clean Pt electrode. The first hypothesis can only be investigated by using *in situ* spectroscopical techniques, which fall within the scope of this chapter (and are later discussed in **chapter 3**). The second hypothesis was tested by studying the stability of the Pt-Bi system.

First, the Pt_p electrode was modified *ex situ* with Bi, achieving coverage of 0.91. The voltammetric profile remained constant after 100 cycles in 0.1 M NaOH, as shown in **fig. 12**, where a reversible peak at 0.65 V can be seen, attributed to the redox behavior of Bi/Bi^{3+} on the Pt surface.^{59,88} Besides this redox behavior, this also attests to the stability of this system. Next, the electrode was transferred to a second cell, where it was used to oxidize glycerol. After 10 oxidation cycles, the electrode was transferred back to the cell containing 0.1 M NaOH, where it was once again cycled in the same potential window. No changes in the H_{UPD} region were observed after it was used to oxidize glycerol, indicating that the adatoms did not leave the Pt surface during oxidation, however the reversible peak at 0.65 V decreased in intensity, indicating that a surface rearrangement occurred, caused by the Bi adatoms and/or glycerol derivatives strongly adsorbed (in our potential window) to the electrode⁸⁷, and this may be the cause for the deactivation observed in **fig. 11**.

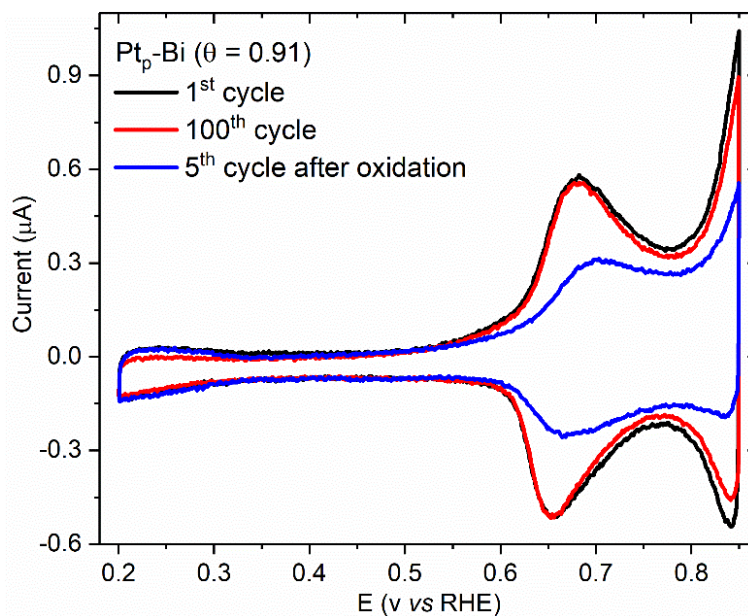


Figure 12: 1st (black) and 100th (red) voltammogram of Pt_p modified *ex situ* by Bi adatoms in 0.1 M NaOH, and 5th cycle (blue) in 0.1 M NaOH after the same electrode was used for 10 cycles of glycerol oxidation in 0.1 M NaOH + 0.1 M glycerol. Both measurements were done with a scan rate of 10 mV/s. Adapted from ref. [82].

A more stable response than what is seen in **fig. 11** was achieved by modifying the Pt_p electrode *in situ*, i. e. by adding Bi or Pb ions to the electrolyte containing glycerol. These results are shown in **fig. 13** below, where the 10th positive scan for each measurement is shown. An initial comparison of this figure with the data shown in **fig. 11** reveals that the oxidation currents are significantly higher after the addition of the ions to the electrolyte, and this is further confirmed when j_{peak} is plotted against the cycle number in **fig. 14**. The results shown in **figs. 13** and **14** combined tell us that at very low concentrations (10^{-8} and 10^{-7} M) these adatoms have little impact on the Pt activity, however from 10^{-6} M onwards there is a change in the voltammetric profile, where high oxidation currents are obtainable at much earlier potentials ($E < 0.6$ V for Pt-Bi, and 0.5 V for Pt-Pb). Further increasing the concentration to 10^{-5} M improves the activity and stability of both systems, however, at 10^{-4} M they become less active, with lower j_{peak} values (however, Pt-Pb at 10^{-4} M Pb²⁺ shows higher oxidation currents at $E < 0.6$ V than with 10^{-5} M Pb²⁺). This indicates that there is an optimal concentration wherein the increase in catalyst activity is at its highest, and above this concentration there is an excessive amount of adatoms being deposited on

the electrode surface, blocking the Pt active sites that would otherwise be available for catalysis. When the Pb^{2+} concentration was further increased to 10^{-3} M the electrode had even smaller oxidation currents, however, its profile remained constant throughout 10 oxidation cycles. Lastly, at 10^{-2} M the Pt electrode was completely inactive towards glycerol oxidation, due to the excess of Pb adatoms.

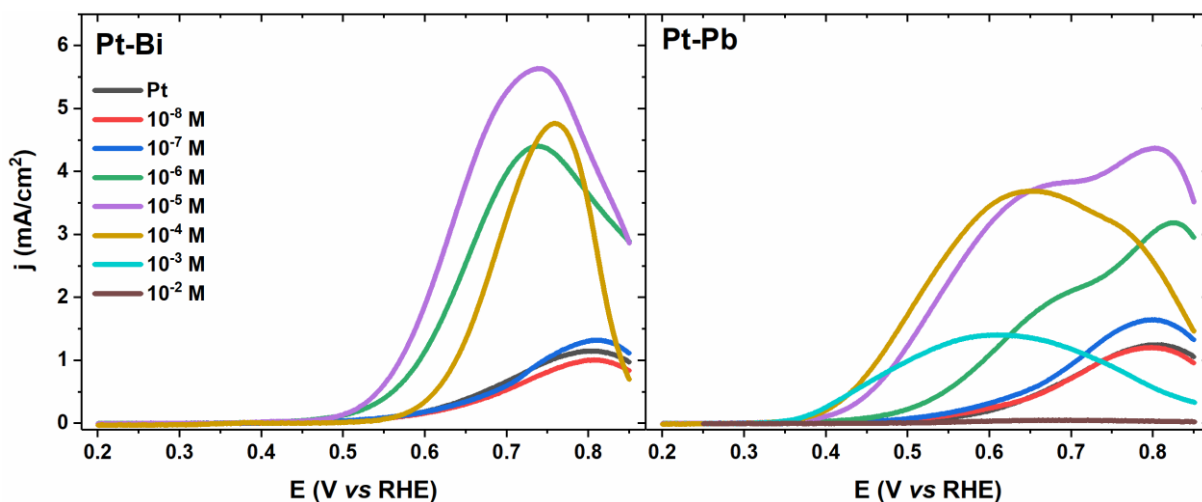


Figure 13: 10th positive scan of the glycerol oxidation on Pt_p in 0.1 M NaOH + 0.1 M glycerol, with a scan rate of 10 mV/s, containing distinct quantities of Bi_2O_3 (left) and Pb^{2+} (right) to the electrolyte. Adapted from refs. [82,83].

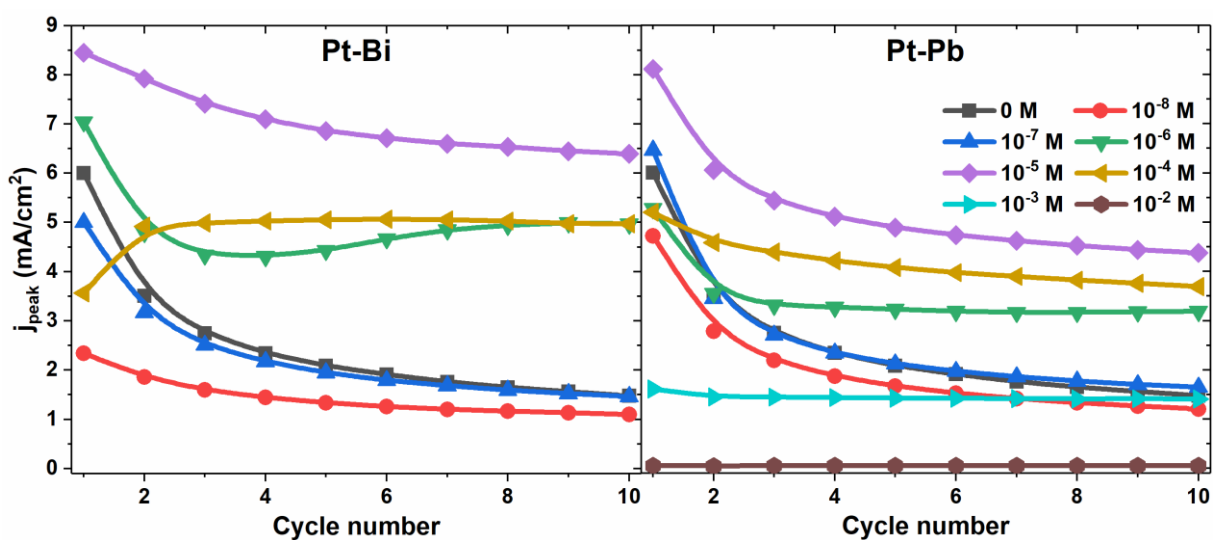


Fig. 14: Change in j_{peak} with cycle number, for the measurements shown previously in fig. 13. Adapted from refs. [82,83].

The results shown here point out that the *in situ* modification provides both higher activity and stability for the electrode than the *ex situ* route, as the oxidation currents remain higher for a longer period. In addition, it becomes clear that the

concentration of 10^{-5} M Pb^{2+} and 10^{-5} M Bi_2O_3 shows the highest improvement in catalyst activity in the Pt-Pb and Pt-Bi systems, respectively. In other words, this concentration offers the highest increase in oxidation current and the slowest decrease of j_{peak} (**fig. 14**). We will denote such a concentration as the optimal concentration of that specific Pt-Adatom system throughout the text from now on.

To better compare these methodologies, a stability test was performed by submitting the Pt_p electrode, both clean and modified by Pb, to 100 oxidation cycles and examining the changes in j_{peak} during this cycling, as shown in **fig. 15**. The bare platinum electrode is only slightly active by the 20th cycle, with a j_{peak} slightly below 1 mA/cm^2 , while the Pt-Pb electrodes have a j_{peak} of 3 and 5 mA/cm^2 using the *ex situ* and *in situ* routes, respectively, with the *in situ* electrode consistently showing higher oxidation current. This data, combined with the results shown in **fig. 12**, confirm that deactivation is due to the adsorption of poisonous intermediates, and not due to adatoms leaving the electrode surface. Since the clean electrode deactivates at a much faster rate, we are led to believe that the adatoms improves the activity by hindering the adsorption poisonous intermediates, and/or by blocking the reaction pathways that lead to their formation. Answering this question is only possible by using *in situ* spectroscopical techniques, which are discussed in **chapter 3**. This improvement in catalytic activity by blocking the adsorption of poisonous intermediates is called the third-body effect⁸⁹, however, we may not yet discard the possibility of other effects taking place, such as a bifunctional mechanism, where the adsorbed atom plays an active role as an extra active site, or by an electronic effect, where the adatoms are changing the electronic properties of superficial Pt atoms.⁶⁴

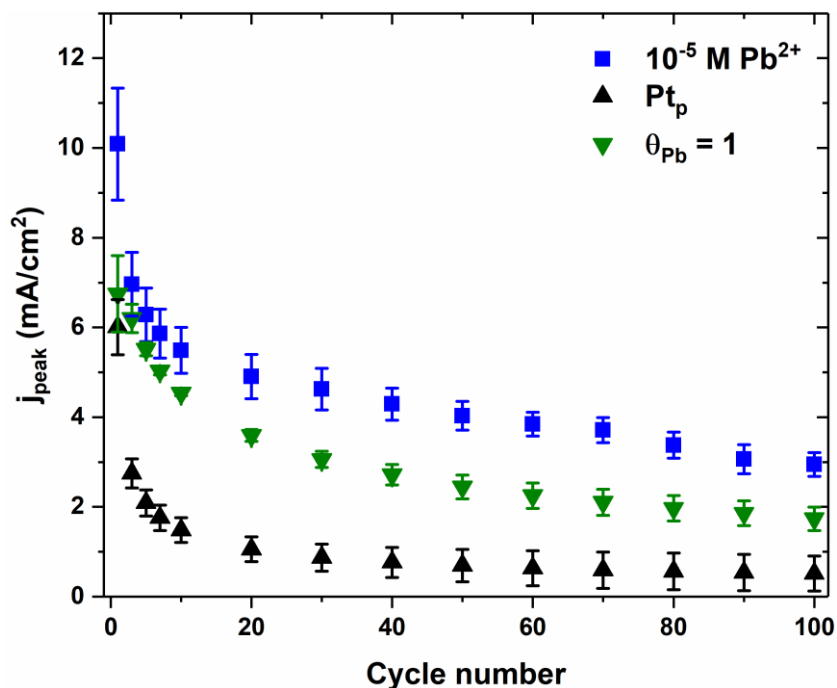


Figure 15: Changes in j_{peak} during 100 oxidation cycles on the same experimental conditions described in **figs. 10** and **13**, for the clean Pt_p electrode and Pt-Pb, modified *ex situ* (green) and *in situ* (blue).

Having determined that the deactivation is caused by strongly adsorbed intermediates and that both elements decrease the rate of electrode poisoning, the next step in our investigation is to understand the interaction between Pt and the adatoms. This was conducted in two steps, first by cycling the Pt_p electrode in the supporting electrolyte with the metallic ions in solution, without glycerol, and second by using Pt single crystals to oxidize glycerol, both with and without modification by Bi and Pb.

The effect of cycling a Pt_p electrode in NaOH with Bi_2O_3 and Pb^{2+} ions in solution is shown in **figs. 16** and **17**, respectively. The Pt-Bi system was discussed in detail in the author's dissertation⁸⁰, and here a shortened version will be presented. The response of those is unimpressive compared to that of glycerol oxidation shown in **fig. 13**, therefore it is safe to consider that the voltammetric response of these electrodes in presence of glycerol is solely due to the catalysis, instead of a combined answer between catalysis and the material.

These results show that the Pt_p electrode becomes progressively more covered by the adatoms with potential cycling, and as their concentration in the solution increases. For both systems, full coverage is not achieved after on both 10^{-8} and 10^{-7}

M after 10 cycles, as the H_{UPD} region can still be seen. A completely covered electrode is only achieved by the 10th cycle at 10^{-6} M, which matches with the improvement in activity seen in **fig. 13**, as this is the concentration where an activity boost is first seen. On Pt-Bi, at this concentration, the redox Bi peak can be observed, which was first described in **fig. 12**, while Pt-Pb shows only a broadening of the oxidation region. At the concentration of 10^{-5} M, both electrodes are completely covered by the first cycle, and while Pt-Pb shows a stable voltammogram since the 1st cycle, Pt-Bi has a broad and irreversible oxidation region between 0.50 and 0.75 V, paired with a reduction peak at 0.35 V, afterwards the voltammogram becomes stable by the 3rd cycle. No significant changes are observed in Pt-Pb by further raising the Pb^{2+} concentration, except that at 10^{-2} M where no oxidation/reduction peaks can be distinguished. For Pt-Bi, on the other hand, at 10^{-4} M the system remained unstable after 10 potential cycles, and oxidation and reduction peaks at 0.40 and 0.30 V, respectively, progressively increased with the cycling. We attribute this feature to a massive (bulk) deposition of Bi adatoms on the electrode, and those peaks correspond to the redox process of Bi on top of Bi.

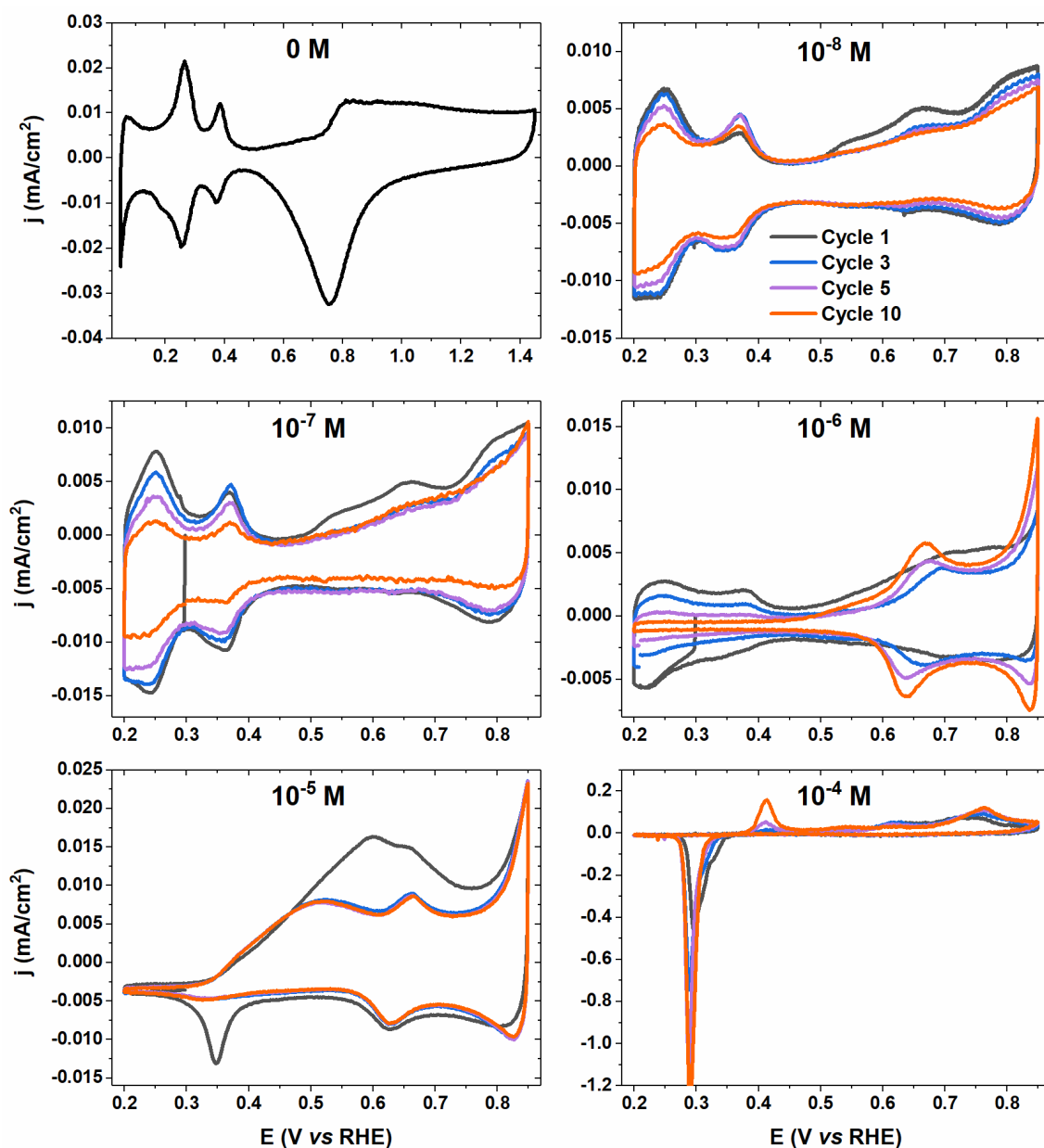


Figure 16: Cycling a Pt_p electrode in 0.1 M NaOH with varying concentrations of Bi₂O₃, with a sweep rate of 10 mV/s. Reprinted with permission from ref.[82]. Copyright 2022 American Chemical Society.

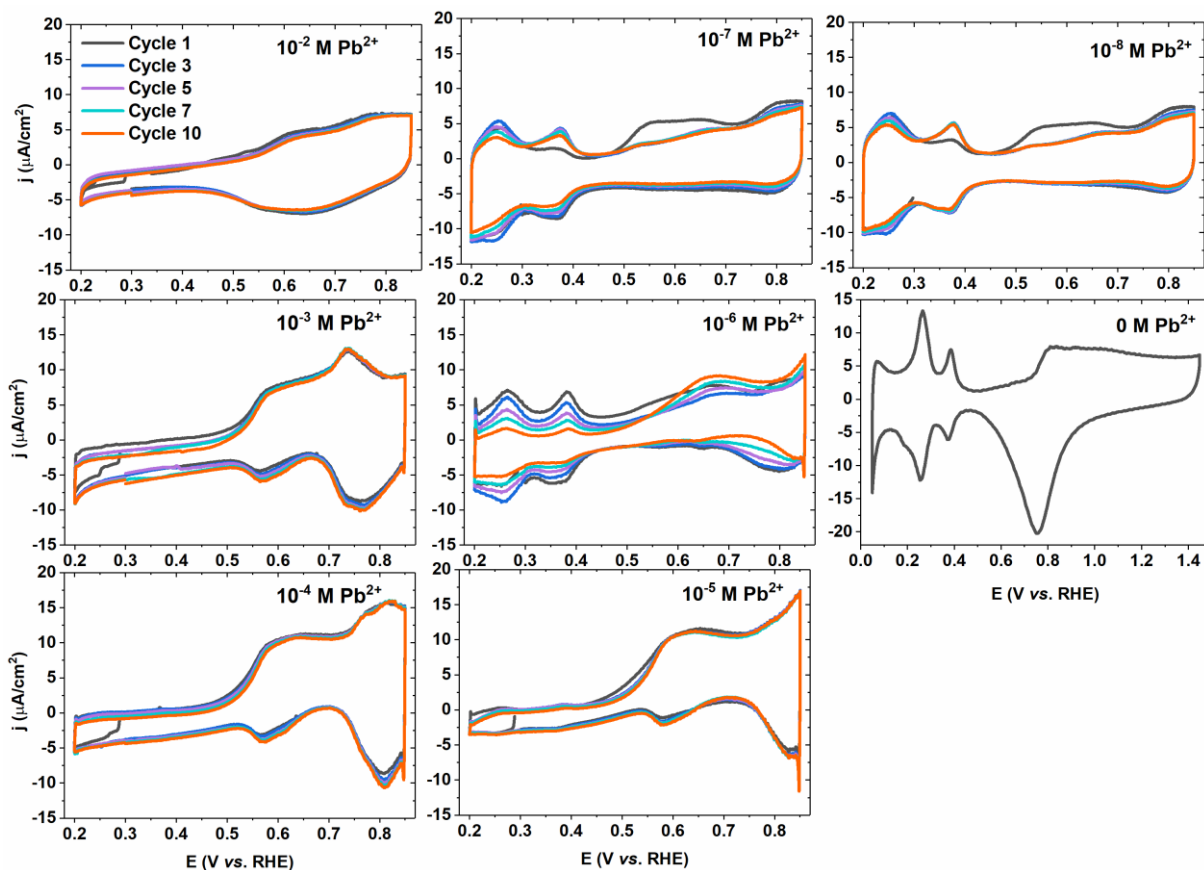


Figure 17: Cycling a Pt_p electrode in 0.1 M NaOH with varying concentrations of Pb^{2+} , with a sweep rate of 10 mV/s. Reprinted with permission from ref.[83]. Copyright 2022 American Chemical Society.

Lastly, Pt single crystals of the main crystallographic orientations, i. e. (111), (110), and (100), were used to oxidize glycerol, both clean and modified by Bi and Pb. Heterogeneous reactions are highly sensitive to the nanoscale and atomic-level structure of the catalyst, and in particular, the glycerol oxidation on Pt has a different response depending on whether a polycrystalline or single crystal electrode is used.⁹⁰ It is important to highlight that the presence of surface defects on single crystal electrodes can cause significant changes to the voltammetric profile of the reaction being studied, which has been shown for glycerol oxidation in acidic media.^{91,92}

Glycerol preferentially binds to the Pt surface by the hydroxyl group, in a nearly parallel orientation, and the adsorption strength on the basal planes follows the trend (110) > (100) > (111)⁹³, meaning that it strongly adsorbs on more open, less-packed terraces.⁹⁴ This same trend is observed on the E_{onset} of the oxidation reaction in alkaline media using Pt single crystals.^{84,85} In particular, the (111) terraces have both the highest E_{onset} and fastest deactivation with potential cycling. **Fig. 18** shows the

results of modifying Pt single crystals *in situ* with Bi and Pb adatoms at their optimal concentrations, and compares it with the response shown for the oxidation using the unmodified electrodes and also Pt_p.

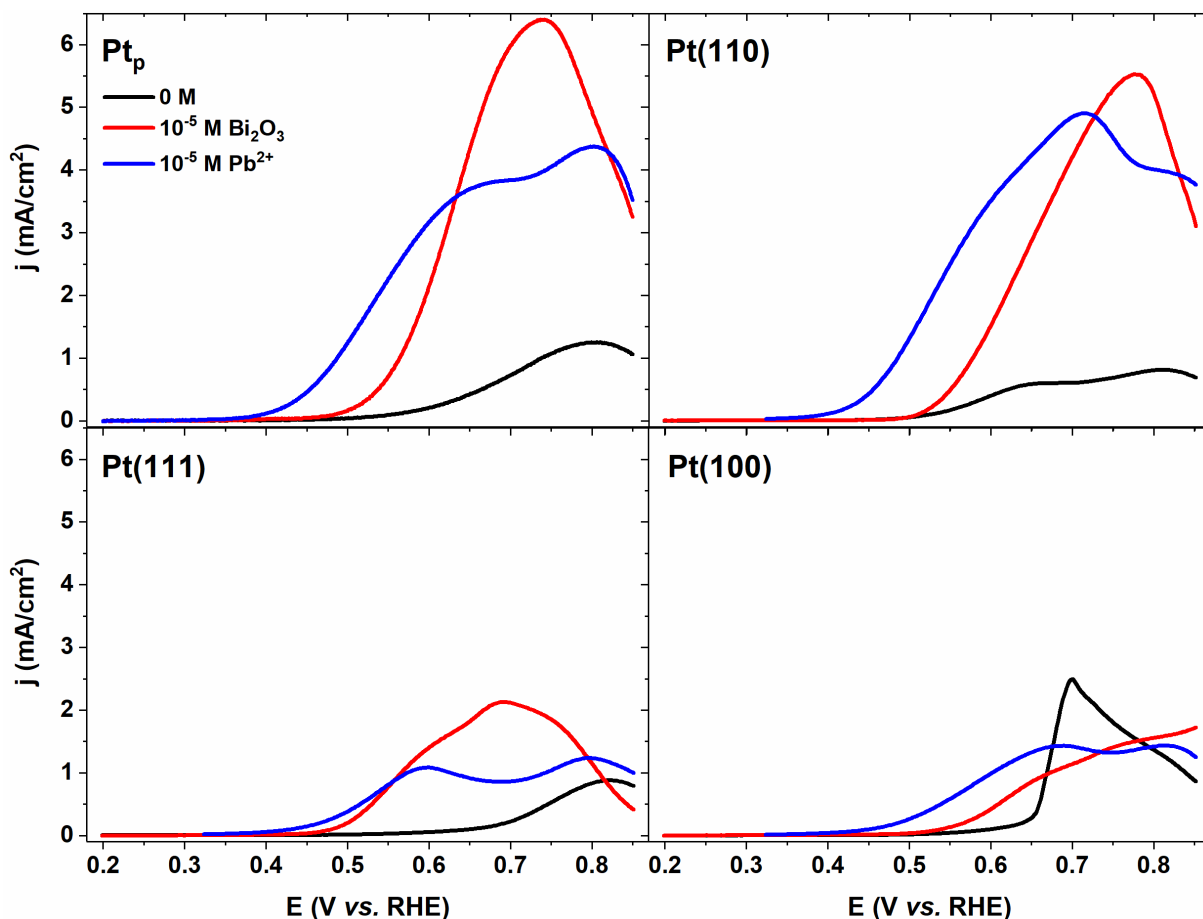


Figure 18: Comparing the 10th positive scan of the glycerol oxidation between Pt_p and Pt single crystals in 0.1 M NaOH + 0.1 M glycerol at a scan rate of 10 mV/s, before and after modification by Bi and Pb. Adapted from ref.[83].

After modification by adatoms, the E_{onset} decreased on all electrodes, and the trend of increasing onset remained at Pt(111) > Pt(100) > Pt(110). The highest current increase was obtained on Pt(110), and its voltammetric response after modification by either Pb or Bi resembles that obtained by Pt_p. The Pt(111) also showed an improvement in oxidation current, while Pt(100) had a lowering of j_{peak} , despite showing higher currents at $E < 0.70$ V.

Pt(110) is the basal plane with the lowest coordination, with a tendency to reorganize due to its high energy, and for this reason, they are often the most reactive sites towards electrochemical reactions, which is reflected in its low E_{onset} values, an

indirect measurement of a reaction activation barrier.⁹⁵ The fact that our modification by Bi and Pb decreased the E_{onset} on all basal planes indicates that their presence is lowering the energetic barrier necessary for the glycerol oxidation to start. Combined with the previous observation that they are hindering the adsorption and/or formation of poisoning intermediates, we now have evidence that at least two distinct mechanisms are contributing to the improvement of the catalyst activity.

2.4. Electrochemical modification by other elements

This section will show the results obtained by modifying platinum with the other seven elements of interest: Tl, Sb, Sn, Se, S, In, and Ge.

Since we have determined that the *in situ* modification offers better results (higher oxidation currents and less deactivation with potential cycling), the Pt electrodes used from now on will only be modified using this methodology. **Fig. 19** summarizes the findings obtained for all the various Pt-adatom systems shown at their optimal concentrations, with Pt-Bi and Pt-Pb included for comparison. Complementary to this, **fig. S1** compares the voltammetric profile of all concentrations for all Pt-Adatom systems. In most cases, there is an increase in activity with the ionic concentration in solution up to a certain point, after which the activity begins to decrease. The only exception was found in Pt-Ge, where it was observed that Pt was heavily deactivated by the presence of Ge^{4+} cations in solution at concentrations as low as 10^{-7} M. This complementary information can be found in the appendix section, **figs. S2 to S8**.

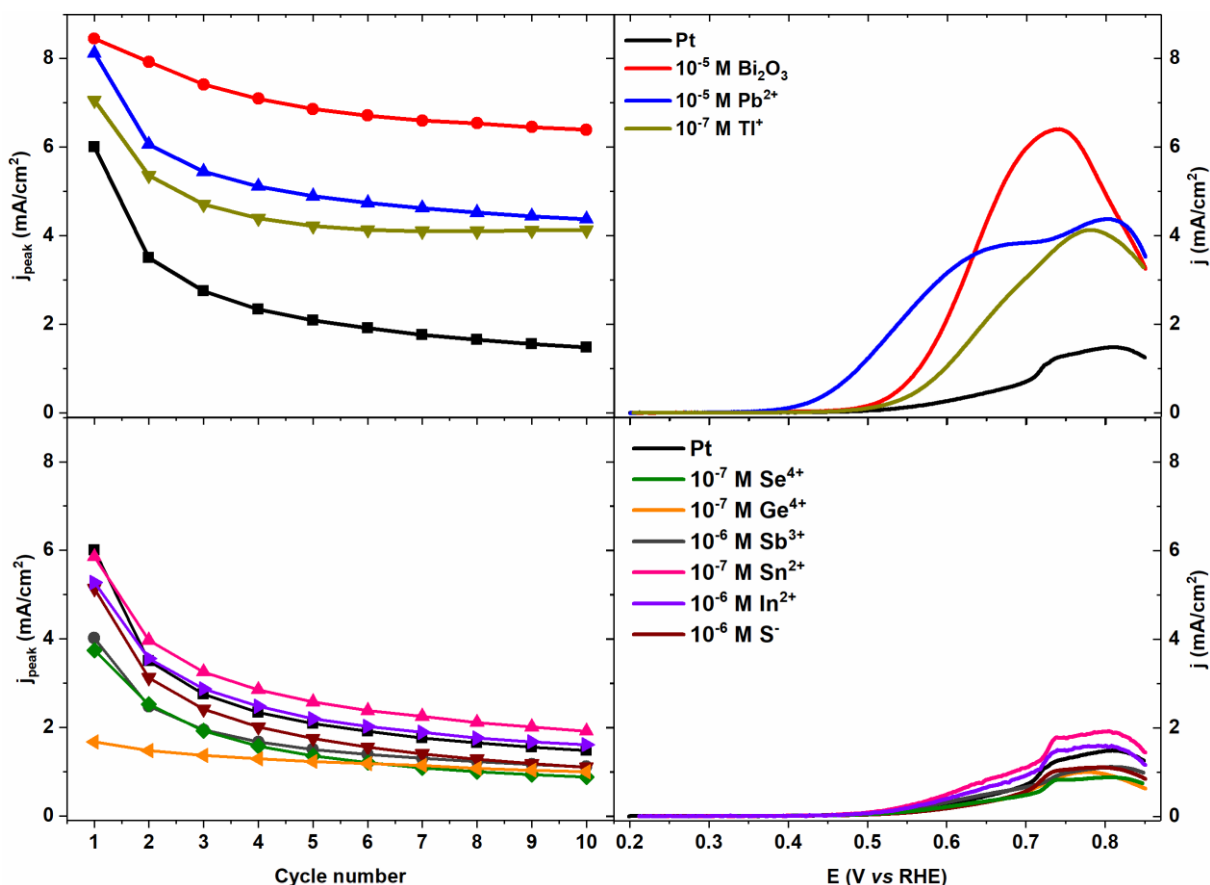


Figure 19: Comparing the j_{peak} evolution with cycle number (left) and the 10th positive scan for the various Pt-Adatom systems that were investigated, with the respective ion concentration indicated. Measurements executed in 0.1 M NaOH + 0.1 M glycerol at 10 mV/s. Using data adapted from refs.[82,83].

Of all elements that were studied, only three improved the electrode performance: Bi, Pb, and Tl. The others either barely impacted the electrode activity or deactivated it.

Starting the discussion, Pt-Sn slightly promotes the glycerol oxidation on platinum in acidic media^{58,96}, increasing the oxidation currents at $E < 0.6$ V. Our results in alkaline media are in line with these reports (**fig. S2**), and we observed only slight changes to the activity: a minor increase in current densities at $E < 0.7$ V and an increase in j_{peak} by roughly 0.5 mA/cm². Thus, we concluded that this element does not alter the activity of Pt in a significant way, and the slight improvement shown is likely coming from a third-body effect exerted by the Sn adatoms, where they are blocking the adsorption of poisonous species by occupying Pt sites.

The modification by indium does not change the electrode activity (**fig. S3**),

except for deactivation at 10^{-4} M In^{2+} . Similar to Pt-Sn, however, the In modification in acidic media slightly increases the Pt activity towards the oxidation reaction.⁵⁸ Little information was found on the use of this element as an electrocatalyst, with a single study⁹⁷ reporting the synthesis of Pd-In nanoparticles and its use in oxidizing alcohols (including glycerol) in alkaline media.

The deactivation shown by the Sb-modified electrodes was a surprising result. This system not only significantly improves the Pt activity towards glycerol oxidation in acidic media⁹⁸, but also changes the selectivity of the reaction, yielding dihydroxyacetone as the primary oxidation product instead of glyceraldehyde⁵⁸, the same result that was been observed for Pt-Bi on the same media, albeit with a higher E_{onset} .²² Pt-Sb is also known to improve the activity toward formic acid oxidation.^{99–101} Our results show deactivation of the electrode at concentrations as low as 10^{-8} M Sb^{3+} (**fig. S4**), and this is maintained as the ion concentration is progressively increased. To understand this discrepancy between the results in alkaline and acidic media, we investigated how the Sb ions interacted with the Pt electrode, similar to what was done to Pt-Bi and Pt-Pb in **figs. 16** and **17**, and the results are shown in **fig. 20**. As was expected, the electrode becomes progressively more covered by the Sb adatoms with increasing concentration (decrease in the H_{UPD} region), with the small redox peak located at 0.65 V at 10^{-8} M becoming a broad region centered on 0.60 V at 10^{-5} M, which matches the redox behavior shown by Sb.¹⁰² With this confirmation that Sb adatoms are showing a stable redox behavior, we hypothesize that the lowering of Pt activity is due to the growth of an inactive $\text{Sb}^{(0)}$ layer, which has been shown to grow on Pt(111) sites in the potential window used in our experiments.¹⁰³ As the Sb^{3+} increases, so does this inactive $\text{Sb}^{(0)}$ layer, resulting in the progressive deactivation of our electrode.

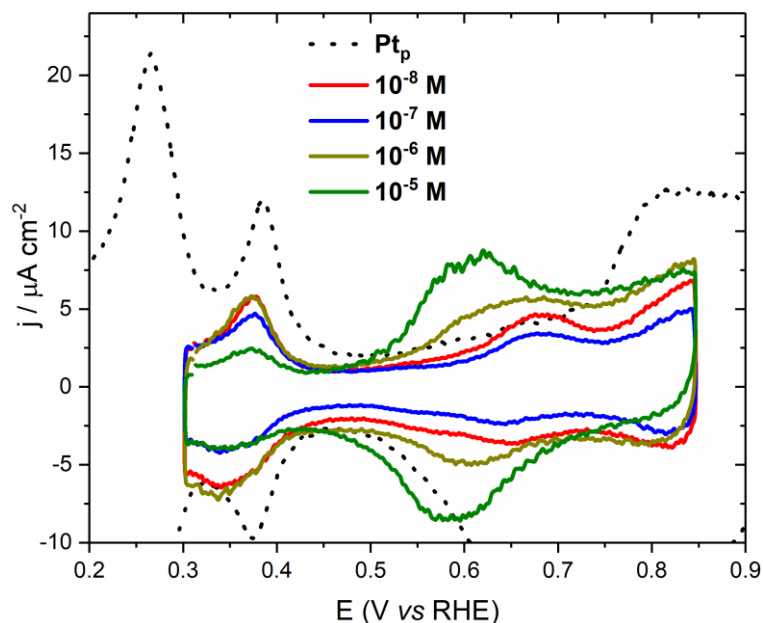


Figure 20: Deposition of Sb^{3+} ions on a Pt_p electrode in 0.1 M NaOH, with a scan rate of 10 mV/s. Shown here is the profile after 10 consecutive potential scans.

Selenium and sulfur are not commonly used to modify electrocatalysts, and previous literature reports have shown that they lower their activity towards the oxidation of several organic molecules.^{104–106} We have obtained similar results for Pt-S and Pt-Se in alkaline media (**figs. S5** and **S6**, respectively) for the glycerol oxidation, where they deactivated the Pt electrodes regardless of the ion concentration. We tentatively explain this by observing the electronegativity difference between these elements and the mechanism by which glycerol interacts with platinum.

Se and S are more electronegative than Pt, so in theory, they would retain a partial negative charge while adsorbed on Pt. Several studies based on both laboratory and computational experiments point out that both species retain a partial negative charge when adsorbed on platinum, thus it is safe to assume that these adatoms would make a negatively-charged adlayer on the catalyst surface.^{100,107–109} Glycerol interacts with the platinum surface through the hydroxyl groups close to the electrode surface^{86,93}, and, in highly alkaline media ($\text{pH} \geq 13$), glycerol undergoes deprotonation on the primary hydroxyl groups, generating the glycerolate ion, a very reactive intermediate with a negative charge, that is considered the primary reactive species for the glycerol oxidation in alkaline media.^{38,110} Therefore, the Se and S adatoms, with a partial negative charge, would exert a shielding effect on the platinum surface, by repelling both the glycerolate ion and glycerol as they approach the

electrode. This would decrease their adsorption rate on Pt sites, resulting in a decrease in electrode activity. This explanation is likely to explain, at least partially, the effect observed on Pt-S and Pt-Se.

Germanium modification significantly decreased the Pt activity, however, the Ge^{4+} concentration did not impact this effect: from 10^{-7} to 10^{-4} M Ge^{4+} , the Pt-Ge electrode showed the same voltammetric profile (**fig. S7**). These results indicate that, at a concentration as low as 10^{-7} M, the Pt surface is already saturated with Ge adatoms, which are hindering the activity by blocking Pt sites. We found no previous registry in the literature concerning Ge as an electrocatalyst for either oxidation or reduction reactions, except for its usage to quantify Pt(100) sites.⁷⁹

Lastly, the thallium modification improved the performance of Pt towards glycerol conversion (**fig. S8**) at low ion concentrations, between 10^{-9} and 10^{-7} M. This catalyst is known to promote the oxidation of formic acid, and results using Pt single crystals¹¹¹ show similar findings to what we observed for Pt-Bi and Pt-Pb in **fig. 18**, i.e., the lowering of E_{onset} and an increase in oxidation currents on the positive-going sweep.^{100,112,113} For these reasons, we hypothesize that Pt-Tl shows similar behavior to that of Pt-Bi and Pt-Pb. To further extend the investigation on the Pt-Tl system, we cycled the electrode in absence of glycerol (**fig. S9**), similar to what was done for Pt-Bi and Pt-Pb in **figs. 16** and **17**, respectively, and we observed that at the optimal Tl^+ concentration (10^{-7} M) the H_{UPD} zone could still be seen. At their respective optimal ion concentrations, Bi and Pb show a full adatom layer (i.e., $\theta = 1.0$ at $Q_{\text{Hydrogen UPD}} = 0$) on Pt. On the other hand, it is worth noticing that the system Pt-Tl never achieves full adatom coverage, even after increasing the Tl^+ concentration from 10^{-7} (optimal) to 10^{-6} M. In other words, there is no universal relationship between $\theta = 1.0$ and improving the electrode activity.

An attempt at explaining why some elements improve while others hinder the activity of Pt can be done with the aid of DFT calculation. Ferre-Vilaplana and co-workers¹⁰⁰ investigated the effect of adatoms on the electrochemical oxidation of formic acid on Pt(111) electrodes, and they found that the improvement in activity obtained through electrochemical experiments is observed when an adatom with a partial positive charge was adsorbed on the electrode surface, as the formate ions chemisorbed on these adatoms and underwent C-H cleavage after interacting with the negatively-charged Pt(111) surface, forming CO_2 as the main product. They found that Bi, Pb, Sb, Te, and As had such a partial positive charge when adsorbed to Pt(111)

and improved its activity, while the opposite was true for Se and S. Our results were different in the case of Pt-Sb; however, this does not mean that they contradict the findings of Ferre-Vilaplana et. al.¹⁰⁰, as our experiments were performed in different electrolytes, a different molecule was oxidized and also different electrode surfaces. Additionally, based on electronegativity differences alone, it is expected that In, Sn, and Tl would hold a positive charge when adsorbed on Pt, and only one of these species improved its activity.

An interesting observation can be made when comparing the cycling of Pt_p in the absence and presence of p-block ions in solution (**fig. 21**). Out of all systems shown here, only Bi and Tl achieve $\theta = 1.0$ after 10 potential cycles. The modification by Bi, Pb, Tl, and Sb shows a broad oxidation region before the oxidation of Pt begins at 0.70 V. While some studies suggest explanations for the nature of these peaks^{59,62,77,102}, there is no solid consensus and, on top of that, there is virtually no investigation towards such interactions in alkaline media. Therefore, it is unclear whether this earlier oxidation is due to oxidation of the adatoms alone, from their metallic to an oxidized state, or if their presence is anticipating the oxidation of Pt adatoms as well.

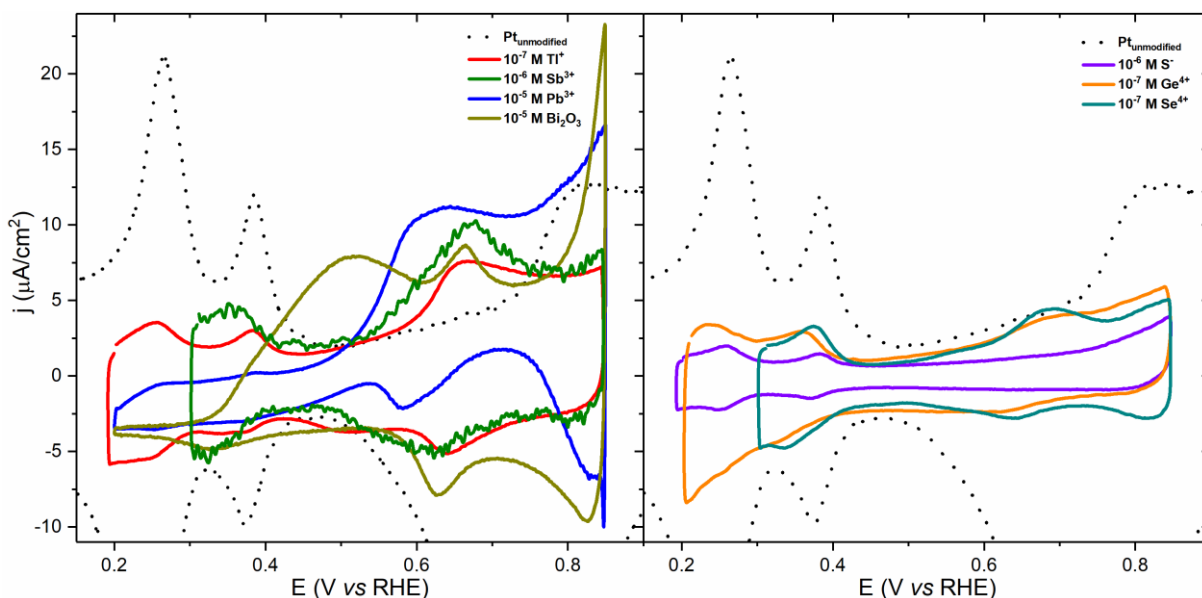


Figure 21: Pt_p electrode after 10 cycles in 0.1 M NaOH in the presence of various ions in solution, at their optimal concentrations. Using data adapted from refs.[82,83].

Another possibility is that any adatom should improve the activity of Pt at low enough coverages through a third-body effect.^{63,101,114,115} Herrero and co-workers⁶³, when studying the formic acid oxidation on Pt(111) modified by Bi and As,

proposed that the adatoms disturb the work function of surface Pt atoms, affecting a distance of seven Pt atoms from the adatom in the case of Bi. In another study¹⁰¹, Sb coverages of as low as 0.03 were enough to completely suppress CO adsorption on Pt(111) electrodes, so our addition of Sb^{3+} to the solution was a considerable excess. A similar observation was also made for Pt-Se, where low amounts of Se adatoms were found to decrease CO adsorption, mainly associated with the disappearance of multi-bonded CO and favoring the formation of linear CO.^{114,115}

3. Spectroscopy applied to electrochemical systems

This chapter describes how spectroscopy techniques were used to perform *in situ* analysis of the electrochemical systems described in the previous chapters. With the aid of spectroscopy and other analytical chemistry techniques (like HPLC analysis), it is possible to elucidate reaction intermediates and products.

3.1. Spectroscopy applied to electrochemical research

Spectroscopy studies the electromagnetic spectra resulting from the interaction between matter (the sample being analyzed) and incident radiation. The spectral acquisition is performed with the aid of a detector, which converts the resulting radiation into either an electric current (photodiode detectors) or stores it as electric charge (charge-couple detectors). There are multiple modes in which this resulting radiation can be interpreted, and they can be roughly divided into i) analyzing the radiation passing through a sample (transmittance or scattering); ii) how much energy the sample absorbed (absorbance); iii) how much of the incident radiation was reflected (reflectance) by the sample, and iv) how much energy is emitted from a decay process (fluorescence) in the sample.

Infrared (IR), along with Raman spectroscopy, are called vibrational spectroscopies, as they study molecular vibrations due to absorption of light/photons. In IR spectroscopy, when the absorbed light matches the vibrational frequency of a chemical bond and it causes a change to the dipole moment of a molecule, an infrared active molecular vibration happens. IR spectroscopy can only detect vibrations caused by changes to the dipole moment, and absorption is measured as a function of frequency.

Concerning electrocatalysis, which studies the reactions occurring on an electrified solid-liquid interface, the most important form of spectroscopy is the Fourier-transform infrared spectroscopy (FTIR). In this technique, the spectra are associated with the potential applied to the WE, and it detects the resulting radiation in either the reflectance or absorbance mode. One of its main purposes in electrochemistry is to study reactions under *in situ* conditions and to understand what is happening at the electrode-electrolyte interface. There are multiple ways to perform the FTIR experiment¹¹⁶, and with the proper experimental setup, it is also viable for time-

resolved studies¹¹⁷ in which one can study fast interface processes, such as reaction kinetics and the dynamics of the electrical double layer.

In Raman spectroscopy, a sample is illuminated by a laser in the UV-visible region, and the frequency of the scattered light is studied. The elastic scattering, with no changes to the frequency, is called Rayleigh scattering. Inelastic scattering, caused by a change to the frequency of the incident beam, is called Raman scattering. This is caused by incident photons being captured by a molecule, where it can either gain or give up energy through changes to its molecular vibrations, before emission as scattered light. Thus, Raman spectroscopy measures vibrational frequencies as a shift from the incident beam frequency.¹¹⁸ This technique is often used in conjunction with FTIR, as it offers the possibility of studying reaction mechanisms that would be otherwise invisible in the IR spectra.^{119,120}

The last type of spectroscopy applied in this work was X-Ray Absorption (XAS). In this technique, the sample is bombarded with x-rays and, after a portion of this incident energy is absorbed, excitation or ejection of a core electron happens. The quantification of this absorbance can be done by measuring the transmitted x-rays, the fluorescence emitted by the excited atom, or measuring the ejected electrons (Auger electrons), and the spectra are registered by shifting the incident beam energy.¹²¹ This technique deals with electronic transitions within an atom, meaning that the x-ray energy can be selectively tuned to excite an individual element within an alloy or composites of various natures.

An XAS spectrum (**figure 22**) is divided into two regions. When the incident energy is increased at a certain point, a sharp increase in absorption is registered, at this point, the incident photons have sufficient energy to excite the electrons of the sample. This jump in absorption is called the x-ray absorption near edge structure (XANES), and the peak is called an absorption edge or white line. The intensity of this absorption peak is sensitive to the oxidation state of the element, as the energy of a core electron is affected by changes in the electronic distribution of the valence orbital (i.e., the energy of the core electron changes because the shielding effect exerted by other electrons is being changed). This means that studying this region allows probing of the oxidation state of the sample, even under electrochemical conditions^{122–124}, providing further information as to how an electrocatalyst changes during operation, which is particularly useful when designing materials for electrochemical devices. The second region is the extended x-ray absorption fine structure (EXAFS), and it refers to

oscillations in the absorption beginning at approximately 50 eV above an absorption edge.¹²⁵ This signal is caused by the backscattering of an exiting photoelectron, produced through absorption, on neighboring atoms, and it is used to study changes to the local atomic structure of a sample.

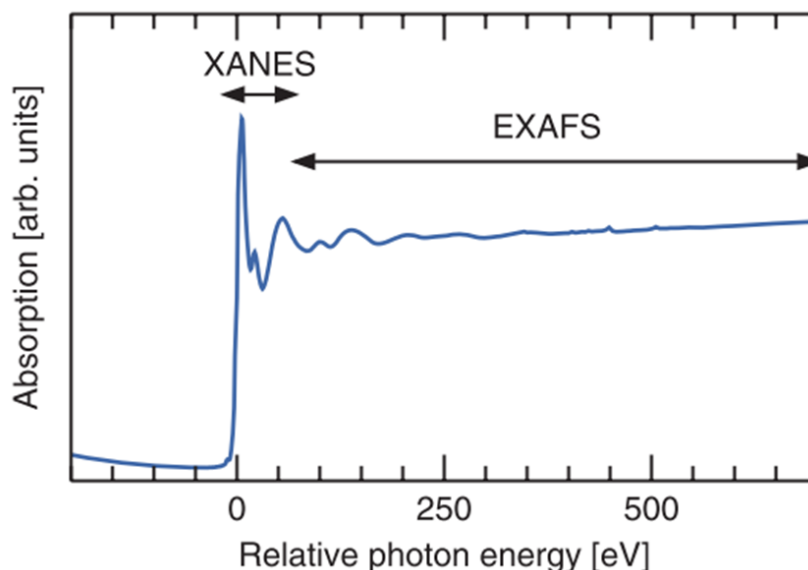


Figure 22: Example of an XAS spectrum around a certain absorption edge, highlighting the XANES and EXAFS regions. Adapted from ref. [125].

3.2. Experimental setup for *in situ* Fourier Transform Infrared Spectroscopy

The *in situ* FTIR experiments were performed in the external reflectance configuration. The incident IR radiation propagates through an IR-transparent window into the electrochemical cell, hitting the electrode, and the reflected beam passes through the same window into a detector. To minimize radiation loss caused by water absorption, the WE is pressed against the IR window, creating a thin electrolyte film.¹²⁶ The spectroelectrochemical (SEC) cell used and this experimental setup is shown in **fig. 23**. The working electrode used was a polycrystalline platinum disk (Pt_{disk}), and the electrodes and the cell were cleaned as described in **section 2.2 of chapter 2**.

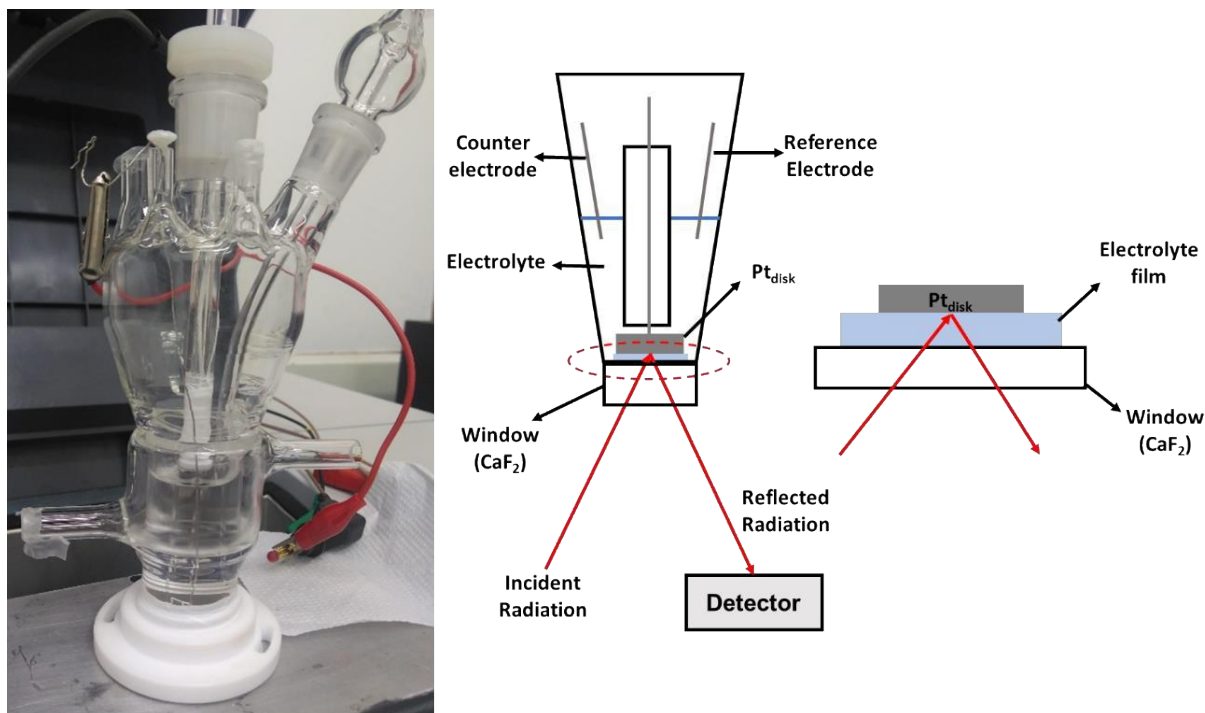


Figure 23: SEC cell used for the *in situ* FTIR measurements, alongside with a schematic of the experiment itself.

Both a window and prism were used, with the latter providing better results by minimizing energy losses due to reflection at either entry or exit points.¹²⁷ The IR-transparent material of choice was CaF_2 for multiple reasons: it has a refractive index close to that of water ($n_{\text{CaF}_2} = 1.4$ vs. $n_{\text{H}_2\text{O}} = 1.33$), it is IR-transparent (i.e., 100% transmittance) from 5000 to 1000 cm^{-1} and it is chemically resistant to most acids and alkalis.

The cell is placed on top of a specular reflection accessory (Veemax II, Pike Technologies), and the spectrometer used was a Shimadzu IR Prestige-21 equipped with an MCT detector. All spectra were recorded as an average of 164 interferograms with a 4 cm^{-1} resolution. The spectra are plotted in absorbance units (a.u.) as $-\log(R/R_0)$, where R is the reflectivity of the sample and R_0 the reflectivity at the reference potential, which was 0.2 V (vs RHE). Before beginning the spectral collection, the electrode is subjected to 9 potential cycles between $0.20 - 0.85\text{ V}$ at 10 mV/s , by forming a meniscus with the electrolyte. This step is done to reach a point where the WE is more stable, i.e., its anodic currents are not changing drastically between each potential cycle (see **figs. 14** and **15** in **chapter 2**). After this step, the WE is polarized at 0.20 V and pressed against the CaF_2 window, and both the mirror

and electrode positions are adjusted to generate a high enough signal on the MCT detector. After a high intensity is achieved, background spectra are taken at this potential, and then a linear potential sweep at 1 mV/s begins simultaneously with the continuous spectral collection.

We performed the experiments using both H₂O and D₂O. Measurements in water were conducted first, to observe initial changes between spectra acquired on Pt_p and the Pt-Adatom electrodes. In the following, we used D₂O instead of water to prepare the solutions because the main stretching mode of water (1600 cm⁻¹) falls in the same region as the various oxidation products from glycerol, obstructing their signal.¹²⁸ Band assignment was done by taking the spectra of several possible oxidation products in alkaline media, shown in **fig. S10**, using the attenuated total reflectance configuration, as well as from data obtained in previous group publications.^{129,130}

The chemicals used in this step, without previous purification, were: deuterium oxide (99.9% atom% D, Sigma-Aldrich), Dihydroxyacetone (Pharmaceutical Secondary Standard, Sigma-Aldrich), D-glyceric acid calcium salt (99%, Sigma-Aldrich), DL-glyceraldehyde (≥90% GC, Sigma-Aldrich), glycolic acid (99% Reagent Plus, Sigma-Aldrich), sodium mesoxalate monohydrate (≥98.0% RT, Sigma-Aldrich), glyoxylic acid monohydrate (98%, Sigma-Aldrich), tartronic acid (97%, Sigma-Aldrich), oxalic acid (99.999%, anhydrous, Sigma-Aldrich), formic acid (≥95% P.A. ACS, Sigma-Aldrich), sodium β-hydroxypyruvate hydrate (≥97%, Sigma-Aldrich), and lactate (≥95% natural).

3.3. *In situ* FTIR results

In the previous chapter, we determined that only Pt modified by Bi, Pb, and Tl showed an improvement in the electrode activity (anodic current) and stability (slower decrease of anodic current with potential cycling). Therefore, FTIR investigation was done only on those systems (in addition to the clean Pt electrode), and the collected spectra are shown in **figures 24** and **25** with the main bands highlighted, while the corresponding band assignment is shown in **figure 26**.

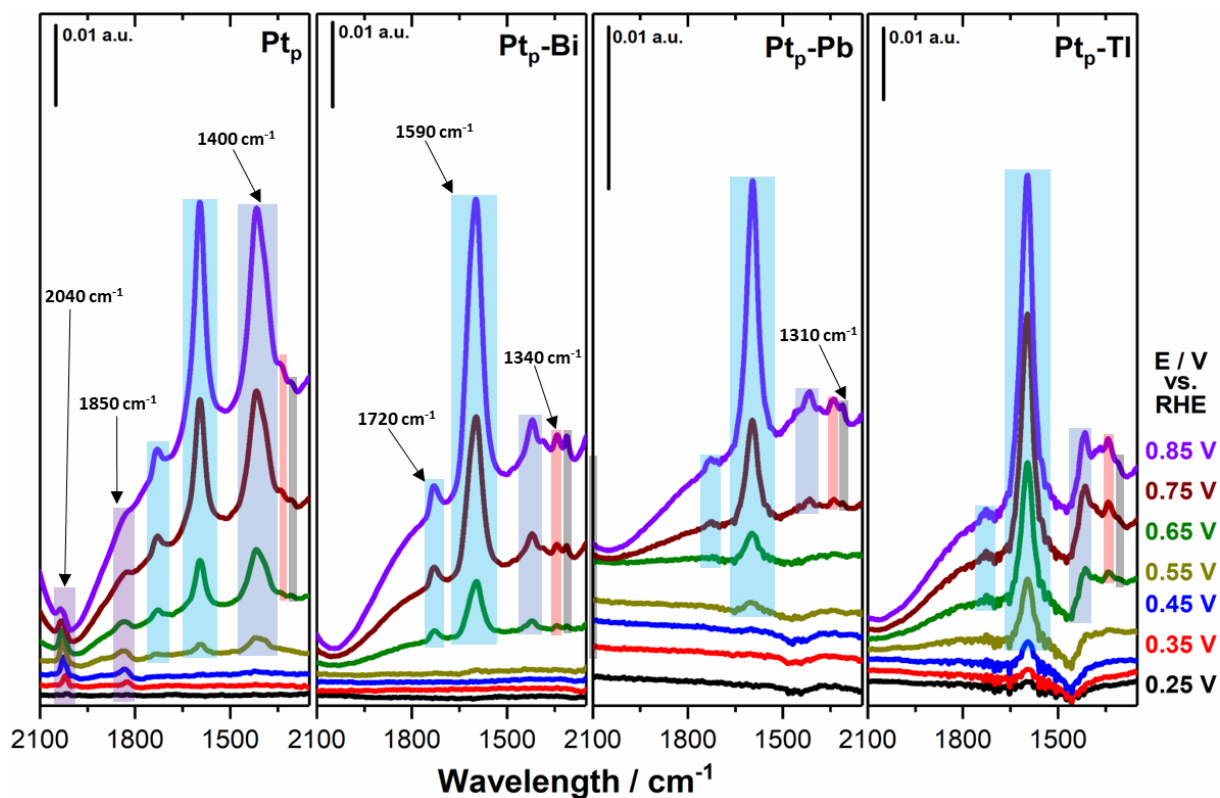


Figure 24: *in situ* FTIR spectra collected in 0.1 M NaOH + 0.1 M glycerol registered during positive-going scan at 1 mV/s. Spectra registered for clean platinum (Pt_p), Pt-Bi (+ 10^{-5} M Bi_2O_3), Pt-Pb (+ 10^{-5} M Pb^{2+}) and Tl⁺ (+ 10^{-7} M Tl^+). Using data adapted from refs.[82,83].

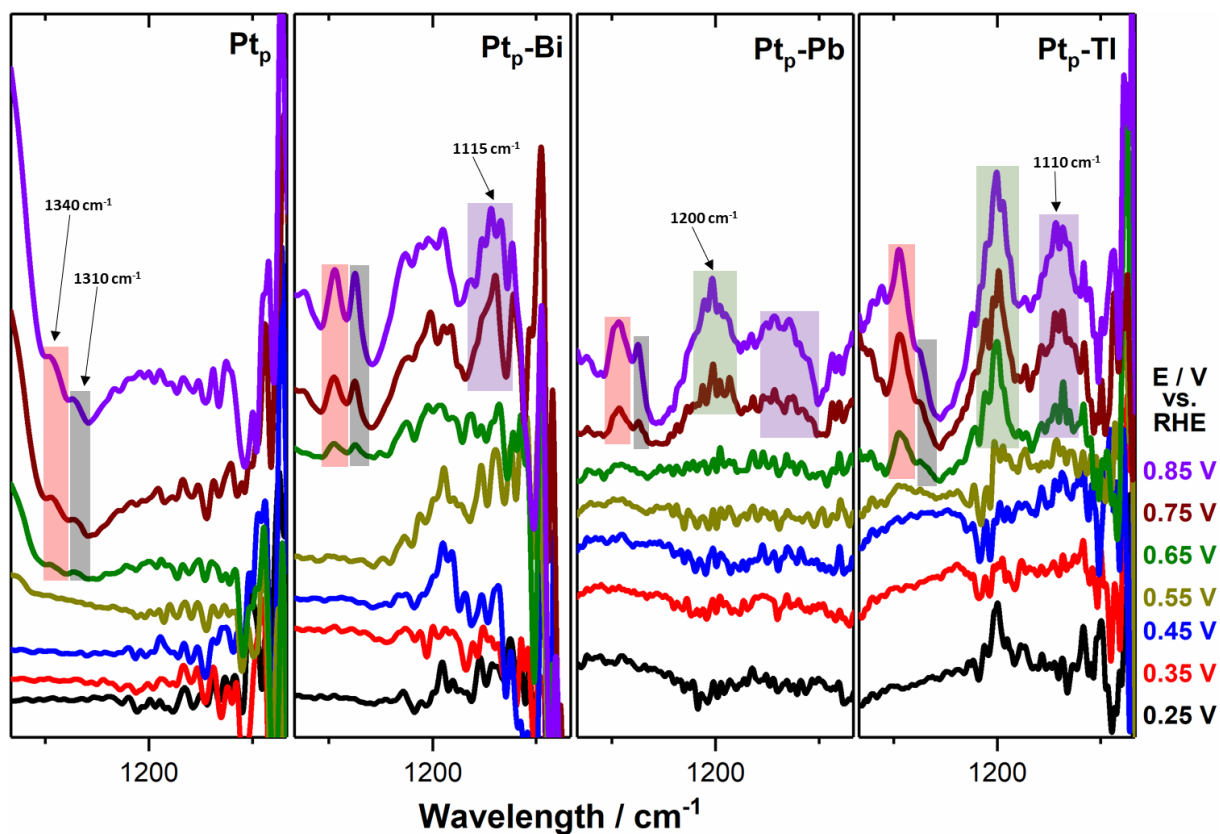


Figure 25: Zoomed-in spectra shown in **figure 24**, between 1400 and 1000 cm⁻¹. Using data adapted from refs.[82,83].

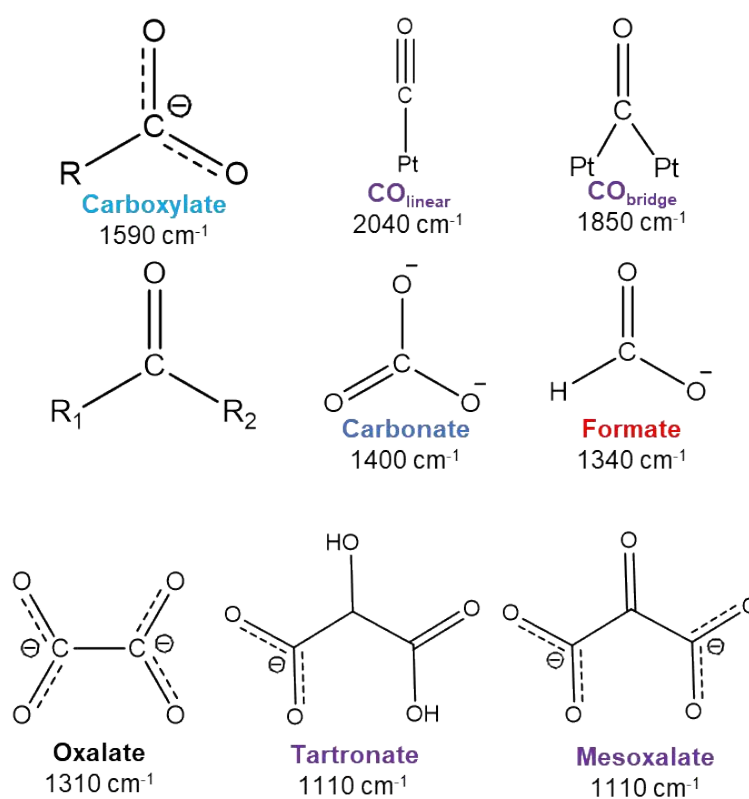


Figure 26: Corresponding band assignment to the *in situ* FTIR spectra shown in **figure 24**. Band assignment was done based on refs.[82,83,129,130].

Since the spectra shown in **fig. 24** are recorded only on the 10th positive-going scan, it is expected to find vibrations attributed to species adsorbed on platinum at potentials as low as 0.25 V, where no anodic processes are expected to happen (see **fig. 19** in **chapter 2**). The spectra for the clean platinum electrode show that two bands, 2040 and 1850 cm⁻¹, are present since the beginning of the spectral collection, and they are associated with linear (CO_{linear}) and bridge (CO_{bridge}) bonded carbon monoxide on the Pt surface. CO is an intermediate species formed during the electrochemical oxidation of various organics^{111,131–134} on platinum electrodes and, in the case of glycerol conversion, it is formed in all pH range.^{57,135} This species is highly poisonous to platinum-based catalysts due to its strong adsorption energy¹³⁶, and, when we compare the spectra obtained for Pt and Pt-Adatoms, these bands are absent from their spectra, findings that are in line with what has been observed for these catalysts in acidic media.^{22,111} In other words, the adatoms on the Pt surface have blocked the formation of CO_{ads}, which partially explains the improvement in catalytic activity, as there is less poison accumulation happening on the electrode surface.

Other alternative explanations for the absence of CO_{ads} bands, that we cannot confirm or discard at the moment, is that: i) CO_{ads} is being formed on the Pt-Adatom surface, however, the adatoms have decreased the adsorption strength of this species to the point where this species is readily desorbed from the Pt surface during the anodic scan, and ii) the reaction pathways that lead to CO formation are being blocked. The first hypothesis can only be ascertained with the aid of time-resolved FTIR, which we did not have access to during the development of this work. The second hypothesis would require both time-resolved spectroscopies¹¹⁷ and DFT calculations to be completely elucidated.

Continuing the spectral investigation, we see a pair of bands at 1720 and 1590 cm⁻¹. The first band corresponds to the carbonyl stretching mode in acidic media²², and does not correlate with the spectra that we registered for the products (**fig. S10**). The second band at 1590 cm⁻¹ is assigned to the stretching of carboxylate and carbonyl groups and, except for glyceraldehyde and carbonate, all oxidation products show a vibrational mode in this region, so no definitive conclusions may be traced from this.

The next band is at 1400 cm⁻¹ and it is associated with carbonate ions. This species comes from the CO₂ generated during the total oxidation of glycerol, which, in

alkaline media, combines with hydroxyl ions to generate carbonate.¹³⁷ In the spectra for clean Pt, the bands 1590 and 1400 cm^{-1} have similar intensity, however, the carbonate band is significantly reduced after adatom deposition. This means that the presence of adatoms is hindering the cleavage of C-C bonds during the oxidation reaction, so it is expected that a higher amount of soluble (non-gaseous) products are being formed on these electrodes.

The last set of bands is the 1340 and 1310 cm^{-1} pair. Oxalate has a sharp peak at 1310 cm^{-1} and it is the only species with a band in this region, according to **fig. S10**, so we attribute this band to this species, while the feature at 1340 cm^{-1} is shared by mesoxalate, tartronate, and formate. Out of those three species, formate is the most likely candidate, as it is formed when a C-C bond is broken during the reaction pathway. Lastly, without CO_{ads} being formed on the Pt-Adatom catalysts, the only possible way for the carbonate band to be seen on those electrodes is via formic acid oxidation to CO_2 , which combines with OH^- into CO_3^{2-} .

Zooming into lower wavenumbers, from 1400 and 1000 cm^{-1} in **fig. 25**, we see a high degree of noise on the spectra, especially on Pt_p and Pt-Bi. Bands in this region are not very defined and difficult to elucidate, however, we see hints of two bands at 1200 and 1110 cm^{-1} being formed at high potentials on the Pt-Adatom systems, however, the 1200 cm^{-1} band is absent from Pt-Bi. No oxidation products show bands at 1200 cm^{-1} , while the 1110 cm^{-1} is a feature shared by both tartronate and mesoxalate.

To summarize, from the *in situ* FTIR experiments, we have evidence that the presence of adatoms on the Pt surface has two main effects: i) blocking the formation of CO_{ads} and ii) hindering the C-C bond breaking. Due to significant overlapping between the bands of the various oxidation products, identification is not precise, however, the spectra point that oxalate, formate, and carbonate are being generated. Any further product identification (and quantification) requires liquid chromatography, which will be discussed in **chapter 4**.

3.4. Experimental setup for *in situ* X-Ray Absorption Spectroscopy

The *in situ* XAS measurements were done using an SEC cell designed by our group, shown in **figure 27**, in collaboration with researchers from the Sirius Synchrotron Facility.¹³⁸ The experimental setup follows the same general scheme

shown in **figure 23**, where incident radiation (X-Ray) is reflected on the WE surface and collected at a detector, however, the differences have to be highlighted. These experiments were conducted at the Carnaúba beamline, which has a beam size of 200 x 500 nm and an energy range between 2.05 – 15 keV. Measurements were taken at the platinum L₃ edge (11564 eV).

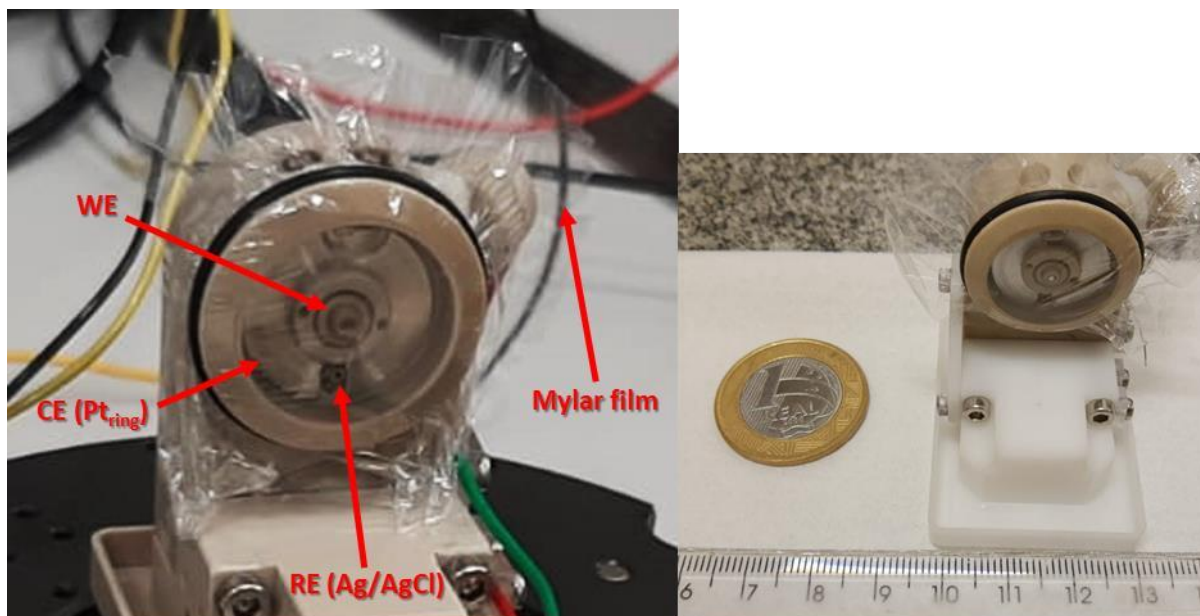


Figure 27: SEC cell used during the *in situ* XAS measurements, highlighting the position of each electrode and the Mylar[®] film used to seal it.

The cell is made of polyether-ether-ketone (PEEK), a material that is resistant to thermal degradation and attacks from both highly acidic and alkaline solutions, cleaned in the same way as a conventional electrochemical cell. The RE is a leak-free Ag/AgCl microelectrode, however, all potentials displayed will be with respect to the RHE scale. The CE is a polycrystalline platinum ring, and the WE is a glassy carbon (GC) electrode with a 1 mm diameter, on top of which nanoparticles are deposited. Before being used, however, the GC electrode has to be cleaned. This is done by manual polishing, where an alumina slurry (0.05 micrometer) to a polishing pad, and doing a figure-eight motion while slightly pressuring the electrode towards the pad, for a few minutes. Afterward, the GC is cleaned with ultrapure water and isopropanol, then dried using a lens cleansing paper tissue. The entire cell is sealed using a Mylar[®] film, a plastic film of biaxially-oriented polyethylene terephthalate (BoPET), a material transparent to X-Rays, held into place by an O-ring. The film must be smoothed before the experiments, otherwise, the wrinkles cause a decrease in the

intensity of the incident X-Rays.

Once the GC electrode is cleaned, we deposit 2 μL of a suspension of spherical platinum nanoparticles ($\text{Pt}_{\text{sphere}}$) on it, and it is then dried in an oven at 60 $^{\circ}\text{C}$. The nanoparticles were synthesized using an adaptation of the colloidal method.¹³⁹ To a round-bottomed flask, we added 100 mL of ultrapure water, 500 μL of sodium polyacrylate (Sigma-Aldrich), and 100 μL of a 0.1 M H_2PtCl_6 solution (from chloroplatinic acid hydrate, $\geq 99.9\%$ trace metal basis, Sigma-Aldrich). After Argon bubbling for 20 min to remove air from the recipient, Pt ions were reduced by bubbling H_2 gas for 5 min, afterward, the flask was sealed and left to stand for one day. On the next day, two pellets of NaOH (semiconductor grade, 99.99% trace metal basis, Sigma-Aldrich) were added to the flask to induce precipitation of the nanoparticles. Once fully precipitated (i.e., the overhead solution was crystal clear), the nanoparticles were washed with ultrapure water 4 times, to remove any remaining reactants.

Quality assurance of said nanoparticles was done using cyclic voltammetry, as Pt nanoparticles with controlled shapes have a specific voltammogram on commonly used supporting electrolytes.^{73,139,140} This was done using CO stripping, a technique in which all organic surfactants are displaced from the Pt surface by forcing the formation of CO_{ads} via polarization at a low enough potential, followed by an anodic sweep to a potential high enough to oxidize this CO layer to CO_2 . The result of such an experiment on our $\text{Pt}_{\text{sphere}}$ particles is shown in **figure 28**. After cleaning a 5 mm GC electrode we deposited 30 μL of the $\text{Pt}_{\text{sphere}}$ slurry and dried it in an oven at 60 $^{\circ}\text{C}$. To perform CO stripping, the GC electrode was polarized at 0.1 V and then pure carbon monoxide was bubbled into the solution for 5 min, to completely cover the Pt surface with CO_{ads} . In the following, pure N_2 was bubbled for 15 min to remove any CO dissolved into the electrolyte. Lastly, the bubbling ceased and the potential sweep began at 20 mV/s, with 0.9 V as the upper vertex potential. From the 2nd cycle onwards, we can observe the H_{UPD} region on the nanoparticles, with its two redox peaks at circa 0.25 and 0.35 V, confirming that we have successfully synthesized spherical Pt nanoparticles.

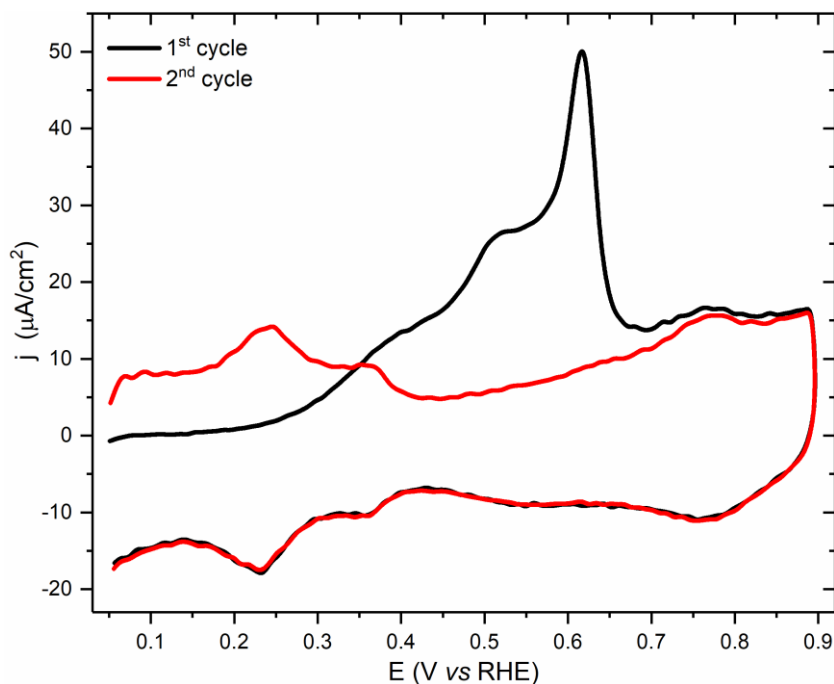


Figure 28: CO stripping experiment in 0.1 M NaOH, at 20 mV/s, to test the quality of the synthesized $\text{Pt}_{\text{sphere}}$ nanoparticles.

Due to the small size of the GC electrode and SEC cell, it is not feasible to perform CO stripping on this cell, because either CO or N_2 bubbling would either rip the Mylar film or cause the cell to leak. Therefore, we had to bubble N_2 on the electrolyte solutions before adding them to the cell (which has a capacity of less than 2 mL), and without executing the CO stripping on the $\text{Pt}_{\text{sphere}}$ deposited on the small GC electrode.

3.5. *In situ* XAS results

Besides executing the measurements for clean Pt, five adatoms were chosen: Pb, Bi, S, Se, and Ge. They were chosen because Pb and Bi retain a partial positive charge when adsorbed to platinum and S and Se have a negative partial charge¹⁰⁷, while Ge is expected to have an almost neutral charge, due to its electronegativity being close to that of platinum.

The primary goal of these objects is to examine the XANES region of the Pt L_3 edge, as the intensity of this absorption edge (also called a white line) depends on the oxidation state of platinum.¹²²

Before spectral collection, the particles were imaged via fluorescence.

Figures S11 and **S12** show the dispersion of $\text{Pt}_{\text{sphere}}$ on top of the GC electrode,

illustrating that while the deposition was successful, there is a very low number of nanoparticles on the electrode surface, owing to either a very dilute colloidal suspension. One of the main issues throughout these experiments was the fact that some of the particles were shifting their position during polarization, causing noise to the spectra acquired. **Figure S13** shows the same cluster as in **figs. S11** and **S12** after spectral acquisition at +1.20 V (*vs* RHE), and its position moved away significantly from the beam center. We believe that this shift in their position was caused mainly by their low fixation on the GC electrode. During the beamline experiments, the nanoparticles were air-dried in a neighboring room in between measurements, instead of inside an oven at 60°C, and due to this they were not sufficiently adhered to the GC surface. To circumvent this issue, we took images of the electrode in between the XANES spectra (without polarization and at either 0.30 or 1.20 V), and changed the beamline position to recentralize the X-Ray beam on the moving cluster.

The *in situ* XAS spectra for the various Pt systems are shown in **figure 29**, where we compare the spectra taken at +0.30 and +1.20 V. While we were able to successfully perform these experiments in our SEC cell, we observed no changes to the intensity of the Pt L₃ white line with either the applied potential or with adatoms present on the Pt surface.

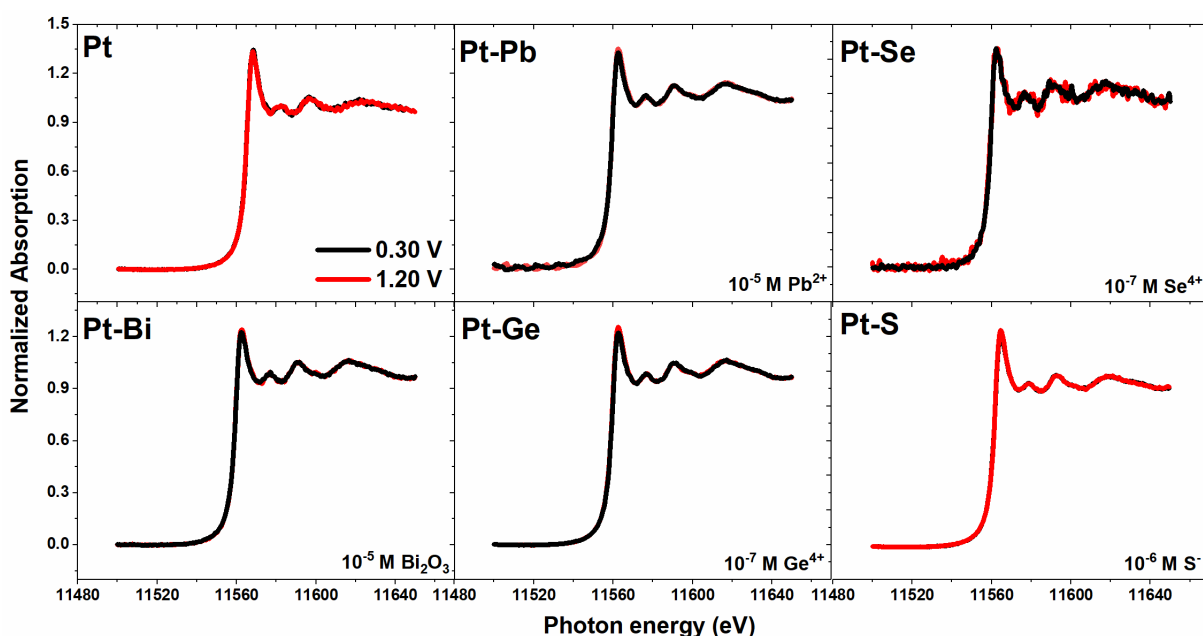


Figure 29: Normalized *in situ* XAS spectra of the various Pt-Adatom systems at the Pt L₃ edge, polarized at two distinct potentials. The base electrolyte was 0.1 M NaOH, with the addition of p-block ions as pointed out in the figure.

To explain these findings, we have to bear in mind that electrochemical techniques, including the *in situ* FTIR, are essentially probing the surface of the material, while X-Rays have a certain penetration depth to them. This means that the X-Rays were penetrating the bulk of the Pt_{sphere} particles instead of only analyzing their surface alone and, since only their (relatively small) surface is being oxidized, the majority of the signal corresponds to metallic Pt⁽⁰⁾ instead of its oxides.

To properly analyze the Pt surface with XAS we would need to use soft (low energy) X-Rays¹⁴¹ with low penetration, instead of the hard (high energy) X-Ray beam that is available at the Carnaúba beamline. Another surface technique that could, in principle, be used to study the oxidation state of Pt is near-ambient pressure X-Ray photoelectron spectroscopy¹⁴², which consists of using X-Ray photoelectron spectroscopy (XPS) under electrochemical conditions.

We have previously used *ex situ* XPS⁸² to investigate if Bi adatoms were in their metallic or oxidized state when deposited on the Pt surface, as seen in **fig. 30**. These results were obtained after cycling the Pt_p electrode in a NaOH + Bi₂O₃ solution, removed from the electrochemical cell and transferred to the XPS chamber, where we only saw the signal corresponding to Bi³⁺. However, exposure to air during this transfer is enough to oxidize metallic bismuth to bismuth oxide. To properly analyze the Bi adatoms the Pt-Bi electrode would need to be transferred to the XPS chamber under vacuum, which was successfully done by Shi-Gang sun and co-workers¹⁰⁸, and they verified that at transfer potentials below 0.91 V (*vs* RHE) the XPS spectra of Bi is made by two-thirds of atomic bismuth and one-third on its oxidized state, so it would be safe to assume that, in our experimental conditions, we should have a mixture of metallic and oxidized bismuth. The main goal of *in situ* XAS was to extend this investigation of the Pt-Bi system in acidic media (their experiment was done in 0.1 M HClO₄, while ours is in 0.1 M NaOH) to alkaline media, as well as other Pt-adatom systems. Previous studies have indicated that adatoms with a partial charge will affect the local electronic structure of its Pt substrate^{100,107}, and it was our objective to obtain direct evidence of it.

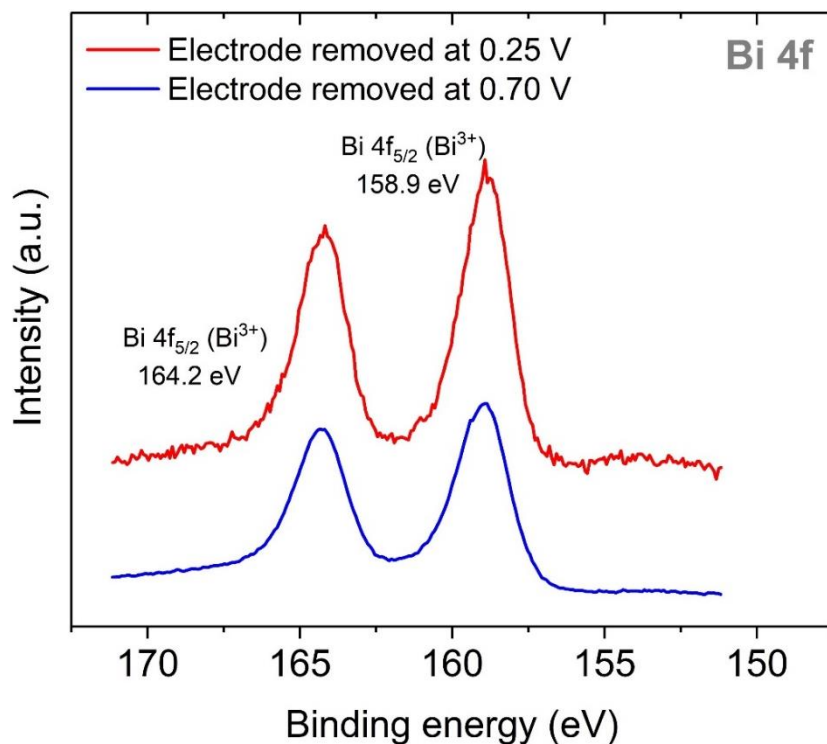


Figure 30: *ex situ* XPS obtained on a Pt_p electrode after cycling it in 0.1 M NaOH + 10⁻⁵ M Bi₂O₃ at 10 mV/s. The electrode was removed from the cell after polarization at 0.25 V and 0.70 V and transferred to an XPS chamber. Reprinted with permission from ref.[82]. Copyright 2022 American Chemical Society.

4. Product identification with liquid chromatography

This section aims to both identify and quantify the soluble oxidation products that are being generated during the glycerol conversion in the various Pt-Adatom systems. This is done using high-pressure liquid chromatography (HPLC), while samples are collected on-line during a linear potential sweep.

4.1. Basics of liquid chromatography

Liquid chromatography is a technique that separates a mixture (the sample or solute) based on the size, shape, charge, or chemical properties of the composition. The separation is dictated by the interaction between three phases: the solute (analyte), the mobile phase (solvent), and the stationary phase (separation column).¹⁴³

Modern liquid chromatography is called high-performance or high-pressure liquid chromatography, hence the name HPLC. This came after improvement to the quality of the separation columns, by packing small ($< 10 \mu\text{m}$) silica nanoparticles into the columns, since well-packed columns improve the separation efficiency and, in turn, increase the columns' internal pressure.¹⁴⁴ It is important to highlight, however, that not all columns use silica as their stationary phase, such as those used in ion exclusion chromatography.

When devising a separation method for HPLC, many parameters have to be taken into account. The injection volume determines how much of a sample is injected, if too little is injected then no peaks associated with the products will be detected, while if the volume is too high the column will overload, distorting the peak shape. The column temperature is another key parameter, as higher temperatures mean faster analysis and lower retention times for the various products. The packing material used in the columns will determine if it is a hydrophilic or hydrophobic column, which will in turn determine if the mobile phase should have a high concentration of an appropriate organic solvent. Lastly, while not a parameter in itself, the detector used affects the resulting chromatograms: appropriate wavelength for a UV detector, changes to the refractory index, degree of fluorescence, etc.

4.2. Experimental setup for on-line sample collection and HPLC separation method

The experimental setup used here is based on the work by Kwon and co-workers, called on-line HPLC by them.¹⁴⁵ In this setup, we use the same Pt_{disk} used during the *in situ* FTIR experiments as our WE, and a PEEK capillary, attached to a fraction collector, is placed as close as possible to the center of our electrode so that electrolyte samples from its surface are collected during a potential sweep. The setup is shown alongside a scheme in **figure 31**. The main advantage of this technique over conventional electrolysis in H-type cells is that we can obtain the product distribution as a function of electrode potential in a fraction of the time that would be necessary using electrolysis since we can collect electrolyte samples over a wide potential range. The main disadvantage is that it requires specialized equipment (fraction collector) and very small amounts of products are being generated, since there is no product accumulation over time, making product identification and quantification somewhat more difficult.

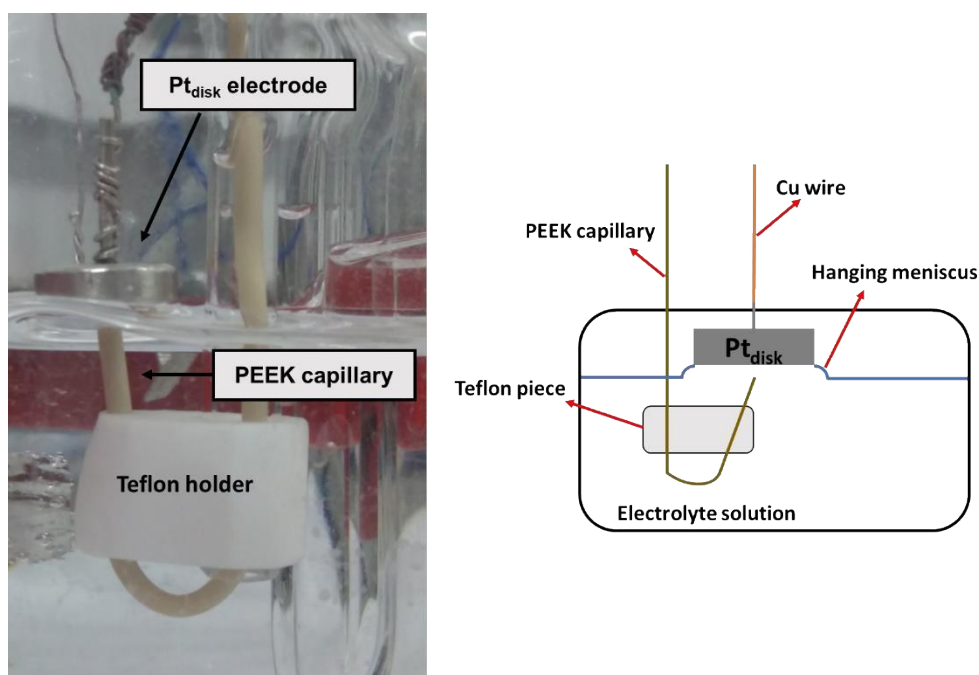


Figure 31: Schematic of the on-line HPLC experiment, where a capillary is used to collect electrolyte samples from the surface of the working electrode. Reproduced from ref.[80].

The experiment is done in conventional glass cells, following the same cleaning instructions for both electrodes and glassware as in **chapter 2**, and the electrolyte solutions were prepared in the same way. The PEEK capillary is cleaned by collecting ultrapure water at 2 mL/min over a few minutes, and the glass tube used

to hold this capillary and Teflon piece used to keep it in place are cleaned by rinsing with ultrapure water. The fraction collector used is a Shimadzu FRC – 10A.

In a similar fashion to the *in situ* FTIR, the sample collection only begins after 9 potential cycles between the 0.20 – 0.85 V potential window at 10 mV/s, to reach a more stable electrode (in terms of maintaining a high j_{peak} with cycling). After these 9 cycles, the electrode is polarized at 0.20 V and N₂ is gently bubbled into the cell for at least 5 min, without breaking the meniscus, to remove any product accumulated at the electrode surface. After this time, bubbling is ceased and the capillary is moved up until it is very close to the center of the WE (**fig. 31**). The collection rate is kept at a constant 60 $\mu\text{L}/\text{min}$, and before the potential sweep begins, a sample from both the bulk electrolyte and at the electrode surface, while polarized at 0.20 V, are collected. In the following, the WE potential is swept at 1 mV/s from 0.20 – 0.85 V while sample acquisition is happening, meaning that each sample corresponds to the electrolyte collected during a 60 mV window, and due to this the samples are labeled as their respective mean potential (i.e., the sample collected from 0.26 to 0.32 V is called 0.29 V and so on).

Samples travel for 7 min at the flow rate of 60 $\mu\text{L}/\text{min}$ in the capillary tubing before leaving the fraction collector, at which point they are stored in 0.5 mL Eppendorf® tubes. Each tube contains 10 μL of a 0.3034 M H₂SO₄ solution, to neutralize the samples and decrease their pH to 3.30, matching the pH of our mobile phase. This step is done to avoid chemical reactions that happen due to our highly alkaline media.¹⁴⁶ Samples are stored at 2 °C on the fridge before analysis, and before injection, they are transferred to 150 μL spring bottom inserts and placed into 1.5 mL vials, loaded to a sample cooler kept at 10 °C on our chromatograph. The chromatograph used is a Shimadzu LC-6AD equipped with a quaternary pump, a column oven, and two detectors, UV and refractory index detector (RID). The mobile phase used was 0.5 mM H₂SO₄, the injection volume was 20 μL , and the flow of 0.6 mL/min. Three columns were used: an Aminex HPX-87H and two Shodex Sugar SH1011, kept at 84 °C and preceded by a BioRad H cation pre-column.

Identification of the possible oxidation products was done using external standards, and quantification using calibration curves. External standards were 1.5 mL solutions composed of an acidified electrolyte (0.1 M NaOH + 0.1 M glycerol, then H₂SO₄ is added until pH = 3.30), and 0.1 mM of each oxidation product. A few milligrams of each oxidation product is diluted in 5 mL of ultrapure water to make

individual stock solutions, which were used to prepare these external standards. The chromatograms for these external standards are shown in **fig. S14** for the RI detector, the wavelengths chosen for the UV detector were 211 and 230 nm, and **fig. S15** shows the chemical structure of the molecules on these standards. To avoid elution discrepancies between samples, each chromatogram was normalized by subtracting their respective void time, and hence the time axis is labeled as the retention time.

Quantification was done by making calibration curves, similarly to the external standards, with the exception that the concentration of the organics was changed to relate their concentration to the peak area. The calibration curves used are shown in **fig. S16**.

4.3. Results for HPLC with on-line sample collection

Complementary to the external standards used to identify the possible products from the glycerol conversion, we also injected 20 μL of each stock solution used to make those standards (**fig. S17**), to check their elution time without interference from other species (i.e., glycerol and others). We see that both mesoxalate and oxalate are eluting immediately after the void time (downward peak), indicating that they are not interacting with our stationary phase. Due to this lack of interaction, we cannot separate these molecules from injected samples, as we would need to change the columns used altogether (and devise a new method). In **fig. 24** of **chapter 3**, we saw an 1100 cm^{-1} band that could be due to the presence of either mesoxalate or tartronate (**fig. S10**), however, since mesoxalate does not interact with our column, we are unable to detect its presence (or lack thereof) using HPLC.

Further examination of **fig. S17** shows that hydroxypyruvate and tartronate are eluting close to each other, but can still be differentiated. On the other hand, glycolate, lactate, formate, glyceraldehyde, and dihydroxyacetone are all eluting at similar times, with the latter two species being eluted as a pair of peaks instead of only one. We do not know why this happens, but the same result was obtained even after changing the reagents used to make the stock solutions. Despite these limitations, this separation method had the best results in separating these 12 different molecules (**fig. S15**).

With that being said, **figure 32** shows the chromatograms of the samples collected on-line during glycerol conversion in the various Pt-Adatom systems, with

each identified product labeled, and **figure 33** shows the product associated with each peak. Peak assignment and its implications will be discussed in the following paragraphs.

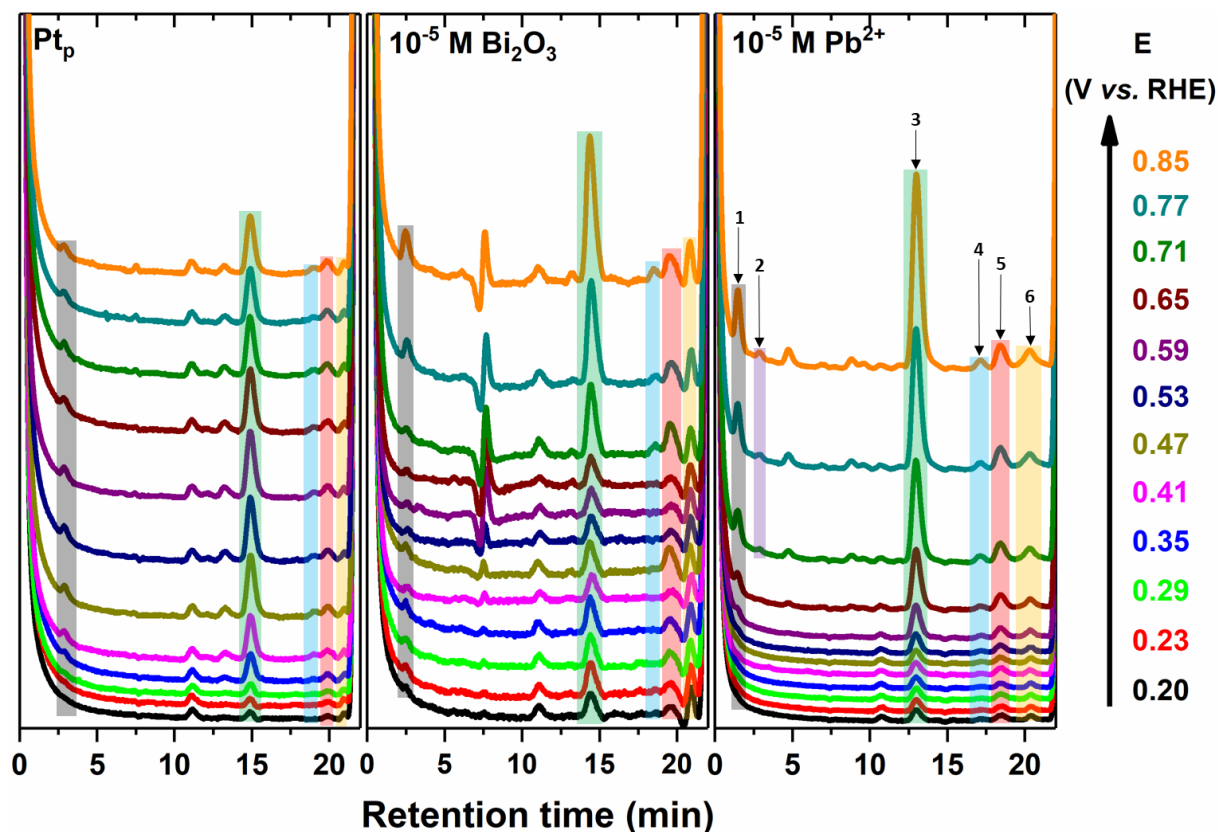


Figure 32: Chromatograms for samples collected on-line during the glycerol conversion at 1 mV/s in 0.1 M NaOH + 0.1 M glycerol for the various Pt-Adatom systems. Using data adapted from ref.[83].

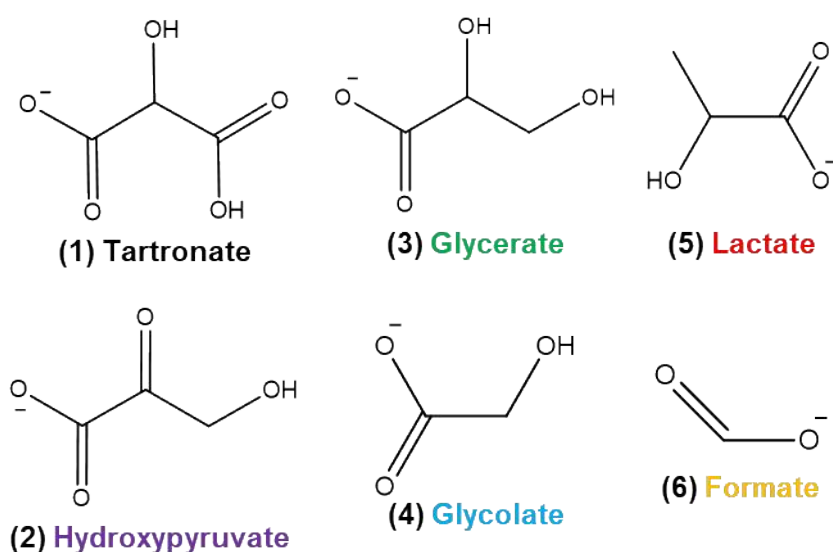


Figure 33: Oxidation products that were identifiable from the chromatograms shown in **fig. 32**.

A first look at **fig. 32** shows that there is a slight discrepancy in the retention times of compounds 5 – 7, namely glycolate, lactate, and formate, between the Pt-Adatom systems studied, and with **fig. S14**. This happened because the experiments were performed at different times, and the columns were cleaned and regenerated during the experiments. To circumvent this, we injected the external standards whenever we did these experiments so that we could properly identify the products despite changes in the stationary phase.

The first product identified was tartronate, observed on both Pt-Bi and Pt-Pb systems. There is a slight indication of its presence on the unmodified electrode, however, the magnitude of this peak is below the detection limit of the RI detector used. Following the elution order, on Pt-Pb we see a small peak at 2.9 min, which indicates the formation of hydroxypyruvate, and then, another peak at 4.7 min that starts to grow steadily at $E > 0.70$ V that we were unable to link to any of the possible products used in our external standards.

Before moving on with the product assignment, a disclaimer has to be made. By zooming in into the chromatograms at very low potentials ($E < 0.29$ V) where no anodic current is expected, as seen in **figure 34**, where we show the linear sweep voltammogram associated with the chromatograms shown in **fig. 32**. Commercial grade glycerol has a purity of $\geq 99.5\%$, meaning that it has a very small percentage of impurities. We investigated this in **fig. S18**, where we see that by injecting NaOH and NaOH + glycerol solutions, the presence of glycerol causes the appearance of four very small peaks from 13 to 20 min. These peaks can be identified when compared to the external standards in **fig. S14** and they are, in order of elution, glycerate, glycolate, lactate, and formate. This means that all alkaline glycerol solutions contain very small amounts of these products, and, when looking back at our chromatograms in **fig. 32**, these four molecules are being generated during the electrochemical conversion of glycerol, both with and without adatoms on the Pt surface.

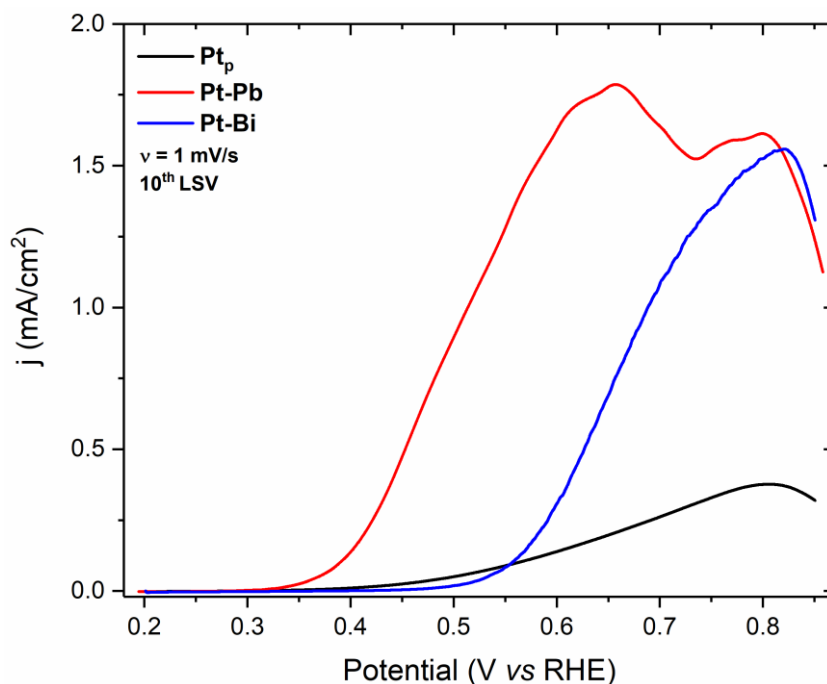


Figure 34: Linear sweep voltammogram at 1 mV/s in a base electrolyte of 0.1 M NaOH + 0.1 M glycerol for the unmodified and the Pt-Adatom systems. Using data adapted from ref.[83].

Having properly identified the oxidation products, the peaks are integrated and converted from peak area to molar concentration with the aid of calibration curves (**fig. S16**), and the product distribution as a function of electrode potential is shown in **figure 35**. Since some products are already present at 0.20 V due to glycerol impurities, we integrate these peaks, and subtract their areas from the integrated peak areas of the other chromatograms, at higher potentials. In other words,

$$A_{peak}^r = A_{peak} - A_{0.20\text{ V}}$$

Where A_{peak}^r is the real peak area, caused by glycerol oxidation on the Pt surface, A_{peak} is the calculated peak area from the chromatogram and $A_{0.20\text{ V}}$ is the calculated peak area at 0.20 V, where no anodic current is observed, and the presence of any product is due to glycerol impurities. Thus, the concentration values in **fig. 35** are obtained by converting A_{peak}^r into molar concentration using the calibration curves shown in **fig. S16**.

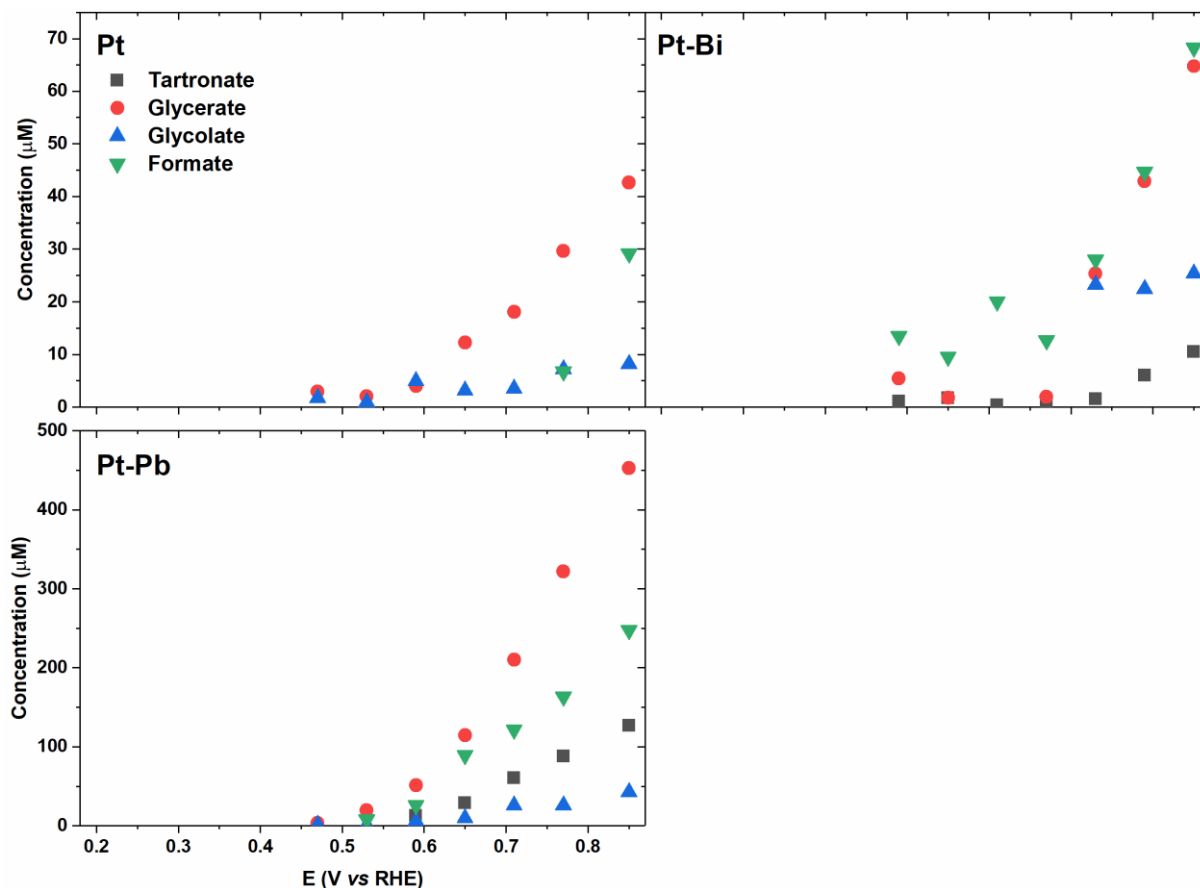


Figure 35: Product concentration vs electrode potential for the various chromatograms shown in **fig. 32**. Using data adapted from ref.[83].

From **figs. 34** and **35** we see that Pt-Pb had higher anodic currents than Pt-Bi, and also it produced a significantly higher amount of oxidation products generating over 400 μM of glycerate at 0.85 V. We saw no significant changes to the reaction selectivity, as we still obtain a mixture of glycerate, glycolate and formate in all cases studied, different from results obtained for both Pt-Bi and Pt-Sb in acidic media, where a change in the reaction selectivity was observed.^{22,58} The most meaningful change was the presence of tartronate on Pt-Bi and Pt-Pb, and hydroxypyruvate on Pt-Pb, which were not previously seen on the clean Pt electrode.

The hydroxypyruvate produced on Pt-Pb was not quantified at the time when this study was published⁸³ because we were not able to confirm its presence. The confirmation only came at a later date, when this data was revisited. The same happened for lactate. At the time when the works concerning the Pt-Bi⁸² and Pt-Pb⁸³ systems were published, we were not able to identify this molecule based on the external standards used at the time. Proper identification of this molecule only came

at a later date, in another work published by our group.¹²⁹ The presence of this species, however, indicates a very important aspect of the reaction pathways at present in our experiments, which was ignored for years in most of the papers in the field, which will be explained below.

The presence of lactate from the electrochemical conversion of glycerol was first seen by Dai et. al.³⁷ while using AuPt nanoparticles as the catalyst. They proposed that this species comes from the base-catalyzed degradation of dihydroxyacetone. In the initial stages of the glycerol oxidation, it is oxidized into either glyceraldehyde (by targeting a primary OH^-) or dihydroxyacetone (targeting the secondary OH^-), products that are detected in the entire pH range when using platinum catalysts.²⁸ We have shown in a previous study⁸² that both molecules are not stable in highly alkaline media, and readily convert into other molecules, however at the time we were not able to identify what species are being formed from their degradation. We have improved this investigation, and the results are shown in **figure 36**, where we investigated which molecules are formed from their degradation after 90s in a pH = 13 solution.

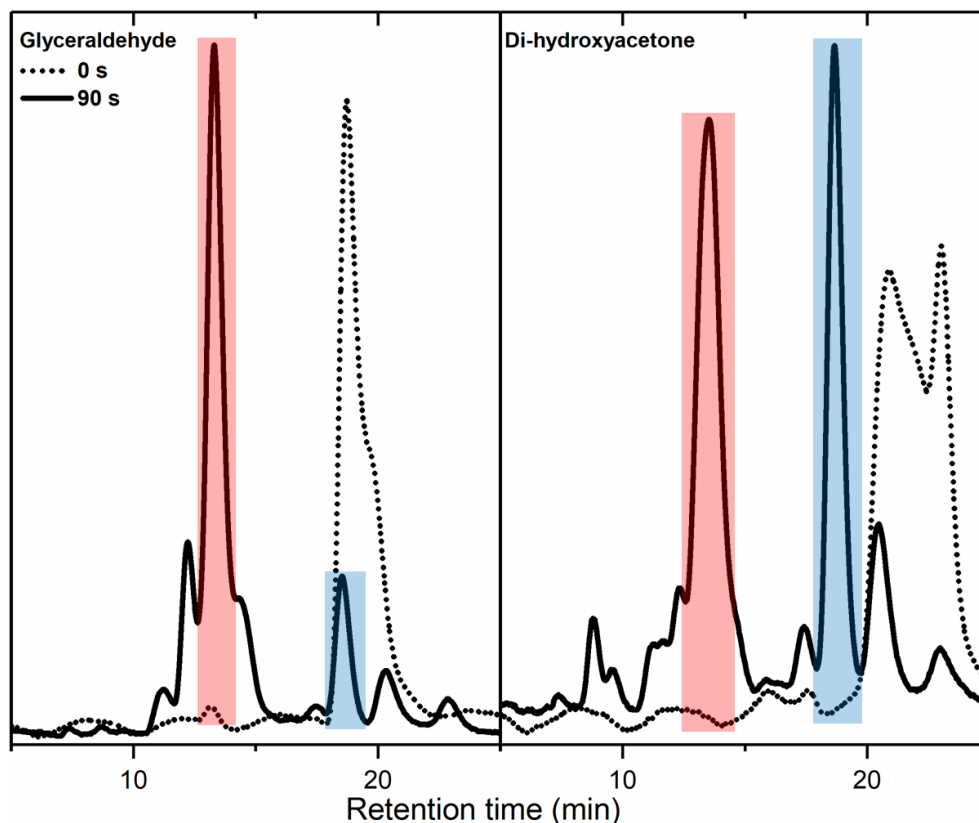


Figure 36: Chromatograms for pure glycerinaldehyde and dihydroxyacetone in water (dotted lines) and after 90s in a pH = 13 solution, which was then acidified with H₂SO₄ (full lines). Red and blue highlights indicate the presence of glycerate and lactate, respectively.

After 90s the ketone and aldehyde are completely degraded, and we were able to detect glycerate and lactate in both cases. Integrating the highlighted peaks in **fig. 36** allows us to compare how much of those species are being generated, and if the ketone and aldehyde have a preferred pathway. For glycerate, $A_{ketone}/A_{aldehyde} = 0.8$, meaning that more glycerate is being produced from the aldehyde degradation. For lactate, $A_{ketone}/A_{aldehyde} = 2.6$, so the degradation of the ketone generates almost three times more lactate than from the aldehyde. In summary, dihydroxyacetone preferentially degrades into lactate in alkaline media, so the lactate observed in **fig. 32** means that dihydroxyacetone was one of the reaction intermediates in our various Pt-Adatom systems, in addition to glycerinaldehyde as a precursor for glycerate.

5. Pt-Bi catalyst applied to glycerol-based microfluidic fuel cells

5.1. Introduction to electrochemical devices

Electrochemical devices allow the conversion of chemical energy into electrical energy or vice-versa. They are made up of at least two electrodes, an anode and cathode, separated by an electrolyte, and are classified according to their purpose, which will impact how they are operated.

Devices for dedicated energy storage can be classified into batteries or capacitors. Batteries store energy in the form of chemical energy, and once they are connected to a circuit, a spontaneous redox reaction occurs within the battery, releasing electrons (electric current) to the external circuit. Depending on the redox reaction happening on these devices, they will be single-use or rechargeable. Capacitors, in general, are devices that store electrostatic energy in an electrostatic field between a set of metallic sheets held closely together.

A fuel cell is a device made for energy generation, it converts chemical energy into electrical energy utilizing a redox reaction and, unlike batteries, they generate electricity continuously as long as fuel is available. The chemical reaction on fuel cells is spontaneous and begins once it is connected to an external circuit, through which electrons will flow. In these devices, the anode and cathode are usually separated by an ion-exchange membrane, allowing the flow of either protons or anions from one side to the other. The versatility of fuel cells allows them to be constructed using multiple architectures, from cells without a liquid electrolyte¹⁴⁷ to their miniaturization on the micrometer scale.¹⁴⁸ These microfluidic fuel cells (μ FC) utilize a laminar flow to separate the reactant streams from the anode and cathode, eliminating costs and ohmic drop related to the use of a membrane. Another important advantage of μ FCs is that they allow the usage of porous electrodes, where the reactant streams are forced through the electrodes, resulting in a significant increase in the energy output from the fuel cell and increased fuel utilization.¹⁴⁹

The last type of device is the electrolyzers, which operate with non-spontaneous redox processes, meaning that they require an electrical input (applied potential) to begin functioning. The main goal of these devices is to convert a molecule (reactant) into another through a redox reaction. It is mainly used in the production of high-purity hydrogen gas through water electrolysis (water splitting)⁴, but may also be used to convert biomass into valuable chemicals¹⁰ or even reduce exhaust CO₂ into

chemicals such as formic acid.¹⁵⁰ In an electrolyzer, the anode, and cathode can be in the same compartment or separated by an ion-exchange membrane, allowing the flow of either protons or anions, so it is possible to use the same device to couple two reactions of interest, one on the cathode and another on the anode.⁸

5.2. Fuel cell fabrication and nanoparticle synthesis

The microfluidic fuel cells used in this work were 3D-printed according to a methodology developed by Guima et. al.⁴⁵ with porous electrodes. This device achieved high power densities owing to the high surface area of the electrode and the improved mass transport conditions (forced convection).

A model of the μ FC is shown in **figure 37**, drawn using the Autodesk Inventor[®] software, sliced using the software Simplify3D[®] and printed using a Sethi[®] 3D-printer model S3. The channels are 150 μ m high with a 0.1 mm resolution, guaranteeing their quality and uniformity. The co-laminar channel piece is printed in polylactic acid, with the bottom plate printed in polyethylene terephthalate glycol, due to its transparency. After the electrodes are placed on the channels (**figure 38**), the two pieces are glued together using polyvinyl chloride glue. After drying, electric contact is made using silver conductive epoxy and aluminum wires on the 2.0 mm holes. The side 2.3 mm holes are for the electrolyte inlet, and the two 1.5 mm on the inferior part are for the electrolyte outlet, also called the exhaust electrolyte, due to mixing of the cathode and anode electrolytes in the microchannel.

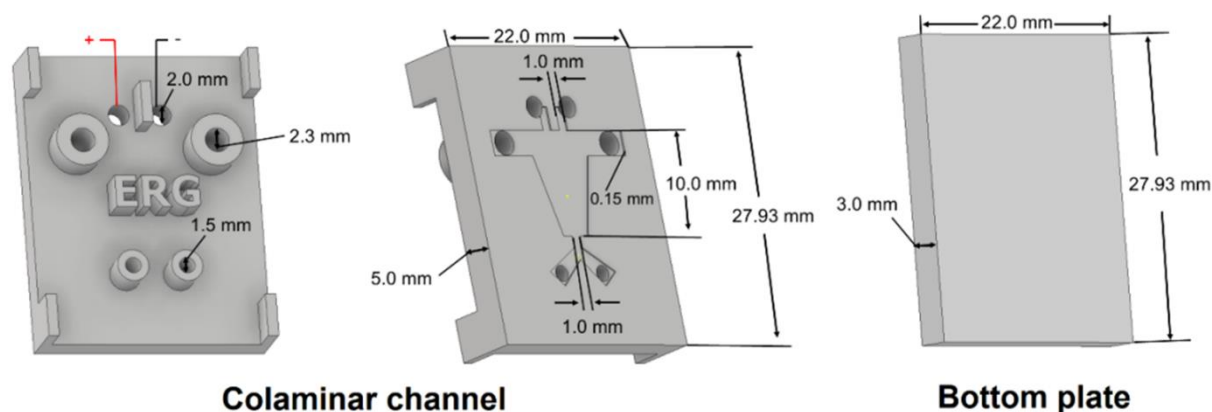


Figure 37: Model of the μ FC used, featuring the co-laminar channel and the bottom plate used to seal the cell. Reprinted with permission from ref[65]. Copyright 2022 American Chemical Society.

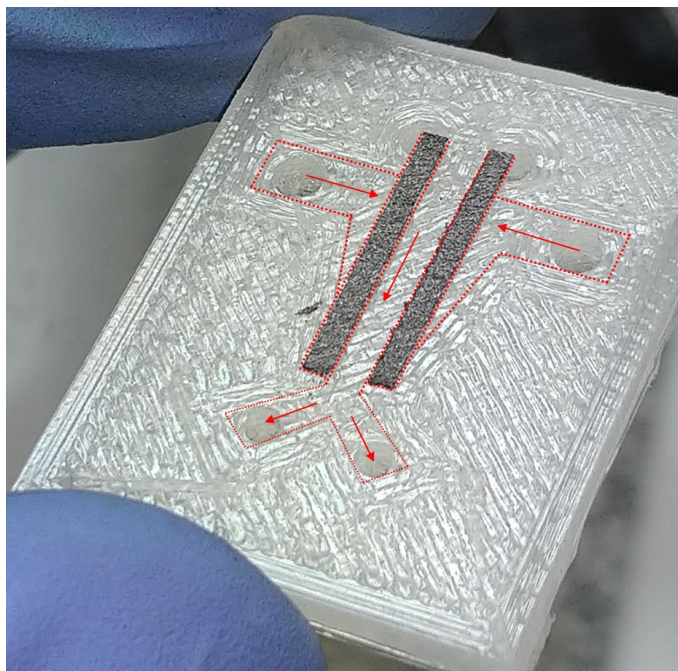


Figure 38: Placement of the electrodes on the microfluidic channels. Arrows indicate the flow of the electrolyte on the cell, with a dotted line indicating the limits of the printed area.

The porous electrodes used in this cell were strips of carbon paper (CP) impregnated with Pt nanoparticles supported on carbon Vulcan (Pt/C), and the final electrode is labeled as Pt/C/CP.

For the synthesis of Pt/C nanoparticles⁶⁵, 483 mg of H_2PtCl_6 (Sigma-Aldrich, ACS reagent $\geq 37.50\%$ Pt basis) is dissolved under constant stirring on a solution made of 50 mL of dimethylformamide (Sigma-Aldrich, ACS Reagent $\geq 99.8\%$) and 39.7 mg of poly(vinylpyrrolidone) (Sigma-Aldrich, K30). When all the H_2PtCl_6 is dissolved, the color of the solution changes from transparent to orange. In the following, 500 mg of NaBH_4 (Sigma-Aldrich, powder $\geq 98.0\%$) is slowly added to the solution to reduce the Pt^{4+} ions over the course of 10 min, after which the solution color changes to black. After 30 min of constant stirring, 121 mg of Carbon Vulcan (Cabot, VXC72) is slowly added to the solution to form the Pt/C nanoparticles, and after an extra 30 min, the stirring was stopped and 50 mL of acetone (Synth, 100% pure) was added to the beaker and transferred to an ultrasonic bath for 1 hour.

After the ultrasound bath, the solution was left undisturbed for between 1 and 2 hours, until a black precipitate was formed at the bottom, and a clear liquid is left on top. This liquid part is collected and discarded, and the precipitate is carefully

redissolved in ultrapure water and transferred to a vacuum filtration system. Filtration was done by alternating between acetone and ultrapure water until the filtrate was transparent. The filter paper containing the solids was carefully transferred to an oven, where they were dried at 60 °C for 12h.

Physical characterization was done using X-Ray diffraction (XRD), to observe crystallinity and crystallite size, and thermogravimetric analysis (TGA) for determining the Pt loading of the nanoparticles. The XRD was done in an XRD-700 Shimadzu equipped with a copper font, operating with a monochromator at 0.02 ° from 20 to 100 2 θ at 2 °/min. The TGA was done in a TA Instruments® TGA 2950 from 25 to 800 °C at 5 °C/min using an oxidant atmosphere. **Figure 39** shows the result of these characterizations. Crystallite size was calculated using the Scherrer equation and the peak ascribed to Pt(111), and the mean crystallite size was 3.75 nm. TGA analysis shows a platinum load of 53.1% after evaporating the carbon Vulcan at approximately 400 °C¹⁵¹, however, two peaks are still present at 180 °C and 260 °C, matching the boiling point of dimethylformamide and melting point of poly(vinylpyrrolidone), respectively, meaning that not all excess reagents were washed off from the nanoparticles.

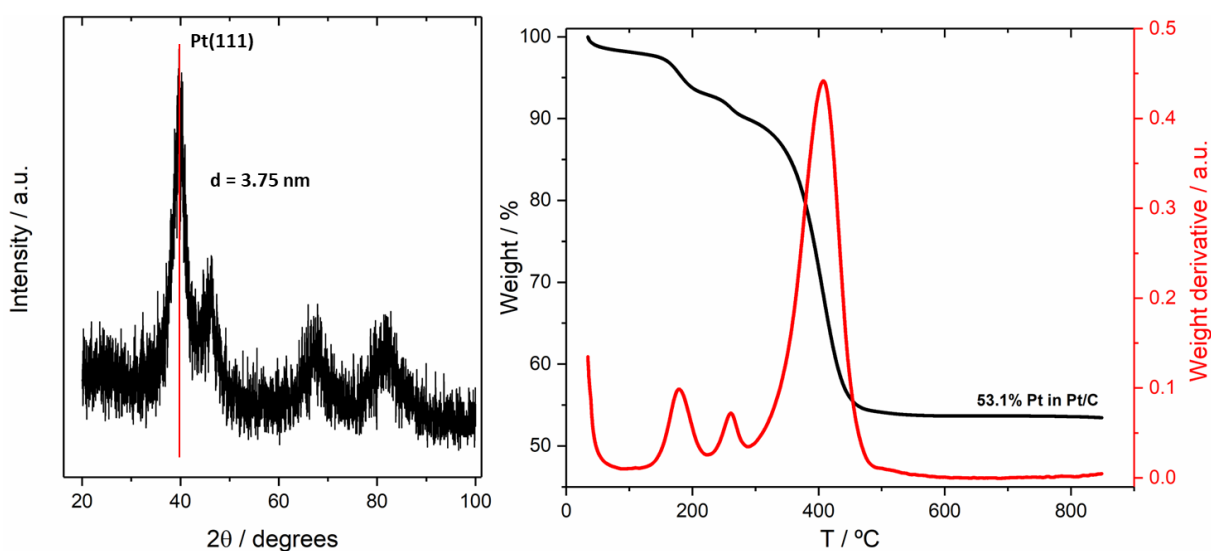


Figure 39: Results of the physical characterization of the Pt/C nanoparticles, with results for XRD (A) and TGA (B). Adapted from ref.[65].

The dried Pt/C particles were used to prepare a catalytic ink. The ink was made by adding 200 mg of the Pt/C nanoparticles to a solution of 7.68 mL ultrapure water, 7.68 mL methanol (Sigma-Aldrich, ACS reagent \geq 99.8%), and 1.78 mL Nafion

5% (Sigma-Aldrich) under constant stirring for 24 hours at room temperature, and stored on the fridge. The carbon paper was cut into 15 x 15 mm squares and cleaned by flame annealing on a butane flame, and after cooling to room temperature they were submerged into the catalytic ink and sonicated for 5 minutes, to improve the dispersion of the nanoparticles. The impregnated carbon paper squares were dried in an oven at 80 °C for 4 hours and then cut into 13 x 1 mm strips to be used as Pt/C/CP electrodes on the μ FC.

The anode of the μ FC was modified with Bi adatoms using two different methodologies, that we chose to name *in situ* and *operando*.⁶⁵ The *in situ* modification consists of the electroless (spontaneous) deposition of the Bi adatoms, inspired by the work of Martins et. al.¹⁵², where the authors decorated a Pt/C electrode with Fe adatoms. In our work, a solution of 0.1 M KOH + 10^{-5} M Bi₂O₃ was pumped on the anode while ultrapure water flowed on the cathode, at a flow rate of 50 μ L/min for 30min. The *operando* modification, on the other hand, consists of adding 10^{-5} M Bi₂O₃ to the 0.1 M KOH + 0.1 M glycerol anode solution, so that Bi deposition happens during the cell operation.

After the operation, some of the μ FCs were opened and the modified anodes were characterized by scanning electron microscopy (SEM) imaging and by measuring the chemical composition of the surface using an energy-dispersive X-ray detector (EDX) coupled to the microscope. The SEM used was a JEOL model JSM-6380LV, and the EDX detector was a Thermo Scientific (Noran System Six).

All solutions were used without previous purification. The anolyte (anode electrolyte) was KOH (ACS grade, Sigma-Aldrich) + glycerol (ACS grade, Sigma-Aldrich), and catholyte (cathode electrolyte) was H₂SO₄ (ISO grade, Merck Emsure) + Na₂S₂O₈ (Reagent grade, Sigma-Aldrich). The electrolyte solutions were pumped into the cell using a syringe pump KDS Legato, model 101, and the cell operation was controlled using a PalmSens3 potentiostat. The cross-sectional area of the porous electrodes was used to normalize the current values obtained during cell operation, and it has a value of 0.026 cm². Fuel cells are operated in a two-electrode system, where both RE and CE are short-circuited and connected to the anode, while the WE is connected to the cathode.

Half-cell measurements were performed in a conventional three-electrode cell, using RHE as the reference electrode and a Pt coil as the CE. The cell and these electrodes were cleaned as described in **chapter 2**.

5.3. Anode modification results

SEM imaging and the elemental mapping of the Bi-Pt/C/CP electrodes modified using the *in situ* (figure 40) and *operando* (figure 41) methodologies are shown in the images below.

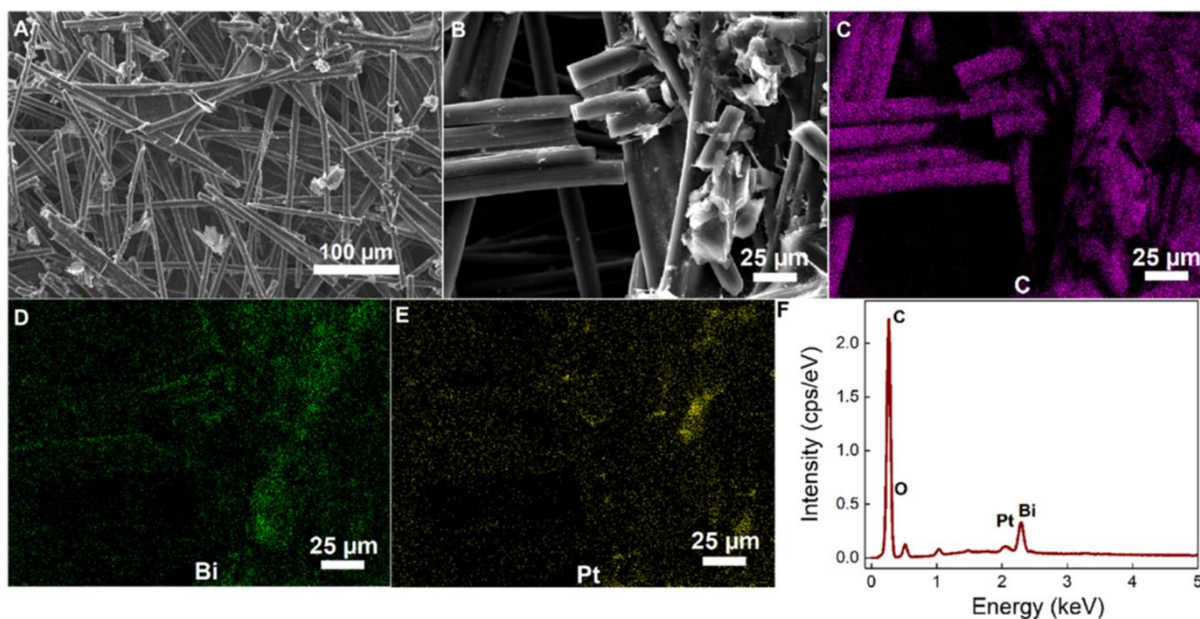


Figure 40: Representative SEM image of the (A) *in situ* Bi-Pt/C/CP electrode. (B) selected region for mapping the elemental composition, detailed for (C) carbon, (D) bismuth, and (E) platinum. (F) Representative energy-dispersive X-Ray spectrum. Reprinted with permission from ref.[65]. Copyright 2022 American Chemical Society.

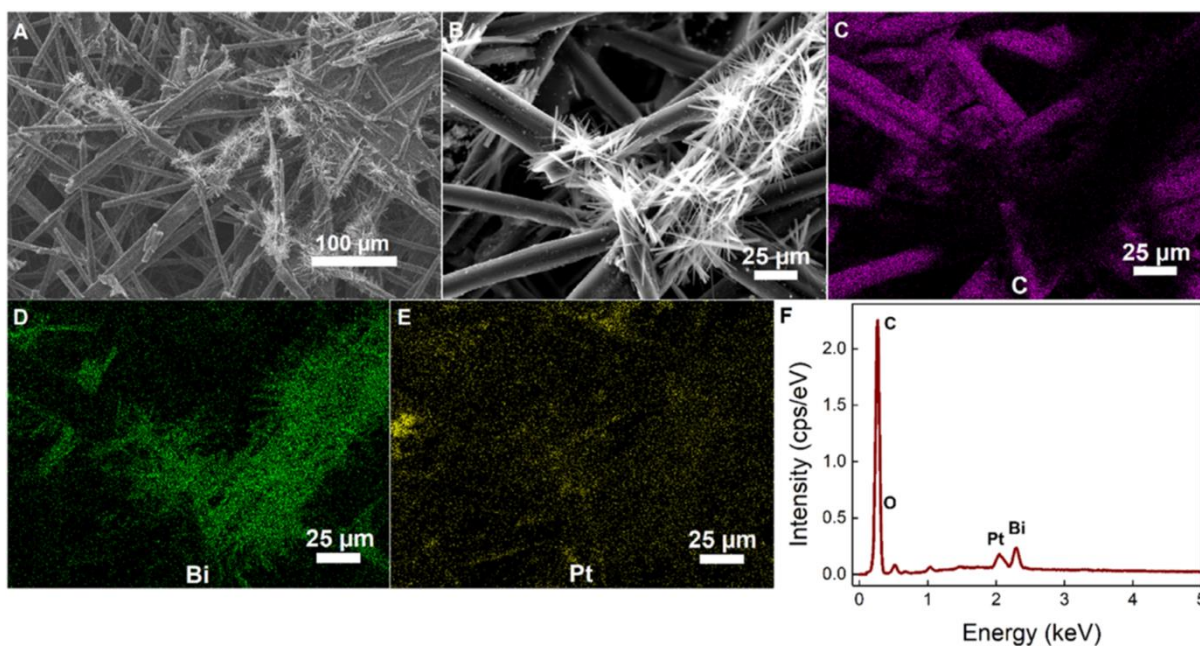


Figure 41: Representative SEM image of the (A) *operando* Bi-Pt/C/CP electrode. (B) selected region for mapping the elemental composition, detailed for (C) carbon, (B) bismuth, and (E) platinum. (F) Representative energy-dispersive X-Ray spectrum. Reprinted with permission from ref.[65]. Copyright 2022 American Chemical Society.

In **figs. 40** and **41**, image (A) shows the carbon fibers that make up the carbon paper, our porous electrode, while image (B) is a representative image of those fibers, chosen for the elemental mapping displayed in images (C), (D) and (E).

Initial comparison of both representative regions in (B) shows that rod-like structures have grown on the carbon fibers of the electrode modified via the *operando* route, in **fig. 41**. The platinum mapping in (E) points out that the Pt/C nanoparticles are well-dispersed on the carbon fibers, and that the aforementioned structures are growing on top of these nanoparticles. Bismuth mapping in (D) revealed significant differences between both methodologies. In **fig. 40** the *in situ* (electroless) deposition of Bi resulted in a uniform distribution of bismuth on top of the Pt/C nanoparticles, meanwhile in **fig. 41** the Bi mapping shows that the rod-like structures are made of Bi, and have grown on top of the Pt/C particles. Similar structures have been reported in the literature from hydrothermal reactions¹⁵³, while ours were obtained at room temperature in a few hours. The exact composition of these particles was not examined, but it can be a mixture of various bismuth oxides such as Bi₂O₄, Bi₄O₇, and δ -Bi₂O₃.

5.4. Cell operational results

The μ FC is evaluated in terms of its open circuit voltage (OCV) and the power density generated by the device. The OCV is its voltage at zero current density, in an open circuit situation without power generation. The theoretical OCV of the cell can be calculated using the Nernst equation for the overall cell reaction:

$$E_{theory}^{OCV} = E_{cathode} - E_{anode}$$

While direct measurement of the OCV can be done with a voltmeter.¹⁵⁴ This parameter is used to estimate the performance of the device because of differences between the measured ($E_{measured}^{OCV}$) and theoretical (E_{theory}^{OCV}) values are linked to a loss of power density. These differences may arise from species crossover (when an ion-exchange membrane is used), catalyst impurities, and side reactions, among other factors. Measurement of the OCV can also be used to study the degradation of a fuel cell.¹⁵⁵

Before operating the μ FCs themselves, half-cell measurements were performed to observe the behavior and E_{onset} of the anodic and cathodic reactions. Due to the electrodes being porous, all currents in these measurements are expressed in amperes without being normalized by the ECSA. **Figure S19** shows the blank voltammogram of the assembled Pt/C/CP electrode in an H_2SO_4 electrolyte, where we can see a small H_{UPD} region at $E < 0.40$ V on the Pt/C nanoparticles, despite it being quite small (likely due to the presence of leftover reagents from the synthesis, as discussed in **section 5.2**).

To find the optimal operation conditions for our electrode, we examined two sets of glycerol and $Na_2S_2O_8$ concentrations for the anode and cathode half-cells, respectively, shown in **figure 42**, while the concentrations of KOH and H_2SO_4 were fixed. The cathode reaction was unstable at a 1 M concentration, losing intensity during potential cycling, so the 0.5 M concentration was chosen for $Na_2S_2O_8$. The anode reaction, glycerol oxidation, had its current decrease with the increasing glycerol concentration, indicating a self-inhibiting effect on this reaction, as described by Gomes and co-workers¹⁵⁶, therefore we chose the 0.1 M concentration. From these experiments we determined their corresponding E_{onset} , using the last voltammetric cycle, and calculated the theoretical OCP in each glycerol/ $Na_2S_2O_8$ pairing, shown in

figure 43. At our chosen concentrations, the onset for glycerol oxidation was 0.442 V, while the onset for sodium persulfate reduction was 1.076 V, netting a theoretical OCV of 0.634 V.

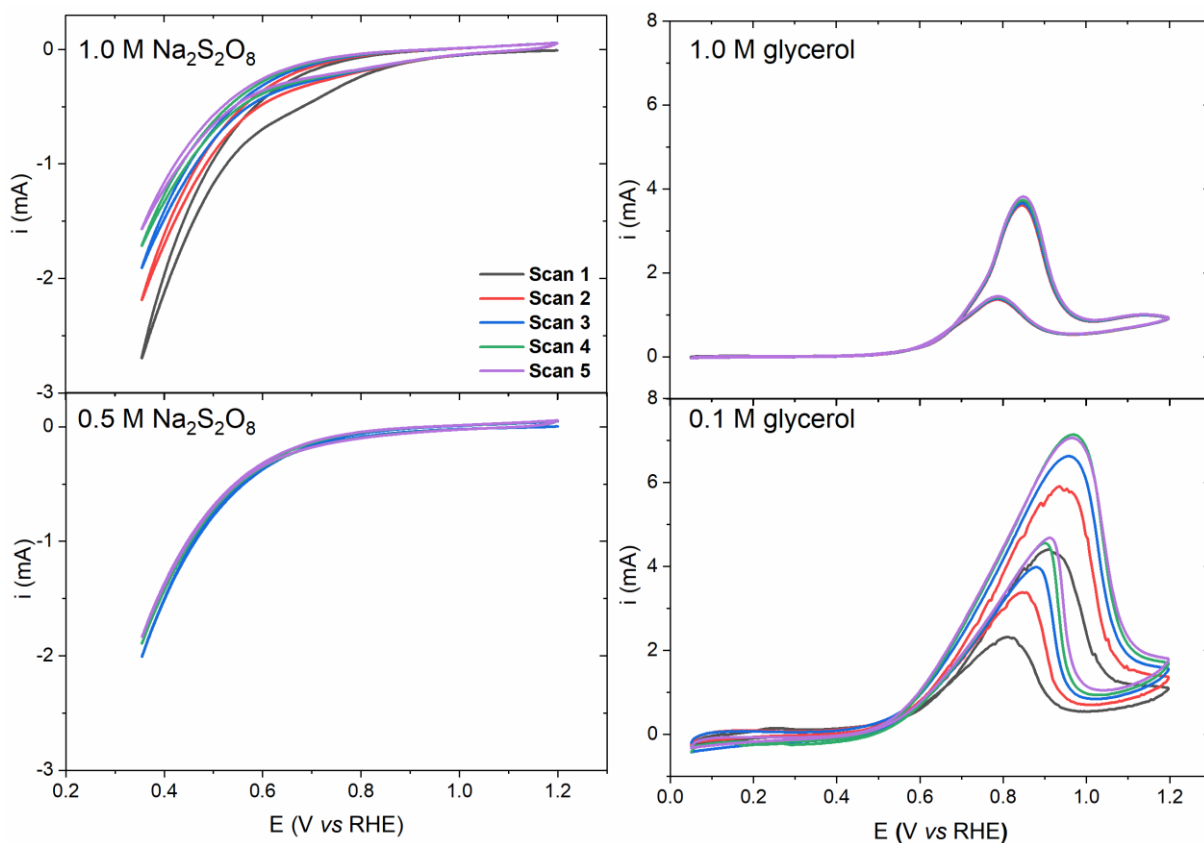


Figure 42: Half-cell reactions for different concentrations of $\text{Na}_2\text{S}_2\text{O}_8$ and glycerol in 1.0 M H_2SO_4 and 0.1 M KOH , respectively, using the Pt/C/CP electrodes, with all measurements at 50 mV/s. Adapted from ref.[65].

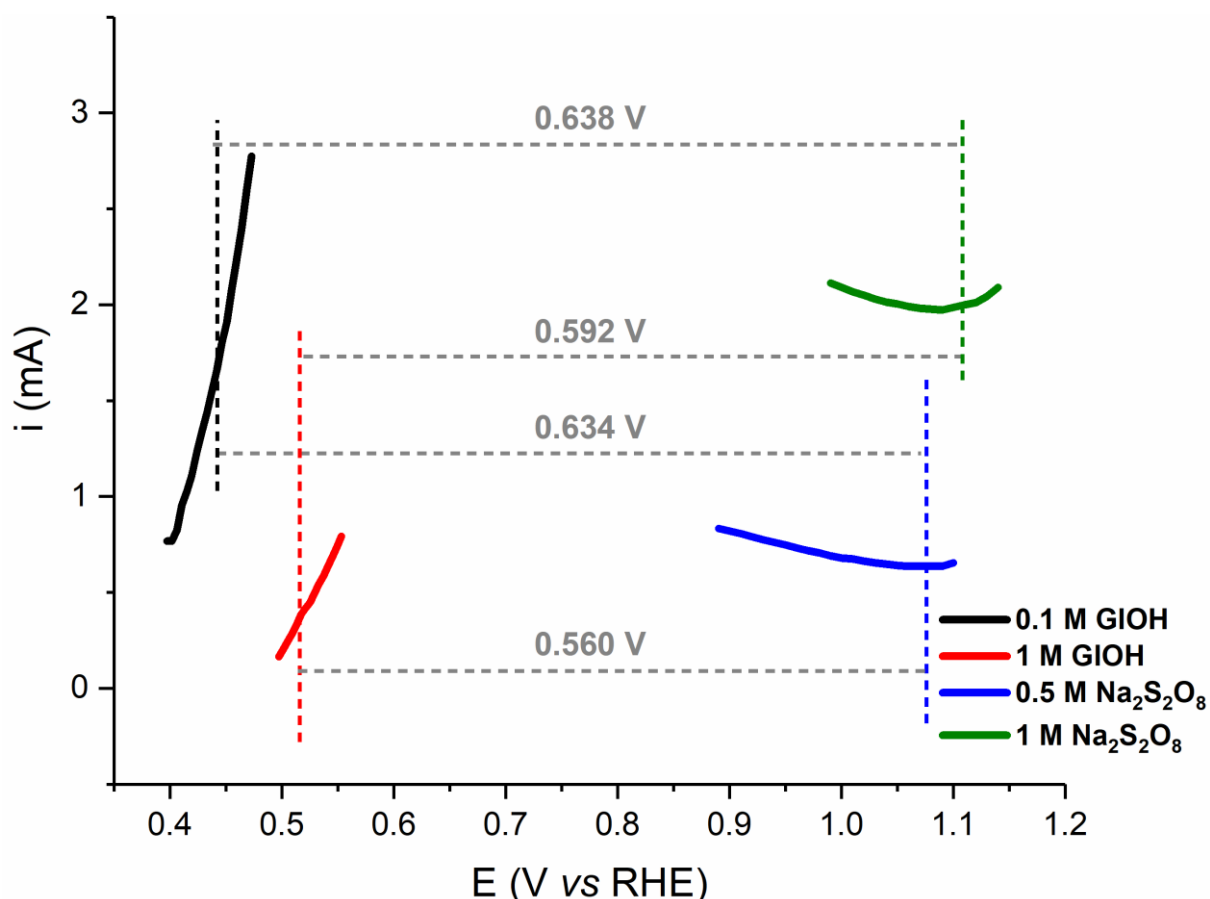


Figure 43: Theoretical OCP values for different pairings of glycerol and $\text{Na}_2\text{S}_2\text{O}_8$, after determining the respective E_{onset} from the voltammograms in **figure 42**.

Concluding the half-cell investigation, the anolyte was fixed at 0.1 M KOH + 0.1 M glycerol, with the catholyte being 1.0 M H_2SO_4 + 0.5 M $\text{Na}_2\text{S}_2\text{O}_8$, and the cell performance under flow conditions was evaluated. Initially, the cell was tested without anode modification, and multiple flow rates from 25 to 300 $\mu\text{L}/\text{min}$ were used, and the results are shown in **figure 44** below. This figure shows the polarization curves ($E - j$) measured from the OCP, after it reaches stability, to 0.01 V at 50 mV/s, and the power density curves ($P - j$) are calculated from the polarization curves

The measured OCV lies between 0.40 and 0.45 V, lower than the theoretical value determined above. The power density was roughly the same at 25 and 50 $\mu\text{L}/\text{min}$, with a maximum value of 0.25 mW/cm^2 , and decreased when the flow was further increased to 100 and 300 $\mu\text{L}/\text{min}$. These OCV and power density values are very low when compared to the performance of this device when using commercial Pt/C nanoparticles, free of impurities, with a maximum power density (P_{max}) of 175 mW/cm^2 at 0.9 V and an OCV of 1.8 V.⁴⁵ Despite the low performance obtained by us,

the μ FC remained stable.

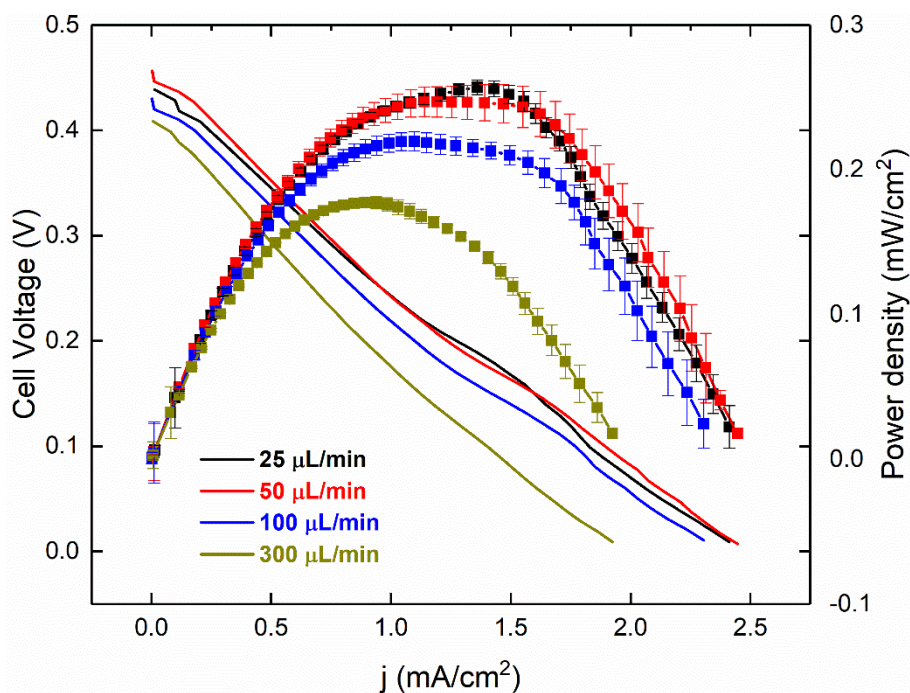


Figure 44: Polarization (lines, left axis) and power density (line + symbol, right axis) curves for the μ FC operating with the unmodified Pt/C/CP anode at different flow rates. Anolyte and catholyte were 0.1 M KOH + 0.1 M glycerol and 1.0 M H₂SO₄ + 0.5 M Na₂S₂O₈. Using data from ref.[65].

The next step was modifying the anode with Bi adatoms. Following the discussion in the previous section, the Bi-modified electrodes modified via the *in situ* and *operando* routes will be labeled as Bi_{uniform} and Bi_{dendrite}, respectively. These systems were examined at the flow rates of 50 and 100 μ L/min, because at either lower or higher flow rates the measured OCV never reached stability. The results are displayed in **figure 45**.

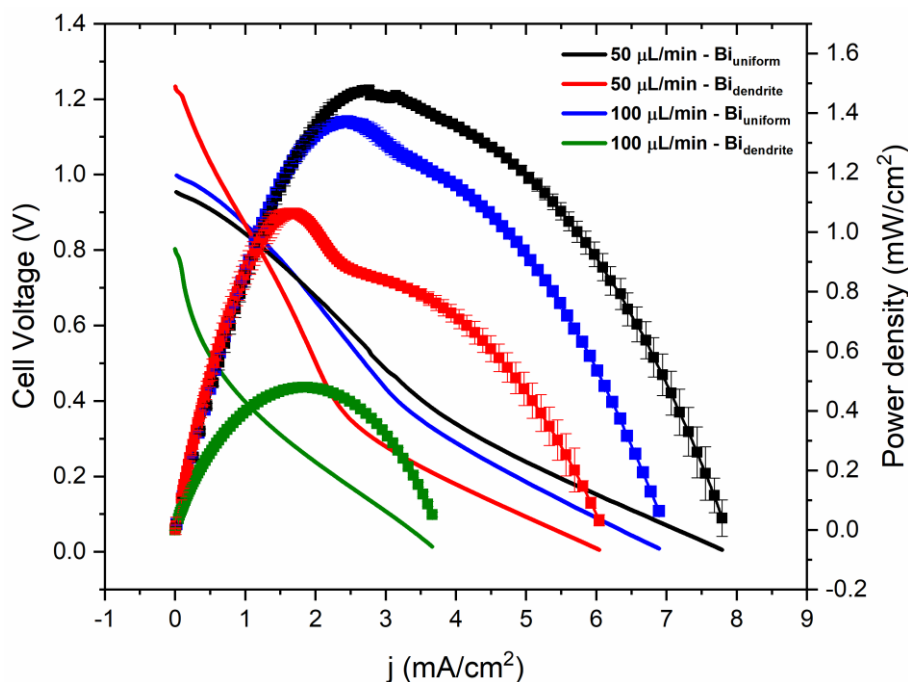


Figure 45: Polarization (left) and power density (right) curves for the μ FC after modifying the anode with Bi via the *in situ* ($\text{Bi}_{\text{uniform}}$) and *operando* ($\text{Bi}_{\text{dendrite}}$) routes, at two different flow rates. Anolyte and catholyte were 0.1 M KOH + 0.1 M glycerol and 1.0 M H_2SO_4 + 0.5 M $\text{Na}_2\text{S}_2\text{O}_8$. Using data from ref.[65].

It is immediately noticeable that the *in situ* modification had significantly better results than the electrode modified with the *operando* methodology at both flow rates. We attribute the lower performance of the *operando* anode to an excessive amount of bismuth oxides on top of the Pt/C nanoparticles that grew into dendrites, as we have previously shown that a bismuth/bismuth oxide electrode is inactive towards the glycerol electrooxidation.⁸² In all scenarios we have a significant increase in both OCV and power density when compared to a cell operating with the bare anode (**figure 46**), at both flow rates.

The highest measured OCV was 1.23 V for the $\text{Bi}_{\text{dendrite}}$ anode at 50 $\mu\text{L}/\text{min}$, however, closer examination of the polarization curve of this cell shows that it is almost a straight line from 1.23 to ca. 0.40 V, after which there is a drastic change in the slope, reflected in the power density curve as a shoulder. This indicates a mass transfer limitation during the operation of the $\text{Bi}_{\text{dendrite}}\text{-}\mu\text{FC}$ ¹⁵⁷, where not enough reactants are reaching the electrode since both the glycerol oxidation and $\text{Na}_2\text{S}_2\text{O}_8$ reduction have fast reaction kinetics.^{158,159} This limitation can be solved by either increasing the convective mass transfer (i.e., increasing the flow rate, seen in **figs. 45** and **46**) or by

increasing the concentration of the ionic species, which in our case would mean increasing the KOH concentration.

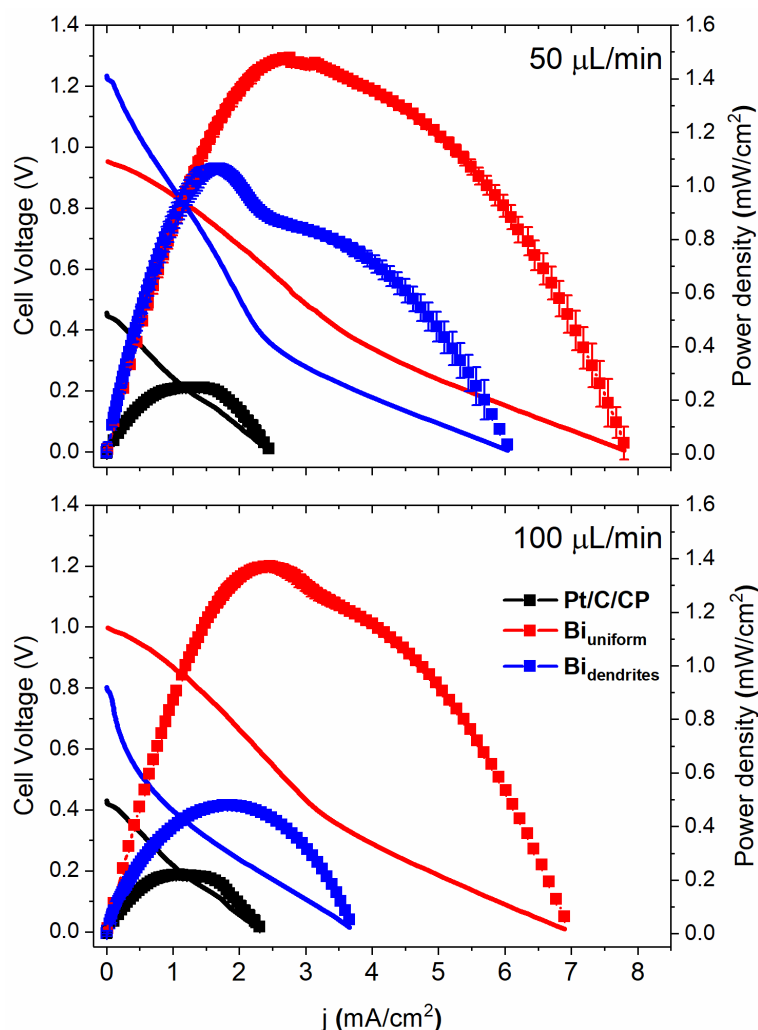


Figure 46: Comparison between the polarization and power density curves of a μ FC operating with the Pt/C/CP (black), $\text{Bi}_{\text{uniform}}$ (red), and $\text{Bi}_{\text{dendrite}}$ (blue) anodes at different flow rates, indicated in the respective images. Anolyte and catholyte were 0.1 M KOH + 0.1 M glycerol and 1.0 M H_2SO_4 + 0.5 M $\text{Na}_2\text{S}_2\text{O}_8$. Using data from ref.[65].

Due to the mass transfer limitation at 50 $\mu\text{L}/\text{min}$, the flow rate of 100 $\mu\text{L}/\text{min}$ was chosen as our optimal operational condition. At this flow rate, measured OCV increased from 0.43 V to 0.80 and 1.0 V for $\text{Bi}_{\text{dendrite}}$ and $\text{Bi}_{\text{uniform}}$, respectively, and P_{max} increased from 0.25 mW/cm^2 to 0.48 and 1.37 mW/cm^2 . Lastly, the soluble products from glycerol were identified and quantified, in addition to quantifying the glycerol consumption. This was done by performing chronoamperometries on the μ FC with the three different anodes at a potential equivalent to $\frac{3}{4}$ of P_{max} . The chronoamperometry data is shown in **figure S20**, while **figure 47** shows the product quantification and

glycerol consumption, with the corresponding chromatograms shown in **figure S21**. This quantification was made after a single passing of the electrolyte, without recirculation.

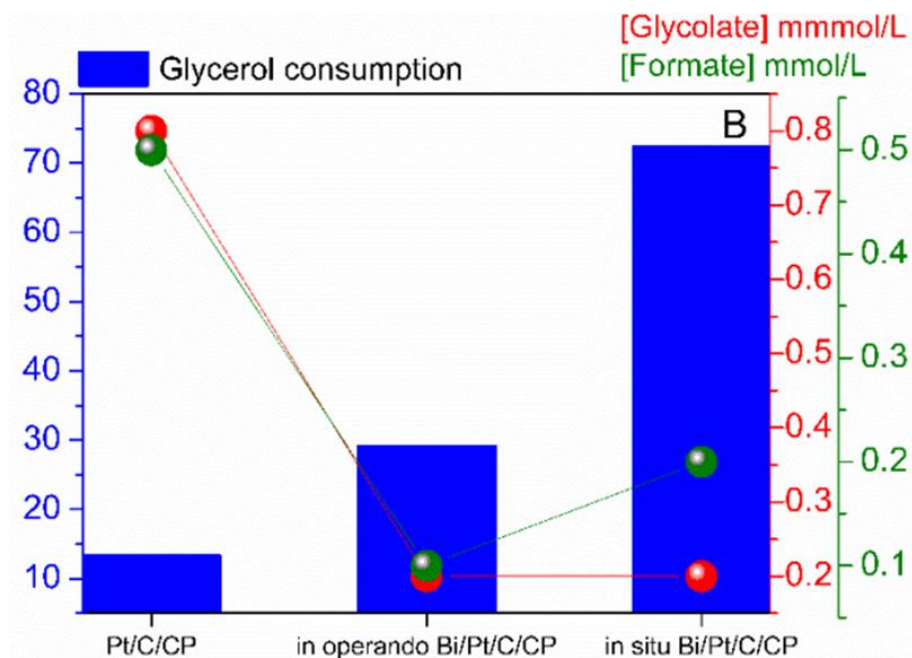


Figure 47: Product concentration and glycerol consumption for each electrode at a potential of $\frac{3}{4} P_{\max}$: 0.33 V for Pt/C/CP, 0.43 V for *operando* Bi-Pt/C/CP, and 0.83 V for *in situ* Bi-Pt/C/CP. Reprinted with permission from ref.[65]. Copyright 2022 American Chemical Society.

The only soluble products detected from glycerol consumption were glycolate and formate. Using the unmodified anode yield the highest concentration of these products, [glycolate] = 86.8 mM and [formate] = 0.5 mM, however glycerol consumption was only 13.4%, indicating that the low power densities extracted from this cell in **fig. 44** are due to partial oxidation of glycerol. After anode modification, glycerol consumption reached 29.2% for the *operando* electrode and an astounding 72.4% for the electrode modified *in situ*. This increased consumption is linked to the total oxidation of glycerol to carbonate, due to the low amounts of glycolate and formate were detected on both cases: for the *in situ*, [glycolate] = [formate] = 0.2 mM, while for *operando* it was [glycolate] = 0.2 mM and [formate] = 0.1 mM.

These results about product quantification are virtually opposite to what was observed for conventional three-electrode cells, as shown in **chapter 4**. We explain these findings based on two factors: i) porous electrodes and ii) forced convective mass transfer. The electrodes on the μ FC are porous, instead of the planar electrodes

used throughout **chapters 2 – 4**. of depositing the catalyst (Pt/C nanoparticles) on a planar surface (glassy carbon electrode), they are being dispersed in a porous matrix, the carbon paper, resulting in a higher surface area and, in turn, a higher activity of the electrodes. Also, in **chapters 2 – 4** the electrolyte used was stagnant, so the mass transfer is governed by diffusion of the species to the electrode surface. When convection is present, mass transfer is improved, resulting in higher currents. This can be achieved by moving the electrode, as seen in experiments using rotating disk electrodes⁷⁰, or by moving the electrolyte, which we are doing in these experiments by pumping it into the μ FC. This convective transport, coupled with porous electrodes, in an arrangement where the electrolyte is forced to cross them (flowing through the electrodes), results in a significant improvement in the sequential and successive collisions of intact and oxidized species. Increasing the number of collisions means we are improving the activity of the electrodes on the fuel cell. This, in turn, means that further oxidation of the soluble products is expected, which explains why (comparatively) very low amounts of glycolate and formate were detected on the Bi-Pt/C/CP anodes, despite the addition of Bi improving the formation of soluble products on planar electrodes, discussed in **chapter 4**. Lastly, a comparison has to be made between the two Bi-Pt/C/CP anodes. The *in situ* electrode has more than double the glycerol consumption shown by the *operando* one, however, it also has a higher amount of formate being generated, when it was expected that an even smaller quantity of products would be detected, following this previous explanation. This apparent discrepancy can be explained on the basis that glycolate is being cleaved into two formate molecules on the *in situ* Bi-Pt/C/CP electrode, due to the successive collisions that are happening on the electrode.

In this chapter, we have successfully applied all knowledge collected during **chapters 2 – 4**, on conventional three-electrode cells, to an electrochemical device (fuel cell). The Bi modification significantly improved the OCV of the cell and the power generated from it, in addition to achieving fuel consumption of over 70%. From HPLC, we showed that a mixture of glycolate and formate are being formed during the cell operation, however, it is not feasible to separate those species from the electrolyte, which also contains a high amount of carbonate, glycerol, and other species.

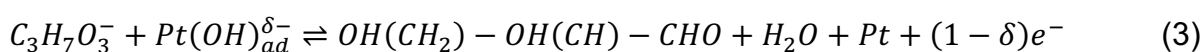
6. Proposal for reaction pathways and suggested mechanism

Based on all the knowledge acquired during **chapters 2 – 5**, published works from our research group^{65,82,83,129,130}, and many others (which will be referenced in the discussions to follow), we propose the reaction pathways shown in **Scheme 1**. Some of the intermediates shown were originally proposed by Garcia et. al.⁸⁶, and our proposed pathways are expanded based on their initial work.

In highly alkaline media glycerol undergoes deprotonation, losing a H_α and forming its corresponding alkoxide, glycerolate.^{38,110} This occurs according to the reaction:



This is a solution-phase reaction, happening solely due to the presence of hydroxyl ions, regardless of the catalyst used. The condition for (1) to happen is that the pH of the solution has to be close to the pKa of glycerol, 14.15. Our 0.1 M NaOH has a pH of 13, and using this pKa value about 6% of the glycerol should exist as the glycerolate ion. The alkoxide species is thought to be more active towards the oxidation reaction than glycerol itself and therefore acts as a precursor for glyceraldehyde formation. This can happen in one of two ways:

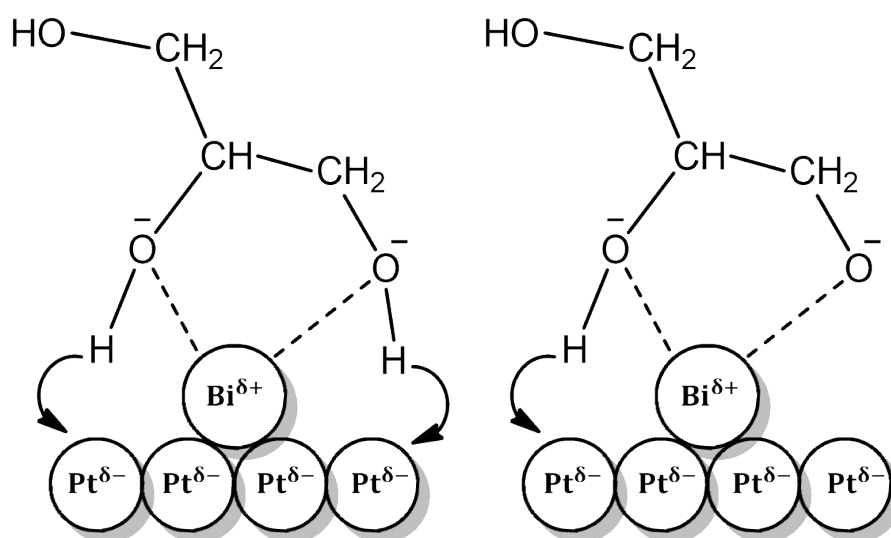


Reaction (2) was originally proposed by Kwon et. al.³⁸, where the alkoxide is converted into the aldehyde through the leaving of a H_β, a chemical reaction that happens mainly due to the highly alkaline media, however, it may still be affected by the catalyst. Reaction (3) was proposed by Shi et. al.¹¹⁰ when studying the role of chemisorbed hydroxyl species on gold electrocatalysts for glycerol conversion in alkaline media.

Based on our proposed scheme, the intermediate formed by adsorption of a primary carbon is converted into glyceraldehyde through reaction (3). This species exists in equilibrium with dihydroxyacetone in alkaline media, where they convert into

one another through an aldose-ketose isomerization.^{160,161} From these species, two routes are possible. They can undergo rearrangement into lactic acid (lactate) in a base-catalyzed dehydration-rearrangement-hydration reaction³⁴, or the glyceraldehyde may undergo further oxidation of its primary carbon, resulting in glyceric acid (glycerate). The chemical oxidation into glyceric acid happens as a parallel, often undesired pathway during their conversion into lactic acid³⁴, whereas glyceraldehyde is readily oxidized into glyceric acid in acidic media on platinum electrodes.⁸⁶ Direct conversion of dihydroxyacetone into glyceric acid was not included in our proposal because it has not been reported during either its chemical (at neutral pH)¹⁶² or electrochemical (at acidic pH)⁸⁶ conversion, so we believe that it first isomerizes into the aldehyde before forming the acid. This hypothesis is backed up by our experiments in **chapter 4**, where we showed that the majority of the dihydroxyacetone added to an alkaline solution is converted into lactic acid instead of glyceric acid, while the opposite happens for the aldehyde.

Before continuing the explanation of **scheme 1**, it is necessary to address the influence of the adatoms. In heterogeneous catalysis, the addition of Bi or Pb to palladium or platinum-based catalysts causes a shift of the reaction selectivity during the oxidation of sugars, where oxidation of secondary hydroxyl groups is preferred to that of the primary groups.^{23,31,163,164} Both Bi and Pb retain a positive partial charge when they are adsorbed on or alloyed into Pt or Pd catalysts, and it is proposed that there is an enediol-type complex formed between the molecule being studied and the positively-charged atoms, as shown in **Scheme 2**, where this complex is made using glycerol and glycerate. For these atoms to retain a positive partial charge, they have to be donating electrons to the Pt or Pd atoms around them (as both Pt and Pd are more electronegative than Bi or Pb), so there is a localized negative charge on the catalyst surface around Bi or Pb atoms.⁶³ The surface metal-organic complex, then, is formed by electrostatic interaction between the oxygen atom of a hydroxyl group and the positively-charged Bi or Pb atoms, while the H atoms of the groups are interacting with the negatively-charged Pt or Pd surface.



Scheme 2: Stabilization of glycerol (left) and glycerate (right) intermediates by forming an enediol intermediate with a positively-charged adatom (Bi, Pb, or Tl), and subsequent interaction of the H atoms of the weakened O–H bonds with the negatively-charged catalyst (Pt or Pd) surface.

This enediol intermediate has been used by previous authors^{22,87} to explain the change in the selectivity of the glycerol oxidation products when using Pt-Bi catalysts in acidic media. However, recently Feng and co-workers¹⁶⁵ have shown that

the O atoms of all three hydroxyl groups are coordinating to the adatom (Bi in their study), with the middle one being coordinated simultaneously to both Bi and Pt, with 2.60 Å for Bi-O and 2.77 Å for Pt-O. In their work, however, they did not consider that Pt atoms around the Bi adatoms would have a partial negative charge, as their Pt-Bi catalyst is supported on mesoporous silica. The idea that nearby Pt atoms retain a partial negative charge around Bi adatoms was originally proposed by Herrero et. al.⁶³ when studying the poison formation during methanol and formic acid oxidation on Bi-modified Pt(111) electrodes, a proposition later confirmed by García-Arárez et. al.^{107,166} when investigating the effect of adatoms on the potential of maximum entropy of Pt(111) electrodes. This potential of maximum entropy is the potential in which there is a maximum disorder of the interfacial water layer near the electrode surface, a parameter closely related to the potential of zero charge of an electrode, an important parameter for electrocatalytic reactions. García-Arárez¹⁰⁷ showed that Bi and Pb adatoms on Pt(111) reduce this potential, a finding that likely can also be extended to Tl adatoms as well, owing to their similar values of electronegativity and work function.^{167,168}

Lastly, it is important to consider the effect of the supporting electrolyte. In the experiments of Herrero et. al.⁶³, they used H₂SO₄ as the supporting electrolyte, and on this electrolyte, glycerol oxidation begins before Pt(OH) species are formed.^{90,94} With HClO₄ instead, oxidation begins on the same potential as Pt(OH) formation.^{87,94} In alkaline media, where hydroxides of the alkali metals are used as the supporting electrolyte, oxidation begins after the formation of surface Pt(OH)¹⁶⁹, however, in these conditions there is also the presence of non-covalent interactions in the form of hydrated metal cations near the electrode surface.¹⁷⁰ The supporting cation (Li⁺, Na⁺ or K⁺) has a direct effect on the activity of Pt towards glycerol oxidation.^{171,172}

Based on the aforementioned discussion, we propose the following scenario is happening in our experiments, focusing on the effects caused by Bi, Pb, and Tl.

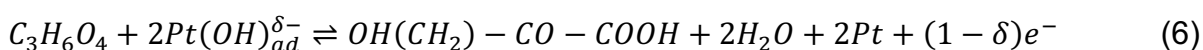
The adatoms adsorbing on platinum retain a positive partial charge while donating electrons to nearby Pt atoms. This causes a lowering of the potential of maximum entropy of platinum, resulting in the interfacial water molecules orienting themselves with the oxygen atoms pointing towards the positive-charged adlayer in our chosen potential window (0.20 – 0.85 V vs RHE). Concerning the non-covalent interactions, the hydrated cations would interact only with this ordered interfacial water layer, with hydrogen atoms pointing towards them. Therefore, it is unlikely that they

would affect the activity of our Pt-Adatom electrodes, however, we cannot fully discard this possibility, as cation effects were not investigated in this work. At potentials as low as 0.20 V vs RHE glycerol adsorbates are already present on the Pt surface⁸⁶, however on Pt-adatom surfaces a different behavior is observed, where these adsorbates adsorb preferentially on more open basal planes.⁸⁷ These glycerol adsorbates are likely interacting with our Pt-Adatom catalysts through the enediol intermediate in **scheme 2**, by displacing the H₂O/OH⁻ molecules at the interface. By increasing the applied potential, glycerol is converted into dihydroxyacetone by oxidation to the middle hydroxyl group, as the H_β is more susceptible to forming a Pt – H bond than the H_α, while glyceroate becomes glyceraldehyde, due to the reactivity of the deprotonated primary hydroxy group. Increasing the potential also causes the adatoms to oxidize, as we saw in **chapter 2**, in addition to the formation of platinum oxides, and these metal-oxygen bonds are formed with the remaining H₂O/OH⁻ molecules present in the interfacial layer.

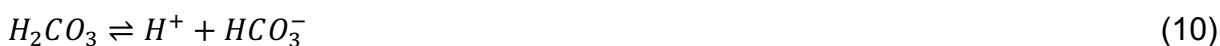
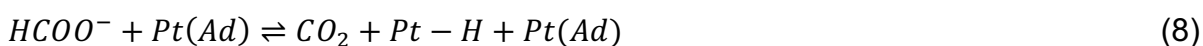
As previously explained, both glyceraldehyde and dihydroxyacetone can be chemically converted into either glyceric or lactic acid. However, there is still the possibility that electrochemical conversion is also happening, at least to a minimum extent, as both species can be oxidized by Pt electrodes.⁸⁶ For this reason, we have added this as a possible reaction pathway in **scheme 1**. Reaction (4) represents the chemical conversion of glyceraldehyde into glyceric acid, while reaction (5) is the possible electrochemical pathway.



Glyceric acid can be chemically oxidized into hydroxypyruvic acid, but it is unlikely to do so in highly alkaline media, as it favors the formation of other species.^{29,162} For this reason, we are only considering its electrochemical conversion, since it was observed on Pt-Pb electrodes, which should happen according to reaction (6).



Also, glyceric acid is mildly electroactive on Pt-Adatom electrodes (**figure S22**), and it may undergo C-C bond breaking, producing glycolic and formic acid as products (which is likely what happened in **chapter 5**). The only possible oxidation pathway for formic acid is to be oxidized into CO₂, which is observed as carbonate in an alkaline medium, according to reactions (7) – (11).¹⁰⁰ For glycolic acid, it can be further oxidized into oxalic acid via a multistep reaction involving 4 electrons, or broken down into two molecules of formic acid (**chapter 5**).



Other possible intermediates are described as follows. Adsorption through two neighboring carbons results in two possibilities, oxidation of the secondary hydroxyl into dihydroxyacetone⁸⁶ or bond-breaking, resulting in glycolic and formic acid. The possible reaction pathways for these molecules were already discussed.

The intermediate formed by adsorption on both primary carbons has been previously thought to be inactive on Pt surfaces⁸⁶, however, we consider it to be active on Pt-Adatom electrodes, as it would explain the observation of tartronic acid, by oxidizing both terminal -CH₂OH groups into -COOH. Besides this intermediate, tartronate may also be generated from the chemical oxidation of glyceric acid in an alkaline medium.²⁹ This would explain the small indication of a tartronate peak seen on the chromatogram of the clean Pt electrode, in **fig. 32** of **chapter 4**, and since it has a much lower anodic current than Pt-Bi or Pt-Pb (see **fig. 34** of **chapter 4**), we can infer that electrochemical production of tartronate on Pt is negligible, while the opposite holds true for Pt-Bi and Pt-Pb.

The last intermediate, formed by adsorption of all three carbon atoms, can only undergo C-C bond breaking and resulting in CO_{ads} on the electrode surface.

Experiments showed that no CO_{ads} is formed on the electrode surface after adatom modification (**fig. 24** in **chapter 3**), so this intermediate may only be generated on the unmodified platinum surface. It is important to highlight, however, that this intermediate may not be the only route for CO_{ads} formation on the clean electrode. In acidic media, it has been shown that glyceraldehyde can readsorb on the Pt surface, and be oxidized to glyceric acid or suffer a C-C bond scission, resulting in CO_{ads} and a C_2 product (likely glycolic acid).¹⁷³ If the aldehyde is being electrochemically oxidized in our experimental conditions, some of it is likely undergoing C-C bond breaking instead of being oxidized to glyceric acid. The CO_{ads} is eventually oxidized into CO_2 at high enough potentials and then detected as carbonate, following reactions (9) – (11).

7. Conclusions and perspectives

In summary, we modified platinum-based electrocatalysts with elements from the p-block and studied how this affected the activity and selectivity of the electrochemical conversion of glycerol.

An initial electrochemical investigation showed that only three elements, bismuth, lead, and thallium, improved the activity of these catalysts. Using single crystals, we showed that they lower the oxidation onset potential on the three main basal planes, and especially improve the activity of Pt(110), the most open plane. These experiments also showed that the adatoms decreased the rate of poisoning on the electrodes. With *in situ* FTIR, we showed that they not only block the formation of CO_{ads} on the Pt surface but also decrease the C-C bond breaking. Without the blocking by CO, deactivation is likely coming from strongly adsorbed glycerol derivatives. We also used XAS to study how the oxidation state of Pt changed with both applied potential and the presence of adatoms, but no changes to the absorption spectra were observed, regardless of the experimental conditions, and later we concluded that the technique was not suitable to our objectives.

We identified the soluble oxidation products using HPLC. There was an overall increase in the concentration of soluble products being generated, after the adatom modification, with two new products being detected: tartronate, on both Pt-Bi and Pt-Pb, and hydroxypyruvate, on Pt-Pb. We used the combined information, derived mainly from *in situ* FTIR and HPLC, to propose several reaction pathways for glycerol electrooxidation in alkaline media.

Lastly, we were able to successfully transfer all knowledge acquired from experiments performed in glass cells to electrochemical devices. We synthesized Pt/C nanoparticles to be used on the anode of a glycerol-based fuel cell and then modified the electrode with Bi adatoms. We had an increase in glycerol consumption from around 13% to 70%, higher cell voltages, and power generated from the device. This improved performance was accompanied by the production of formic and glycolic acid from the anode, proving that it is possible to generate value-added products and energy from the same device, however, such conditions are not feasible for a more scale-up process.

With this work, we have improved the general knowledge surrounding the electrochemical valorization of glycerol. We showed that it is possible to significantly improve catalyst activity, while blocking the formation of poisonous species, by adding trace amounts of p-block elements to its surface. This knowledge was then applied to a fuel cell, where a significant improvement in power generation and fuel consumption was observed. Concerning the reaction mechanism, we have proposed new reaction pathways that add up to what has been currently built, and also took extra steps to differentiate between electrochemical and chemical reactions, the latter one playing a major role when in alkaline electrolytes.

In the foreseeable future, it is possible to continue the investigation of the platinum-adatom systems, using a combination of computational and spectroscopical techniques. We do not fully understand why only three elements, out of nine investigated, improved the electrode activity. All species block the formation of CO_{ads} on platinum, a third-body effect. The retention of a positive charge and the enediol intermediate is not enough to explain our findings, as other elements should retain a positive charge while adsorbed on platinum, and yet they either decreased or had little effect on its activity.

Concerning electrochemical devices, it is possible to continue the investigation of Pt-Adatom anodes on fuel cells, experimenting with different types of adatoms and conditions for the anode modification. Likely, these catalysts would significantly improve the performance of electrolyzers, since they further decrease the already low onset potential of glycerol oxidation. This is a highly desirable scenario, where this reaction could be used to improve hydrogen generation on the cathode side of the device (or another reaction of interest, such as products from CO_2 reduction), in addition to generating a mixture of value-added products on the anode.

8. References

- (1) Rohde, R. A.; Hausfather, Z. The Berkeley Earth Land/Ocean Temperature Record. *Earth Syst. Sci. Data* **2020**, *12* (4), 3469–3479. <https://doi.org/10.5194/essd-12-3469-2020>.
- (2) Oliveira, A. M.; Beswick, R. R.; Yan, Y. A Green Hydrogen Economy for a Renewable Energy Society. *Curr. Opin. Chem. Eng.* **2021**, *33*, 100701. <https://doi.org/10.1016/j.coche.2021.100701>.
- (3) *Global Hydrogen Review 2021*; OECD, 2021. <https://doi.org/10.1787/39351842-en>.
- (4) Yu, M.; Budiyanoto, E.; Tüysüz, H. Principles of Water Electrolysis and Recent Progress in Cobalt-, Nickel-, and Iron-Based Oxides for the Oxygen Evolution Reaction. *Angew. Chemie Int. Ed.* **2022**, *61* (1). <https://doi.org/10.1002/anie.202103824>.
- (5) Smolinka, T.; Bergmann, H.; Garche, J.; Kusnezoff, M. The History of Water Electrolysis from Its Beginnings to the Present. In *Electrochemical Power Sources: Fundamentals, Systems, and Applications*; Elsevier B.V., 2022; pp 83–164. <https://doi.org/10.1016/b978-0-12-819424-9.00010-0>.
- (6) Ouimet, R. J.; Glenn, J. R.; De Porcellinis, D.; Motz, A. R.; Carmo, M.; Ayers, K. E. The Role of Electrocatalysts in the Development of Gigawatt-Scale PEM Electrolyzers. *ACS Catal.* **2022**, *12*, 6159–6171. <https://doi.org/10.1021/acscatal.2c00570>.
- (7) Miller, H. A.; Bouzek, K.; Hnat, J.; Loos, S.; Bernäcker, C. I.; Weißgärber, T.; Röntzsch, L.; Meier-Haack, J. Green Hydrogen from Anion Exchange Membrane Water Electrolysis: A Review of Recent Developments in Critical Materials and Operating Conditions. *Sustain. Energy Fuels* **2020**, *4* (5), 2114–2133. <https://doi.org/10.1039/c9se01240k>.
- (8) Zhao, H.; Lu, D.; Wang, J.; Tu, W.; Wu, D.; Koh, S. W.; Gao, P.; Xu, Z. J.; Deng, S.; Zhou, Y.; You, B.; Li, H. Raw Biomass Electroreforming Coupled to Green Hydrogen Generation. *Nat. Commun.* **2021**, *12* (1), 1–10. <https://doi.org/10.1038/s41467-021-22250-9>.
- (9) Hibino, T.; Kobayashi, K.; Ito, M.; Ma, Q.; Nagao, M.; Fukui, M.; Teranishi, S. Efficient Hydrogen Production by Direct Electrolysis of Waste Biomass at Intermediate Temperatures. *ACS Sustain. Chem. Eng.* **2018**, *6* (7), 9360–9368.

- <https://doi.org/10.1021/acssuschemeng.8b01701>.
- (10) Holade, Y.; Tuleushova, N.; Tingry, S.; Servat, K.; Napporn, T. W.; Guesmi, H.; Cornu, D.; Kokoh, K. B. Recent Advances in the Electrooxidation of Biomass-Based Organic Molecules for Energy, Chemicals and Hydrogen Production. *Catal. Sci. Technol.* **2020**, *10* (10), 3071–3112. <https://doi.org/10.1039/C9CY02446H>.
- (11) Li, R.; Xiang, K.; Peng, Z.; Zou, Y.; Wang, S. Recent Advances on Electrolysis for Simultaneous Generation of Valuable Chemicals at Both Anode and Cathode. *Adv. Energy Mater.* **2021**, *11* (46), 2102292. <https://doi.org/10.1002/aenm.202102292>.
- (12) Lamy, C. Electrocatalytic Oxidation of Low Weight Oxygenated Organic Compounds: A Review on Their Use as a Chemical Source to Produce Either Electricity in a Direct Oxidation Fuel Cell or Clean Hydrogen in an Electrolysis Cell. *J. Electroanal. Chem.* **2020**, *875*, 114426. <https://doi.org/10.1016/j.jelechem.2020.114426>.
- (13) Costa, A. A. F. da; de Oliveira, A. de N.; Esposito, R.; Len, C.; Luque, R.; Noronha, R. C. R.; Rocha Filho, G. N. da; Nascimento, L. A. S. do. Glycerol and Catalysis by Waste/Low-Cost Materials—A Review. *Catalysts* **2022**, *12* (5), 570. <https://doi.org/10.3390/catal12050570>.
- (14) Guschakowski, M.; Schröder, U. Direct and Indirect Electrooxidation of Glycerol to Value-Added Products. *ChemSusChem* **2021**, 1–11. <https://doi.org/10.1002/cssc.202100556>.
- (15) Othman, P. N. A. M.; Karim, N. A.; Kamarudin, S. K. Research and Innovation in the Electrocatalyst Development toward Glycerol Oxidation Reaction. *Int. J. Energy Res.* **2021**, *45* (9), 12693–12727. <https://doi.org/10.1002/er.6712>.
- (16) Fan, L.; Liu, B.; Liu, X.; Senthilkumar, N.; Wang, G.; Wen, Z. Recent Progress in Electrocatalytic Glycerol Oxidation. *Energy Technol.* **2020**, *2000804*, 2000804. <https://doi.org/10.1002/ente.202000804>.
- (17) Houache, M. S. E.; Hughes, K.; Baranova, E. A. Study on Catalyst Selection for Electrochemical Valorization of Glycerol. *Sustain. Energy Fuels* **2019**, *3* (8), 1892–1915. <https://doi.org/10.1039/c9se00108e>.
- (18) Coutanceau, C.; Baranton, S.; Kouamé, R. S. B. Selective Electrooxidation of Glycerol Into Value-Added Chemicals : A Short Overview. *Front. Chem.* **2019**, *7* (February), 1–15. <https://doi.org/10.3389/fchem.2019.00100>.

- (19) Coutanceau, C.; Baranton, S. Electrochemical Conversion of Alcohols for Hydrogen Production: A Short Overview. *Wiley Interdiscip. Rev. Energy Environ.* **2016**, *5* (4), 388–400. <https://doi.org/10.1002/wene.193>.
- (20) Katryniok, B.; Kimura, H.; Skrzyńska, E.; Girardon, J.-S.; Fongarland, P.; Capron, M.; Ducoulombier, R.; Mimura, N.; Paul, S.; Dumeignil, F. Selective Catalytic Oxidation of Glycerol: Perspectives for High Value Chemicals. *Green Chem.* **2011**, *13* (8), 1960. <https://doi.org/10.1039/c1gc15320j>.
- (21) Lidia, S. R.; Stanisław, B. Production of Dihydroxyacetone from an Aqueous Solution of Glycerol in the Reaction Catalyzed by an Immobilized Cell Preparation of Acetic Acid Bacteria *Gluconobacter Oxydans* ATCC 621. *Eur. Food Res. Technol.* **2012**, *235* (6), 1125–1132. <https://doi.org/10.1007/s00217-012-1846-0>.
- (22) Kwon, Y.; Birdja, Y.; Spanos, I.; Rodriguez, P.; Koper, M. T. M. Highly Selective Electro-Oxidation of Glycerol to Dihydroxyacetone on Platinum in the Presence of Bismuth. *ACS Catal.* **2012**, *2* (5), 759–764. <https://doi.org/10.1021/cs200599g>.
- (23) Kimura, H.; Tsuto, K.; Wakisaka, T.; Kazumi, Y.; Inaya, Y. Selective Oxidation of Glycerol on a Platinum-Bismuth Catalyst. *Appl. Catal. A, Gen.* **1993**, *96* (2), 217–228. [https://doi.org/10.1016/0926-860X\(90\)80011-3](https://doi.org/10.1016/0926-860X(90)80011-3).
- (24) Garcia, R.; Besson, M.; Gallezot, P. Chemoselective Catalytic Oxidation of Glycerol with Air on Platinum Metals. *Appl. Catal. A, Gen.* **1995**, *127* (1–2), 165–176. [https://doi.org/10.1016/0926-860X\(95\)00048-8](https://doi.org/10.1016/0926-860X(95)00048-8).
- (25) Clough, S. R. Glyceraldehyde. In *Encyclopedia of Toxicology*; Elsevier, 2005; pp 448–449. <https://doi.org/10.1016/B0-12-369400-0/00456-7>.
- (26) Habe, H.; Fukuoka, T.; Kitamoto, D.; Sakaki, K. Biotechnological Production of D-Glyceric Acid and Its Application. *Appl. Microbiol. Biotechnol.* **2009**, *84* (3), 445–452. <https://doi.org/10.1007/s00253-009-2124-3>.
- (27) Zhou, X.; Yan, H.; Feng, X.; Zhao, H.; Liu, Y.; Chen, X.; Chen, D.; Yang, C. Producing Glyceric Acid from Glycerol via Integrating Vacuum Dividing Wall Columns: Conceptual Process Design and Techno-Economic-Environmental Analysis. *Green Chem.* **2021**, *23* (10), 3664–3676. <https://doi.org/10.1039/d1gc00327e>.
- (28) Kwon, Y.; Schouten, K. J. P.; Koper, M. T. M. Mechanism of the Catalytic Oxidation of Glycerol on Polycrystalline Gold and Platinum Electrodes.

- ChemCatChem* **2011**, *3* (7), 1176–1185.
<https://doi.org/10.1002/cctc.201100023>.
- (29) Fordham, P.; Besson, M.; Gallezot, P. Selective Catalytic Oxidation of Glyceric Acid to Tartronic and Hydroxypyruvic Acids. *Appl. Catal. A Gen. Gen.* **1995**, *133*, L179–L184.
- (30) Li, T.; Harrington, D. A. An Overview of Glycerol Electrooxidation Mechanisms on Pt, Pd and Au. *ChemSusChem* **2021**, *14* (6), 1472–1495.
<https://doi.org/10.1002/cssc.202002669>.
- (31) Gallezot, P. Selective Oxidation with Air on Metal Catalysts. *Catal. Today* **1997**, *37*, 405–418.
- (32) Abbadi, A.; Van Bekkum, H. Selective Chemo-Catalytic Routes for the Preparation of β -Hydroxypyruvic Acid. *Applied Catalysis A: General*. 1996, pp 113–122. [https://doi.org/10.1016/S0926-860X\(96\)00229-3](https://doi.org/10.1016/S0926-860X(96)00229-3).
- (33) Zalineeva, A.; Serov, A.; Padilla, M.; Martinez, U.; Artyushkova, K.; Baranton, S.; Coutanceau, C.; Atanassov, P. B. Glycerol Electrooxidation on Self-Supported Pd₁Sn_x Nanoparticules. *Appl. Catal. B Environ.* **2015**, *176–177*, 429–435.
<https://doi.org/10.1016/j.apcatb.2015.04.037>.
- (34) Purushothaman, R. K. P.; van Haveren, J.; van Es, D. S.; Melián-Cabrera, I.; Meeldijk, J. D.; Heeres, H. J. An Efficient One Pot Conversion of Glycerol to Lactic Acid Using Bimetallic Gold-Platinum Catalysts on a Nanocrystalline CeO₂ Support. *Appl. Catal. B Environ.* **2014**, *147*, 92–100.
<https://doi.org/10.1016/j.apcatb.2013.07.068>.
- (35) Jem, K. J.; Tan, B. The Development and Challenges of Poly (Lactic Acid) and Poly (Glycolic Acid). *Adv. Ind. Eng. Polym. Res.* **2020**, *3* (2), 60–70.
<https://doi.org/10.1016/j.aiepr.2020.01.002>.
- (36) Deshmukh, G.; Manyar, H. Production Pathways of Acetic Acid and Its Versatile Applications in the Food Industry. In *Biotechnological Applications of Biomass*; IntechOpen, 2021; p 13. <https://doi.org/10.5772/intechopen.92289>.
- (37) Dai, C.; Sun, L.; Liao, H.; Khezri, B.; Webster, R. D.; Fisher, A. C.; Xu, Z. J. An Efficient One Pot Conversion of Glycerol to Lactic Acid Using Bimetallic Gold-Platinum Catalysts on a Nanocrystalline CeO₂ Support. *J. Catal.* **2017**, *356*, 14–21. <https://doi.org/10.1016/j.jcat.2017.10.010>.
- (38) Kwon, Y.; Lai, S. C. S.; Rodriguez, P.; Koper, M. T. M. Electrocatalytic Oxidation of Alcohols on Gold in Alkaline Media: Base or Gold Catalysis? *J. Am. Chem.*

- Soc.* **2011**, 133 (18), 6914–6917. <https://doi.org/10.1021/ja200976j>.
- (39) Pozdniakov, M. A.; Zhuk, I. V.; Lyapunova, M. V.; Salikov, A. S.; Botvin, V. V.; Filimoshkin, A. G. Glyoxylic Acid: Synthesis, Isolation, and Crystallization. *Russ. Chem. Bull.* **2019**, 68 (3), 472–479. <https://doi.org/10.1007/s11172-019-2442-2>.
- (40) Schuler, E.; Demetriou, M.; Shiju, N. R.; Gruter, G. J. M. Towards Sustainable Oxalic Acid from CO₂ and Biomass. *ChemSusChem* **2021**, 14 (18), 3636–3664. <https://doi.org/10.1002/cssc.202101272>.
- (41) M. Walgode, P.; Lucas, L. C.; Rui, R. P.; E. Rodrigues, A. Dihydroxyacetone Production: From Glycerol Catalytic Oxidation with Commercial Catalysts to Chromatographic Separation. *Ind. Eng. Chem. Res.* **2021**, 60 (29), 10551–10565. <https://doi.org/10.1021/acs.iecr.1c00275>.
- (42) Arcanjo, M. R. A.; Silva, I. J.; Cavalcante, C. L.; Iglesias, J.; Morales, G.; Paniagua, M.; Melero, J. A.; Vieira, R. S. Glycerol Valorization: Conversion to Lactic Acid by Heterogeneous Catalysis and Separation by Ion Exchange Chromatography. *Biofuels, Bioprod. Biorefining* **2020**, 14 (2), 357–370. <https://doi.org/10.1002/bbb.2055>.
- (43) Beltrán-Prieto, J. C.; Pecha, J.; Kašpárková, V.; Kolomazník, K. Development of an HPLC Method for the Determination of Glycerol Oxidation Products. *J. Liq. Chromatogr. Relat. Technol.* **2013**, 36 (19), 2758–2773. <https://doi.org/10.1080/10826076.2012.725695>.
- (44) Li, Y.; Wei, X.; Chen, L.; Shi, J.; He, M. Nickel-Molybdenum Nitride Nanoplate Electrocatalysts for Concurrent Electrolytic Hydrogen and Formate Productions. *Nat. Commun.* **2019**, 10 (1), 1–12. <https://doi.org/10.1038/s41467-019-13375-z>.
- (45) Guima, K.-E.; Coelho, P.-H. L.; Trindade, M. A. G.; Martins, C. A. 3D-Printed Glycerol Microfluidic Fuel Cell. *Lab Chip* **2020**, 20 (12), 2057–2061. <https://doi.org/10.1039/D0LC00351D>.
- (46) Medford, A. J.; Vojvodic, A.; Hummelshøj, J. S.; Voss, J.; Abild-Pedersen, F.; Studt, F.; Bligaard, T.; Nilsson, A.; Nørskov, J. K. From the Sabatier Principle to a Predictive Theory of Transition-Metal Heterogeneous Catalysis. *J. Catal.* **2015**, 328, 36–42. <https://doi.org/10.1016/j.jcat.2014.12.033>.
- (47) She, Z. W.; Kibsgaard, J.; Dickens, C. F.; Chorkendorff, I.; Nørskov, J. K.; Jaramillo, T. F. Combining Theory and Experiment in Electrocatalysis: Insights into Materials Design. *Science* (80-.). **2017**, 355 (6321). <https://doi.org/10.1126/science.aad4998>.

- (48) Resasco, J.; Abild-Pedersen, F.; Hahn, C.; Bao, Z.; Koper, M. T. M.; Jaramillo, T. F. Enhancing the Connection between Computation and Experiments in Electrocatalysis. *Nat. Catal.* **2022**, *5* (5), 374–381. <https://doi.org/10.1038/s41929-022-00789-0>.
- (49) Hirasawa, S.; Nakagawa, Y.; Tomishige, K. Selective Oxidation of Glycerol to Dihydroxyacetone over a Pd-Ag Catalyst. *Catal. Sci. Technol.* **2012**, *2* (6), 1150–1152. <https://doi.org/10.1039/c2cy20062g>.
- (50) Carrettin, S.; McMorn, P.; Johnston, P.; Griffin, K.; Hutchings, G. J. Selective Oxidation of Glycerol to Glyceric Acid Using a Gold Catalyst in Aqueous Sodium Hydroxide. *Chem. Commun. (Camb.)* **2002**, No. 7, 696–697. <https://doi.org/10.1039/b201112n>.
- (51) Chornaja, S.; Dubencov, K.; Kampars, V.; Stepanova, O.; Zhizhkun, S.; Serga, V.; Kulikova, L. Oxidation of Glycerol with Oxygen in Alkaline Aqueous Solutions in the Presence of Supported Palladium Catalysts Prepared by the Extractive-Pyrolytic Method. *React. Kinet. Mech. Catal.* **2013**, *108* (2), 341–357. <https://doi.org/10.1007/s11144-012-0516-3>.
- (52) Lakshmanan, P.; Upare, P. P.; Le, N.-T.; Hwang, Y. K.; Hwang, D. W.; Lee, U.-H.; Kim, H. R.; Chang, J.-S. Facile Synthesis of CeO₂-Supported Gold Nanoparticle Catalysts for Selective Oxidation of Glycerol into Lactic Acid. *Appl. Catal. A Gen.* **2013**, *468*, 260–268. <https://doi.org/10.1016/j.apcata.2013.08.048>.
- (53) Bełtowska-Brzezinska, M. Untersuchungen Zum Mechanismus Der Elektrochemischen Oxidation von Alkoholen an Gold. *Electrochim. Acta* **1980**, *25* (3), 267–271.
- (54) Shen, P. K.; Xu, C. Alcohol Oxidation on Nanocrystalline Oxide Pd/C Promoted Electrocatalysts. *Electrochem. commun.* **2006**, *8* (1), 184–188. <https://doi.org/10.1016/j.elecom.2005.11.013>.
- (55) Xu, C.; Tian, Z.; Shen, P.; Jiang, S. P. Oxide (CeO₂, NiO, Co₃O₄ and Mn₃O₄)-Promoted Pd/C Electrocatalysts for Alcohol Electrooxidation in Alkaline Media. *Electrochim. Acta* **2008**, *53* (5), 2610–2618. <https://doi.org/10.1016/j.electacta.2007.10.036>.
- (56) Bambagioni, V.; Bianchini, C.; Marchionni, A.; Filippi, J.; Vizza, F.; Teddy, J.; Serp, P.; Zhiani, M. Pd and Pt–Ru Anode Electrocatalysts Supported on Multi-Walled Carbon Nanotubes and Their Use in Passive and Active Direct Alcohol

- Fuel Cells with an Anion-Exchange Membrane (Alcohol=methanol, Ethanol, Glycerol). *J. Power Sources* **2009**, *190* (2), 241–251. <https://doi.org/10.1016/j.jpowsour.2009.01.044>.
- (57) Simões, M.; Baranton, S.; Coutanceau, C. Electro-Oxidation of Glycerol at Pd Based Nano-Catalysts for an Application in Alkaline Fuel Cells for Chemicals and Energy Cogeneration. *Appl. Catal. B Environ.* **2010**, *93* (3–4), 354–362. <https://doi.org/10.1016/j.apcatb.2009.10.008>.
- (58) Kwon, Y.; Hersbach, T. J. P.; Koper, M. T. M. Electro-Oxidation of Glycerol on Platinum Modified by Adatoms: Activity and Selectivity Effects. *Top. Catal.* **2014**, *57* (14–16), 1272–1276. <https://doi.org/10.1007/s11244-014-0292-6>.
- (59) Clavilier, J.; Feliu, J. M.; Aldaz, A. An Irreversible Structure Sensitive Adsorption Step in Bismuth Underpotential Deposition at Platinum Electrodes. *J. Electroanal. Chem. Interfacial Electrochem.* **1988**, *243* (2), 419–433. [https://doi.org/10.1016/0022-0728\(88\)80045-7](https://doi.org/10.1016/0022-0728(88)80045-7).
- (60) Clavilier, J.; Fernandez-Vega, A.; Feliu, J. M.; Aldaz, A. Heterogeneous Electrocatalysis on Well Defined Platinum Surfaces Modified by Controlled Amounts of Irreversibly Adsorbed Adatoms. Part I. Formic Acid Oxidation on the Pt(111)-Bi System. *J. Electroanal. Chem. Interfacial Electrochem.* **1989**, *258* (1), 89–100. [https://doi.org/10.1016/0022-0728\(89\)85164-2](https://doi.org/10.1016/0022-0728(89)85164-2).
- (61) Clavilier, J.; Fernandez-Vega, A.; Feliu, J. M.; Aldaz, A. Heterogeneous Electrocatalysis on Well Defined Platinum Surfaces Modified by Controlled Amounts of Irreversibly Adsorbed Adatoms. Part III. Formic Acid Oxidation on the Pt(100)-Bi System. *J. Electroanal. Chem. Interfacial Electrochem.* **1989**, *261* (1), 113–125. [https://doi.org/10.1016/0022-0728\(89\)87130-X](https://doi.org/10.1016/0022-0728(89)87130-X).
- (62) Clavilier, J.; Orts, J. M.; Feliu, J. M.; Aldaz, A. Study of the Conditions for Irreversible Adsorption of Lead at Pt(h,k,l) Electrodes. *J. Electroanal. Chem.* **1990**, *293* (1–2), 197–208. [https://doi.org/10.1016/0022-0728\(90\)80063-C](https://doi.org/10.1016/0022-0728(90)80063-C).
- (63) Herrero, E.; Fernandez-Vega, A.; Feliu, J. M.; Aldaz, A. Poison Formation Reaction from Formic Acid and Methanol on Pt(111) Electrodes Modified by Irreversibly Adsorbed Bi and As. *J. Electroanal. Chem.* **1993**, *350*, 73–88.
- (64) Climent, V.; García-Arez, N.; Feliu, J. M. Clues for the Molecular-Level Understanding of Electrocatalysis on Single-Crystal Platinum Surfaces Modified by p-Block Adatoms. In *Fuel Cell Catalysis*; Koper, M. T. M., Wieckowski, A., Eds.; John Wiley & Sons, Inc.: Hoboken, NJ, USA, 2008; pp 209–244.

- <https://doi.org/10.1002/9780470463772.ch7>.
- (65) de Souza, M. B. C.; Guima, K.; Fernández, P. S.; Martins, C. A. Glycerol Is Converted into Energy and Carbonyl Compounds in a 3D-Printed Microfluidic Fuel Cell: In Situ and In Operando Bi-Modified Pt Anodes. *ACS Appl. Mater. Interfaces* **2022**, *14* (22), 25457–25465. <https://doi.org/10.1021/acsami.2c04313>.
- (66) Houache, M. S. E.; Cossar, E.; Ntais, S.; Baranova, E. A. Electrochemical Modification of Nickel Surfaces for Efficient Glycerol Electrooxidation. *J. Power Sources* **2018**, *375*, 310–319. <https://doi.org/10.1016/j.jpowsour.2017.08.089>.
- (67) Andreu, T.; Mallafré, M.; Molera, M.; Sarret, M.; Oriol, R.; Sirés, I. Effect of Thermal Treatment of Nickel-cobalt Electrocatalyst for Glycerol Oxidation. *ChemElectroChem* **2022**, *202200100*, 1–7. <https://doi.org/10.1002/celec.202200100>.
- (68) Houache, M. S. E.; Hughes, K.; Safari, R.; Botton, G. A.; Baranova, E. A. Modification of Nickel Surfaces by Bismuth: Effect on Electrochemical Activity and Selectivity toward Glycerol. *ACS Appl. Mater. Interfaces* **2020**, *12* (13), 15095–15107. <https://doi.org/10.1021/acsami.9b22378>.
- (69) Habibi, B.; Delnavaz, N. Electrooxidation of Glycerol on Nickel and Nickel Alloy (Ni–Cu and Ni–Co) Nanoparticles in Alkaline Media. *RSC Adv.* **2016**, *6* (38), 31797–31806. <https://doi.org/10.1039/C5RA26006J>.
- (70) Bard, A. J.; Faulkner, L. R. *Electrochemical Methods - Fundamentals and Applications*, 2nd ed.; Harris, D., Swain, E., Robey, C., Aiello, E., Eds.; John Wiley & Sons, Inc: New York, NY, 2000.
- (71) Elgrishi, N.; Rountree, K. J.; McCarthy, B. D.; Rountree, E. S.; Eisenhart, T. T.; Dempsey, J. L. A Practical Beginner's Guide to Cyclic Voltammetry. *J. Chem. Educ.* **2018**, *95* (2), 197–206. <https://doi.org/10.1021/acs.jchemed.7b00361>.
- (72) Clavilier, J.; Faure, R.; Guinet, G.; Durand, R. Preparation of Monocrystalline Pt Microelectrodes and Electrochemical Study of the Plane Surfaces Cut in the Direction of the {111} and {110} Planes. *J. Electroanal. Chem.* **1979**, *107* (1), 205–209. [https://doi.org/10.1016/S0022-0728\(79\)80022-4](https://doi.org/10.1016/S0022-0728(79)80022-4).
- (73) Vidal-Iglesias, F. J.; Arán-Ais, R. M.; Solla-Gullón, J.; Herrero, E.; Feliu, J. M. Electrochemical Characterization of Shape-Controlled Pt Nanoparticles in Different Supporting Electrolytes. *ACS Catal.* **2012**, *2* (5), 901–910. <https://doi.org/10.1021/cs200681x>.

- (74) Clavilier, J.; Durand, R.; Guinet, G.; Faure, R. Electrochemical Adsorption Behaviour of Pt(100) in Sulphuric Acid Solution. *J. Electroanal. Chem.* **1981**, *127* (1–3), 281–287. [https://doi.org/10.1016/S0022-0728\(81\)80488-3](https://doi.org/10.1016/S0022-0728(81)80488-3).
- (75) McCrum, I. T.; Janik, M. J. Deconvoluting Cyclic Voltammograms To Accurately Calculate Pt Electrochemically Active Surface Area. *J. Phys. Chem. C* **2017**, *121* (11), 6237–6245. <https://doi.org/10.1021/acs.jpcc.7b01617>.
- (76) Feliu, J. M.; Fernandez-Vega, A.; Aldaz, A.; Clavilier, J. New Observations of a Structure Sensitive Electrochemical Behaviour of Irreversibly Adsorbed Arsenic and Antimony from Acidic Solutions on Pt (111) and Pt (100) Orientations. *J. Electroanal. Chem.* **1988**, *256* (1), 149–163. [https://doi.org/10.1016/0022-0728\(88\)85014-9](https://doi.org/10.1016/0022-0728(88)85014-9).
- (77) Rodriguez, P.; García-Aráez, N.; Herrero, E.; Feliu, J. M. New Insight on the Behavior of the Irreversible Adsorption and Underpotential Deposition of Thallium on Platinum (111) and Vicinal Surfaces in Acid Electrolytes. *Electrochim. Acta* **2015**, *151*, 319–325. <https://doi.org/10.1016/j.electacta.2014.11.019>.
- (78) Herrero, E.; Climent, V.; Feliu, J. M. On the Different Adsorption Behavior of Bismuth, Sulfur, Selenium and Tellurium on a Pt(775) Stepped Surface. *Electrochem. commun.* **2000**, *2* (9), 636–640. [https://doi.org/10.1016/S1388-2481\(00\)00093-X](https://doi.org/10.1016/S1388-2481(00)00093-X).
- (79) Gómez, R.; Llorca, M. J.; Feliu, J. M.; Aldaz, A. The Behaviour of Germanium Adatoms Irreversibly Adsorbed on Platinum Single Crystals. *J. Electroanal. Chem.* **1992**, *340* (1–2), 349–355. [https://doi.org/10.1016/0022-0728\(92\)80310-Z](https://doi.org/10.1016/0022-0728(92)80310-Z).
- (80) Batista Cordeiro de Souza, M. Study of Glycerol Electrooxidation on Platinum and Gold Surfaces Modified by Metal Adatoms, Universidade Estadual de Campinas, Campinas, 2018. <https://doi.org/10.47749/T/UNICAMP.2018.1061102>.
- (81) Furuya, N.; Motoo, S. Arrangement of Ad-Atoms of Various Kinds on Substrates. Part I. Platinum Substrate. *J. Electroanal. Chem.* **1979**, *98*, 189–194.
- (82) de Souza, M. B. C.; Vicente, R. A.; Yukuhiro, V. Y.; V. M. T. Pires, C. T. G.; Cheuquepán, W.; Bott-Neto, J. L.; Solla-Gullón, J.; Fernández, P. S. Bi-Modified Pt Electrodes toward Glycerol Electrooxidation in Alkaline Solution: Effects on Activity and Selectivity. *ACS Catal.* **2019**, *9* (6), 5104–5110.

- <https://doi.org/10.1021/acscatal.9b00190>.
- (83) de Souza, M. B. C.; Yukuhiro, V. Y.; Vicente, R. A.; Vilela Menegaz Teixeira Pires, C. T. G.; Bott-Neto, J. L.; Fernández, P. S. Pb- and Bi-Modified Pt Electrodes toward Glycerol Electrooxidation in Alkaline Media. Activity, Selectivity, and the Importance of the Pt Atoms Arrangement. *ACS Catal.* **2020**, *10* (3), 2131–2137. <https://doi.org/10.1021/acscatal.9b04805>.
- (84) Sandrini, R. M. L. M.; Sempionatto, J. R.; Herrero, E.; Feliu, J. M.; Souza-Garcia, J.; Angelucci, C. A. Mechanistic Aspects of Glycerol Electrooxidation on Pt(111) Electrode in Alkaline Media. *Electrochem. commun.* **2018**, *86* (December 2017), 149–152. <https://doi.org/10.1016/j.elecom.2017.11.027>.
- (85) Sandrini, R. M. L. M.; Sempionatto, J. R.; Tremiliosi-Filho, G.; Herrero, E.; Feliu, J. M.; Souza-Garcia, J.; Angelucci, C. A. Electrocatalytic Oxidation of Glycerol on Platinum Single Crystals in Alkaline Media. *ChemElectroChem* **2019**, *6* (16), 4238–4245. <https://doi.org/10.1002/celec.201900311>.
- (86) Garcia, A. C.; Kolb, M. J.; Van Nierop Y Sanchez, C.; Vos, J.; Birdja, Y. Y.; Kwon, Y.; Tremiliosi-Filho, G.; Koper, M. T. M. Strong Impact of Platinum Surface Structure on Primary and Secondary Alcohol Oxidation during Electro-Oxidation of Glycerol. *ACS Catal.* **2016**, *6* (7), 4491–4500. <https://doi.org/10.1021/acscatal.6b00709>.
- (87) Garcia, A. C.; Birdja, Y. Y.; Tremiliosi-Filho, G.; Koper, M. T. M. Glycerol Electro-Oxidation on Bismuth-Modified Platinum Single Crystals. *J. Catal.* **2017**, *346*, 117–124. <https://doi.org/10.1016/j.jcat.2016.12.013>.
- (88) Evans, R. W.; Attard, G. A. The Redox Behaviour of Compressed Bismuth Overlayers Irreversibly Adsorbed on Pt(111). *J. Electroanal. Chem.* **1993**, *345* (1–2), 337–350. [https://doi.org/10.1016/0022-0728\(93\)80488-4](https://doi.org/10.1016/0022-0728(93)80488-4).
- (89) Angerstein-Kozłowska, H.; MacDougall, B.; Conway, B. E. Origin of Activation Effects of Acetonitrile and Mercury in Electrocatalytic Oxidation of Formic Acid. *J. Electrochem. Soc.* **1973**, *120* (6), 756. <https://doi.org/10.1149/1.2403551>.
- (90) Fernández, P. S.; Martins, C. A.; Angelucci, C. A.; Gomes, J. F.; Camara, G. A.; Martins, M. E.; Tremiliosi-Filho, G. Evidence for Independent Glycerol Electrooxidation Behavior on Different Ordered Domains of Polycrystalline Platinum. *ChemElectroChem* **2015**, *2* (2), 263–268. <https://doi.org/10.1002/celec.201402291>.
- (91) Fernández, P. S.; Gomes, J. F.; Angelucci, C. A.; Tereshchuk, P.; Martins, C. A.;

- Camara, G. A.; Martins, M. E.; Da Silva, J. L. F.; Tremiliosi-Filho, G. Establishing a Link between Well-Ordered Pt(100) Surfaces and Real Systems: How Do Random Superficial Defects Influence the Electro-Oxidation of Glycerol? *ACS Catal.* **2015**, *5* (7), 4227–4236. <https://doi.org/10.1021/acscatal.5b00451>.
- (92) Fernández, P. S.; Tereshchuk, P.; Angelucci, C. A.; Gomes, J. F.; Garcia, A. C.; Martins, C. A.; Camara, G. A.; Martins, M. E.; Da Silva, J. L. F.; Tremiliosi-Filho, G. How Do Random Superficial Defects Influence the Electro-Oxidation of Glycerol on Pt(111) Surfaces? *Phys. Chem. Chem. Phys.* **2016**, *18* (36), 25582–25591. <https://doi.org/10.1039/C6CP04768H>.
- (93) Tereshchuk, P.; Chaves, A. S.; Silva, J. L. F. Da. Glycerol Adsorption on Platinum Surfaces: A Density Functional Theory Investigation with van Der Waals Corrections. *J. Phys. Chem. C* **2014**, *118* (28), 15251–15259. <https://doi.org/10.1021/jp502969s>.
- (94) Climent, V.; Feliu, J. M. Surface Electrochemistry with Pt Single-Crystal Electrodes. In *Advances in Electrochemical Science and Engineering: Nanopatterned and Nanoparticle-Modified Electrodes*; Alkire, R. C., Bartlett, P. N., Lipkowski, J., Eds.; Wiley-VCH Verlag GmbH & Co. KGaA, 2017; pp 1–57.
- (95) Koper, M. T. M. M. Structure Sensitivity and Nanoscale Effects in Electrocatalysis. *Nanoscale* **2011**, *3* (5), 2054. <https://doi.org/10.1039/c0nr00857e>.
- (96) Pupo, M. M. S.; López-Suárez, F. E.; Bueno-López, A.; Meneses, C. T.; Eguiluz, K. I. B.; Salazar-Banda, G. R. Sn@Pt and Rh@Pt Core-Shell Nanoparticles Synthesis for Glycerol Oxidation. *J. Appl. Electrochem.* **2014**, *45* (2), 139–150. <https://doi.org/10.1007/s10800-014-0757-0>.
- (97) Serov, A.; Martinez, U.; Atanassov, P. Novel Pd-In Catalysts for Alcohols Electrooxidation in Alkaline Media. *Electrochem. commun.* **2013**, *34*, 185–188. <https://doi.org/10.1016/j.elecom.2013.06.003>.
- (98) Caneppele, G. L.; Almeida, T. S.; Zanata, C. R.; Teixeira-Neto, É.; Fernández, P. S.; Camara, G. A.; Martins, C. A. Exponential Improving in the Activity of Pt/C Nanoparticles towards Glycerol Electrooxidation by Sb Ad-Atoms Deposition. *Appl. Catal. B Environ.* **2017**, *200*, 114–120. <https://doi.org/10.1016/j.apcatb.2016.06.072>.
- (99) Lee, J. K.; Jeon, H.; Uhm, S.; Lee, J. Influence of Underpotentially Deposited Sb onto Pt Anode Surface on the Performance of Direct Formic Acid Fuel Cells.

- Electrochim. Acta* **2008**, *53* (21), 6089–6092.
<https://doi.org/10.1016/j.electacta.2008.02.089>.
- (100) Ferre-Vilaplana, A.; Perales-Rondón, J. V.; Feliu, J. M.; Herrero, E. Understanding the Effect of the Adatoms in the Formic Acid Oxidation Mechanism on Pt(111) Electrodes. *ACS Catal.* **2015**, *5* (2), 645–654.
<https://doi.org/10.1021/cs501729j>.
- (101) Climent, V.; Herrero, E.; Feliu, J. M. Electrocatalysis of Formic Acid and CO Oxidation on Antimony-Modified Pt(111) Electrodes. *Electrochim. Acta* **1998**, *44* (8–9), 1403–1414. [https://doi.org/10.1016/S0013-4686\(98\)00263-1](https://doi.org/10.1016/S0013-4686(98)00263-1).
- (102) Bertin, E.; Fleury, A.; Roy, C.; Martin, M. H.; Garbarino, S.; Guay, D. Preferentially (100) Oriented Pt Thin Film with Less than a Monolayer of Bi, Pd and Sb Adatoms Application for Formic Acid Oxidation. *Electrochim. Acta* **2015**, *162*, 237–244. <https://doi.org/10.1016/j.electacta.2014.11.153>.
- (103) Zhao, J.; Jung, C.; Rhee, C. K. Adlayers of Sb Irreversibly Adsorbed on Pt(111): An Electrochemical Scanning Tunneling Microscopy Study. *J. Phys. Chem. B* **2006**, *110* (22), 10814–10821. <https://doi.org/10.1021/jp057422l>.
- (104) Binder, H.; Kohling, A.; Sandstede, G. Acceleration by Adsorbed Sulphur and Selenium of the Electrochemical Oxidation of Formic Acid on Platinum Catalysts. *Nature* **1967**, *214*, 268–269.
- (105) Loučka, T. Adsorption and Oxidation of Organic Compounds on a Platinum Electrode Partly Covered by Adsorbed Sulphur. *J. Electroanal. Chem.* **1972**, *36* (2), 355–367. [https://doi.org/10.1016/S0022-0728\(72\)80258-4](https://doi.org/10.1016/S0022-0728(72)80258-4).
- (106) Jayaram, R.; Contractor, A. Q.; Lal, H. Formic Acid Oxidation at Platinized Platinum Electrodes. Part IV. Effect of Preadsorbed Sulfur and Related Studies. *J. Electroanal. Chem.* **1978**, *87*, 225–237.
- (107) García-Aráez, N.; Climent, V.; Feliu, J. M. Evidence of Water Reorientation on Model Electrocatalytic Surfaces from Nanosecond-Laser-Pulsed Experiments. *J. Am. Chem. Soc.* **2008**, *130* (12), 3824–3833. <https://doi.org/10.1021/ja0761481>.
- (108) Sun, S. G.; Chen, S. P.; Li, N. H.; Lu, G. Q.; Chen, B. Z.; Xu, F. C. Chemical States of Bismuth and Sulfur Adatoms on the Polycrystalline Pt Electrode Surface towards HCOOH Oxidation - Combined Studies of Cyclic Voltammetry, in Situ FTIRS and XPS on the Origin of Electrocatalytic Activity of Adatoms. *Colloids Surfaces A Physicochem. Eng. Asp.* **1998**, *134* (1–2), 207–220. [https://doi.org/10.1016/S0927-7757\(97\)00335-X](https://doi.org/10.1016/S0927-7757(97)00335-X).

- (109) Lin, W.; Sun, S.; Tian, Z. Investigations of Coadsorption of Carbon Monoxide with S or Bi Adatoms at a Platinum Electrode by In-Situ FTIR Spectroscopy and Quantum Chemistry Analysis. *J. Electroanal. Chem.* **1994**, *364*, 1–7.
- (110) Shi, X.; Simpson, D. E.; Roy, D. The Role of Chemisorbed Hydroxyl Species in Alkaline Electrocatalysis of Glycerol on Gold. *Phys. Chem. Chem. Phys.* **2015**, *17* (17), 11432–11444. <https://doi.org/10.1039/C5CP00313J>.
- (111) Perales-Rondón, J. V.; Busó-Rogero, C.; Solla-Gullón, J.; Herrero, E.; Feliu, J. M. Formic Acid Electrooxidation on Thallium Modified Platinum Single Crystal Electrodes. *J. Electroanal. Chem.* **2017**, *800*, 82–88. <https://doi.org/10.1016/j.jelechem.2016.09.020>.
- (112) Hartung, T.; Willsau, J.; Heitbaum, J. Catalytic Effects of Hg and Tl Submonolayers on the Electrooxidation of Formic Acid on Pt. *J. Electroanal. Chem.* **1986**, *205* (1–2), 135–149. [https://doi.org/10.1016/0022-0728\(86\)90228-7](https://doi.org/10.1016/0022-0728(86)90228-7).
- (113) Busó-Rogero, C.; Perales-Rondón, J. V.; Farias, M. J. S.; Vidal-Iglesias, F. J.; Solla-Gullon, J.; Herrero, E.; Feliu, J. M. Formic Acid Electrooxidation on Thallium-Decorated Shape-Controlled Platinum Nanoparticles: An Improvement in Electrocatalytic Activity. *Phys. Chem. Chem. Phys.* **2014**, *16* (27), 13616–13624. <https://doi.org/10.1039/C4CP00304G>.
- (114) Herrero, E.; Rodes, A.; Pérez, J. M.; Feliu, J. M.; Aldaz, A. CO Adsorption and Oxidation on Pt(111) Electrodes Modified by Irreversibly Adsorbed Selenium and Tellurium. *J. Electroanal. Chem.* **1996**, *412* (1–2), 165–174. [https://doi.org/10.1016/0022-0728\(96\)04626-8](https://doi.org/10.1016/0022-0728(96)04626-8).
- (115) Llorca, M. J.; Herrero, E.; Feliu, J. M.; Aldaz, A. Formic Acid Oxidation on Pt(111) Electrodes Modified by Irreversibly Adsorbed Selenium. *J. Electroanal. Chem.* **1994**, *373* (1–2), 217–225. [https://doi.org/10.1016/0022-0728\(94\)03326-9](https://doi.org/10.1016/0022-0728(94)03326-9).
- (116) Lozeman, J. J. A.; Führer, P.; Olthuis, W.; Odijk, M. Spectroelectrochemistry, the Future of Visualizing Electrode Processes by Hyphenating Electrochemistry with Spectroscopic Techniques. *Analyst* **2020**, *145* (7), 2482–2509. <https://doi.org/10.1039/c9an02105a>.
- (117) Cuesta, A. ATR-SEIRAS for Time-Resolved Studies of Electrode–Electrolyte Interfaces. *Curr. Opin. Electrochem.* **2022**, *35*, 101041. <https://doi.org/10.1016/j.coelec.2022.101041>.
- (118) Nakamoto, K.; Brown, C. W. *Introductory Raman Spectroscopy*; 1994.

- <https://doi.org/10.1016/c2009-0-21238-4>.
- (119) Heck, K. N.; Janesko, B. G.; Scuseria, G. E.; Halas, N. J.; Wong, M. S. Using Catalytic and Surface-Enhanced Raman Spectroscopy-Active Gold Nanoshells to Understand the Role of Basicity in Glycerol Oxidation. *ACS Catal.* **2013**, *3* (11), 2430–2435. <https://doi.org/10.1021/cs400643f>.
- (120) Huang, Y.-F.; Kooyman, P. J.; Koper, M. T. M. Intermediate Stages of Electrochemical Oxidation of Single-Crystalline Platinum Revealed by in Situ Raman Spectroscopy. *Nat. Commun.* **2016**, *7* (1), 12440. <https://doi.org/10.1038/ncomms12440>.
- (121) Calvin, S. *XAFS for Everyone*; CRC Press, 2013. <https://doi.org/10.1201/b14843>.
- (122) Wang, M.; Árnadóttir, L.; Xu, Z. J.; Feng, Z. In Situ X-Ray Absorption Spectroscopy Studies of Nanoscale Electrocatalysts. *Nano-Micro Lett.* **2019**, *11* (1), 1–18. <https://doi.org/10.1007/s40820-019-0277-x>.
- (123) Lima, F. H. B.; Gonzalez, E. R. Electrocatalysis of Ethanol Oxidation on Pt Monolayers Deposited on Carbon-Supported Ru and Rh Nanoparticles. *Appl. Catal. B Environ.* **2008**, *79* (4), 341–346. <https://doi.org/10.1016/j.apcatb.2007.10.028>.
- (124) Lima, F. H. B.; Gonzalez, E. R. Ethanol Electro-Oxidation on Carbon-Supported Pt-Ru, Pt-Rh and Pt-Ru-Rh Nanoparticles. *Electrochim. Acta* **2008**, *53* (6), 2963–2971. <https://doi.org/10.1016/j.electacta.2007.11.007>.
- (125) Willmott, P. *An Introduction to Synchrotron Radiation*, 1st ed.; Wiley: West Sussex, 2011. <https://doi.org/10.1002/9781119970958>.
- (126) Iwasita, T.; Nart, F. C. In Situ Infrared Spectroscopy at Electrochemical Interfaces. *Prog. Surf. Sci.* **1997**, *55* (4), 271–340. [https://doi.org/10.1016/S0079-6816\(97\)00032-4](https://doi.org/10.1016/S0079-6816(97)00032-4).
- (127) Kas, R.; Ayemoba, O.; Firet, N. J.; Middelkoop, J.; Smith, W. A.; Cuesta, A. In-Situ Infrared Spectroscopy Applied to the Study of the Electrocatalytic Reduction of CO₂: Theory, Practice and Challenges. *ChemPhysChem* **2019**, *20* (22), 2904–2925. <https://doi.org/10.1002/cphc.201900533>.
- (128) Schnaidt, J.; Heinen, M.; Denot, D.; Jusys, Z.; Jürgen Behm, R. Electrooxidation of Glycerol Studied by Combined in Situ IR Spectroscopy and Online Mass Spectrometry under Continuous Flow Conditions. *J. Electroanal. Chem.* **2011**, *661* (1), 250–264. <https://doi.org/10.1016/j.jelechem.2011.08.011>.

- (129) Lima, C. C.; Rodrigues, M. V. F.; Neto, A. F. M.; Zanata, C. R.; Pires, C. T. G. V. M. T.; Costa, L. S.; Solla-Gullón, J.; Fernández, P. S. Highly Active Ag/C Nanoparticles Containing Ultra-Low Quantities of Sub-Surface Pt for the Electrooxidation of Glycerol in Alkaline Media. *Appl. Catal. B Environ.* **2020**, 279 (May), 119369. <https://doi.org/10.1016/j.apcatb.2020.119369>.
- (130) Santiago, P. V. B.; Lima, C. C.; Bott-Neto, J. L.; Fernández, P. S.; Angelucci, C. A.; Souza-Garcia, J. Perovskite Oxides as Electrocatalyst for Glycerol Oxidation. *J. Electroanal. Chem.* **2021**, 896 (January), 115198. <https://doi.org/10.1016/j.jelechem.2021.115198>.
- (131) Martins, C. A.; Fernández, P. S.; Troiani, H. E.; Martins, M. E.; Camara, G. A. Ethanol vs. Glycerol: Understanding the Lack of Correlation between the Oxidation Currents and the Production of CO₂ on Pt Nanoparticles. *J. Electroanal. Chem.* **2014**, 717–718, 231–236. <https://doi.org/10.1016/j.jelechem.2014.01.027>.
- (132) De Lima, R. B.; Paganin, V.; Iwasita, T.; Vielstich, W. On the Electrocatalysis of Ethylene Glycol Oxidation. *Electrochim. Acta* **2003**, 49 (1), 85–91. <https://doi.org/10.1016/j.electacta.2003.05.004>.
- (133) Dubau, L.; Hahn, F.; Coutanceau, C.; Léger, J. M.; Lamy, C. On the Structure Effects of Bimetallic PtRu Electrocatalysts towards Methanol Oxidation. *J. Electroanal. Chem.* **2003**, 554–555 (1), 407–415. [https://doi.org/10.1016/S0022-0728\(03\)00308-5](https://doi.org/10.1016/S0022-0728(03)00308-5).
- (134) Mello, G. A. B.; Cheuquepán, W.; Briega-Martos, V.; Feliu, J. M. Glucose Electro-Oxidation on Pt(100) in Phosphate Buffer Solution (PH 7): A Mechanistic Study. *Electrochim. Acta* **2020**, 354, 136765. <https://doi.org/10.1016/j.electacta.2020.136765>.
- (135) Martins, C. A.; Giz, M. J.; Camara, G. A. Generation of Carbon Dioxide from Glycerol: Evidences of Massive Production on Polycrystalline Platinum. *Electrochim. Acta* **2011**, 56, 4549–4553. <https://doi.org/10.1016/j.electacta.2011.02.076>.
- (136) Hammer, B.; Nørskov, J. K. Theoretical Surface Science and Catalysis—Calculations and Concepts. In *Advances in Catalysis*; 2000; Vol. 45, pp 71–129. [https://doi.org/10.1016/S0360-0564\(02\)45013-4](https://doi.org/10.1016/S0360-0564(02)45013-4).
- (137) Jeffery, D. Z.; Camara, G. A. The Formation of Carbon Dioxide during Glycerol Electrooxidation in Alkaline Media: First Spectroscopic Evidences. *Electrochem.*

- commun.* **2010**, *12* (8), 1129–1132.
<https://doi.org/10.1016/j.elecom.2010.06.001>.
- (138) Bott-Neto, J. L.; Rodrigues, M. V. F.; Silva, M. C.; Carneiro-Neto, E. B.; Wosiak, G.; Mauricio, J. C.; Pereira, E. C.; Figueroa, S. J. A.; Fernández, P. S. Versatile Spectroelectrochemical Cell for In Situ Experiments: Development, Applications, and Electrochemical Behavior. *ChemElectroChem* **2020**, *7* (21), 4306–4313. <https://doi.org/10.1002/celec.202000910>.
- (139) Solla-Gullón, J.; Vidal-Iglesias, F. J.; Herrero, E.; Feliu, J. M.; Aldaz, A. CO Monolayer Oxidation on Semi-Spherical and Preferentially Oriented (100) and (111) Platinum Nanoparticles. *Electrochem. commun.* **2006**, *8* (1), 189–194. <https://doi.org/10.1016/j.elecom.2005.11.008>.
- (140) Solla-Gullón, J.; Vidal-Iglesias, F. J.; López-Cudero, A.; Garnier, E.; Feliu, J. M.; Aldaz, A. Shape-Dependent Electrocatalysis: Methanol and Formic Acid Electrooxidation on Preferentially Oriented Pt Nanoparticles. *Phys. Chem. Chem. Phys.* **2008**, *10* (25), 3689–3698. <https://doi.org/10.1039/b802703j>.
- (141) Tsunekawa, S.; Yamamoto, F.; Wang, K. H.; Nagasaka, M.; Yuzawa, H.; Takakusagi, S.; Kondoh, H.; Asakura, K.; Kawai, T.; Yoshida, M. Operando Observations of a Manganese Oxide Electrocatalyst for Water Oxidation Using Hard/Tender/Soft X-Ray Absorption Spectroscopy. *J. Phys. Chem. C* **2020**, *124* (43), 23611–23618. <https://doi.org/10.1021/acs.jpcc.0c05571>.
- (142) Saveleva, V. A.; Papaefthimiou, V.; Daletou, M. K.; Doh, W. H.; Ulhaq-Bouillet, C.; Diebold, M.; Zafeiratos, S.; Savinova, E. R. Operando Near Ambient Pressure XPS (NAP-XPS) Study of the Pt Electrochemical Oxidation in H₂O and H₂O/O₂ Ambients. *J. Phys. Chem. C* **2016**, *120* (29), 15930–15940. <https://doi.org/10.1021/acs.jpcc.5b12410>.
- (143) Snyder, L. R.; Kirkland, J. J.; Dolan, J. W. *Introduction to Modern Liquid Chromatography*; 2010. <https://doi.org/10.1002/9780470508183>.
- (144) Snyder, L. R.; Dolan, J. W. Milestones in the Development of Liquid Chromatography. In *Liquid Chromatography*; Elsevier, 2013; pp 1–17. <https://doi.org/10.1016/B978-0-12-415807-8.00001-8>.
- (145) Kwon, Y.; Koper, M. T. M. Combining Voltammetry with HPLC: Application to Electro-Oxidation of Glycerol. *Anal. Chem.* **2010**, *82* (13), 5420–5424. <https://doi.org/10.1021/ac101058t>.
- (146) Birdja, Y. Y.; Koper, M. T. M. The Importance of Cannizzaro-Type Reactions

- during Electrocatalytic Reduction of Carbon Dioxide. *J. Am. Chem. Soc.* **2017**, *139* (5), 2030–2034. <https://doi.org/10.1021/jacs.6b12008>.
- (147) Zhu, B.; Raza, R.; Fan, L.; Sun, C. *Solid Oxide Fuel Cells. From Electrolyte-Based to Electrolyte-Free Devices*, 1st ed.; Zhu, B., Raza, R., Fan, L., Sun, C., Eds.; Wiley, 2020.
- (148) De, B. S.; Khare, N.; Elias, A.; Basu, S. Microfluidic Concept-Based Fuel Cells. In *Nanotechnology in Fuel Cells*; Elsevier, 2022; pp 11–40. <https://doi.org/10.1016/B978-0-323-85727-7.00005-9>.
- (149) Kjeang, E.; Michel, R.; Harrington, D. A.; Djilali, N.; Sinton, D. A Microfluidic Fuel Cell with Flow-through Porous Electrodes. *J. Am. Chem. Soc.* **2008**, *130* (12), 4000–4006. <https://doi.org/10.1021/ja078248c>.
- (150) Díaz-Sainz, G.; Alvarez-Guerra, M.; Solla-Gullón, J.; García-Cruz, L.; Montiel, V.; Irabien, A. CO₂ Electroreduction to Formate: Continuous Single-Pass Operation in a Filter-Press Reactor at High Current Densities Using Bi Gas Diffusion Electrodes. *J. CO₂ Util.* **2019**, *34* (May), 12–19. <https://doi.org/10.1016/j.jcou.2019.05.035>.
- (151) Sellin, R.; Clacens, J. M.; Coutanceau, C. A Thermogravimetric Analysis/Mass Spectroscopy Study of the Thermal and Chemical Stability of Carbon in the Pt/C Catalytic System. *Carbon N. Y.* **2010**, *48* (8), 2244–2254. <https://doi.org/10.1016/j.carbon.2010.02.034>.
- (152) Martins, C. A.; Ibrahim, O. A.; Pei, P.; Kjeang, E. In Situ Decoration of Metallic Catalysts in Flow-through Electrodes: Application of Fe/Pt/C for Glycerol Oxidation in a Microfluidic Fuel Cell. *Electrochim. Acta* **2019**, *305*, 47–55. <https://doi.org/10.1016/j.electacta.2019.03.018>.
- (153) Luo, J.; Jia, S.; Zhao, J.; Jiang, D.; Zhan, Q.; Shang, T.; Xu, Y. Facile Synthesis of δ -Bi₂O₃ Particles/Rod-like Bi₄O₇ Composite with Enhanced Visible Light-Driven Photocatalytic Performance. *J. Mater. Sci. Mater. Electron.* **2022**, *33* (7), 4681–4693. <https://doi.org/10.1007/s10854-021-07655-y>.
- (154) Zhang, J.; Zhang, H.; Wu, J.; Zhang, J. Fuel Cell Open Circuit Voltage. *Pem Fuel Cell Test. Diagnosis* **2013**, 187–200. <https://doi.org/10.1016/b978-0-444-53688-4.00007-3>.
- (155) Zhang, J.; Zhang, H.; Wu, J.; Zhang, J. *Fuel Cell Degradation and Failure Analysis*; 2013. <https://doi.org/10.1016/b978-0-444-53688-4.00011-5>.
- (156) Gomes, J. F.; Martins, C. A.; Giz, M. J.; Tremiliosi-Filho, G.; Camara, G. A.

- Insights into the Adsorption and Electro-Oxidation of Glycerol: Self-Inhibition and Concentration Effects. *J. Catal.* **2013**, *301*, 154–161. <https://doi.org/10.1016/j.jcat.2013.02.007>.
- (157) You, X.; Ye, Q.; Cheng, P. The Dependence of Mass Transfer Coefficient on the Electrolyte Velocity in Carbon Felt Electrodes: Determination and Validation. *J. Electrochem. Soc.* **2017**, *164* (11), E3386–E3394. <https://doi.org/10.1149/2.0401711jes>.
- (158) Roquet, L.; Belgsir, E. M.; Léger, J.-M.; Lamy, C. Kinetics and Mechanisms of the Electrocatalytic Oxidation of Glycerol as Investigated by Chromatographic Analysis of the Reaction Products: Potential and PH Effects. *Electrochim. Acta* **1994**, *39* (16), 2387–2394. [https://doi.org/10.1016/0013-4686\(94\)E0190-Y](https://doi.org/10.1016/0013-4686(94)E0190-Y).
- (159) Shafiee, S. A.; Aarons, J.; Hamzah, H. H. Review—Electroreduction of Peroxodisulfate: A Review of a Complicated Reaction. *J. Electrochem. Soc.* **2018**, *165* (13), H785–H798. <https://doi.org/10.1149/2.1161811jes>.
- (160) A. Yaylayan, V.; Harty-Majors, S.; A. Ismail, A. Investigation of DL-Glyceraldehyde-Dihydroxyacetone Interconversion by FTIR Spectroscopy. *Carbohydr. Res.* **1999**, *318* (1–4), 20–25. [https://doi.org/10.1016/S0008-6215\(99\)00077-4](https://doi.org/10.1016/S0008-6215(99)00077-4).
- (161) Nagorski, R. W.; Richard, J. P. Mechanistic Imperatives for Aldose - Ketose Isomerization in Water: Specific, General Base- and Metal Ion-Catalyzed Isomerization of Glyceraldehyde with Proton and Hydride Transfer. *Journal of the American Chemical Society.* 2001, pp 794–802. <https://doi.org/10.1021/ja003433a>.
- (162) Hu, W.; Lowry, B.; Varma, A. Kinetic Study of Glycerol Oxidation Network over Pt-Bi/C Catalyst. *Appl. Catal. B Environ.* **2011**, *106* (1–2), 123–132. <https://doi.org/10.1016/j.apcatb.2011.05.015>.
- (163) Abbadi, A.; van Bekkum, H. Highly Selective Oxidation of Aldonic Acids to 2-Keto-Aldonic Acids over Pt-Bi and Pt-Pb Catalysts. *Appl. Catal. A, Gen.* **1995**, *124* (2), 409–417. [https://doi.org/10.1016/0926-860X\(94\)00285-1](https://doi.org/10.1016/0926-860X(94)00285-1).
- (164) Wenkin, M.; Ruiz, P.; Delmon, B.; Devillers, M. The Role of Bismuth as Promoter in Pd-Bi Catalysts for the Selective Oxidation of Glucose to Gluconate. *J. Mol. Catal. A Chem.* **2002**, *180* (1–2), 141–159. [https://doi.org/10.1016/S1381-1169\(01\)00421-6](https://doi.org/10.1016/S1381-1169(01)00421-6).
- (165) Feng, S.; Yi, J.; Miura, H.; Nakatani, N.; Hada, M.; Shishido, T. Experimental and

- Theoretical Investigation of the Role of Bismuth in Promoting the Selective Oxidation of Glycerol over Supported Pt–Bi Catalyst under Mild Conditions. *ACS Catal.* **2020**, *10* (11), 6071–6083. <https://doi.org/10.1021/acscatal.0c00974>.
- (166) Climent, V.; Garcia-Araez, N.; Compton, R. G.; Feliu, J. M. Effect of Deposited Bismuth on the Potential of Maximum Entropy of Pt(111) Single-Crystal Electrodes. *J. Phys. Chem. B* **2006**, *110* (42), 21092–21100. <https://doi.org/10.1021/jp061982i>.
- (167) Trasatti, S. Work Function, Electronegativity, and Electrochemical Behaviour of Metals. *J. Electroanal. Chem. Interfacial Electrochem.* **1971**, *33* (2), 351–378. [https://doi.org/10.1016/S0022-0728\(71\)80123-7](https://doi.org/10.1016/S0022-0728(71)80123-7).
- (168) Trasatti, S. Electronegativity, Work Function, and Heat of Adsorption of Hydrogen on Metals. *J. Chem. Soc. Faraday Trans. 1 Phys. Chem. Condens. Phases* **1972**, *68*, 229. <https://doi.org/10.1039/f19726800229>.
- (169) Avramov-Ivić, M.; Léger, J. M.; Beden, B.; Hahn, F.; Lamy, C. Adsorption of Glycerol on Platinum in Alkaline Medium Effect of the Electrode Structure. *J. Electroanal. Chem.* **1993**, *351* (1–2), 285–297. [https://doi.org/10.1016/0022-0728\(93\)80240-I](https://doi.org/10.1016/0022-0728(93)80240-I).
- (170) Strmcnik, D.; Kodama, K.; van der Vliet, D.; Greeley, J.; Stamenkovic, V. R.; Marković, N. M. The Role of Non-Covalent Interactions in Electrocatalytic Fuel-Cell Reactions on Platinum. *Nat. Chem.* **2009**, *1* (6), 466–472. <https://doi.org/10.1038/nchem.330>.
- (171) Angelucci, C. A.; Varela, H.; Tremiliosi-Filho, G.; Gomes, J. F. The Significance of Non-Covalent Interactions on the Electro-Oxidation of Alcohols on Pt and Au in Alkaline Media. *Electrochem. commun.* **2013**, *33*, 10–13. <https://doi.org/10.1016/j.elecom.2013.03.039>.
- (172) Melle, G.; de Souza, M. B. C.; Santiago, P. V. B.; Corradini, P. G.; Mascaro, L. H.; Fernández, P. S.; Sitta, E. Glycerol Electro-Oxidation at Pt in Alkaline Media: Influence of Mass Transport and Cations. *Electrochim. Acta* **2021**, *398*, 139318. <https://doi.org/10.1016/j.electacta.2021.139318>.
- (173) Melle, G. B.; Machado, E. G.; Mascaro, L. H.; Sitta, E. Effect of Mass Transport on the Glycerol Electro-Oxidation. *Electrochim. Acta* **2019**, *296*, 972–979. <https://doi.org/10.1016/j.electacta.2018.11.085>.

9. Appendix

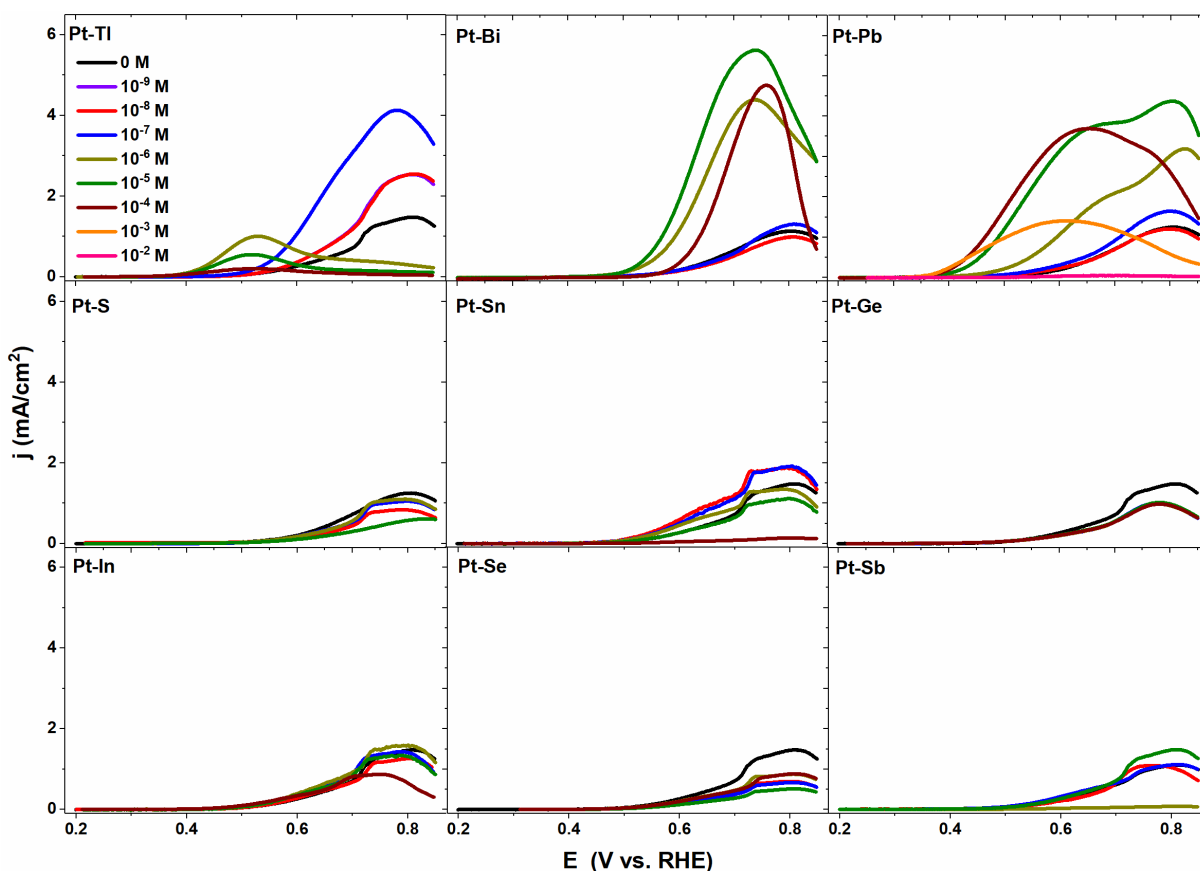


Figure S1: Comparing the 10th positive scan of the glycerol oxidation in 0.1 M NaOH + 0.1 M glycerol on various Pt-adatom systems at 10 mV/s, for all concentrations examined. Using data from refs.[82,83].

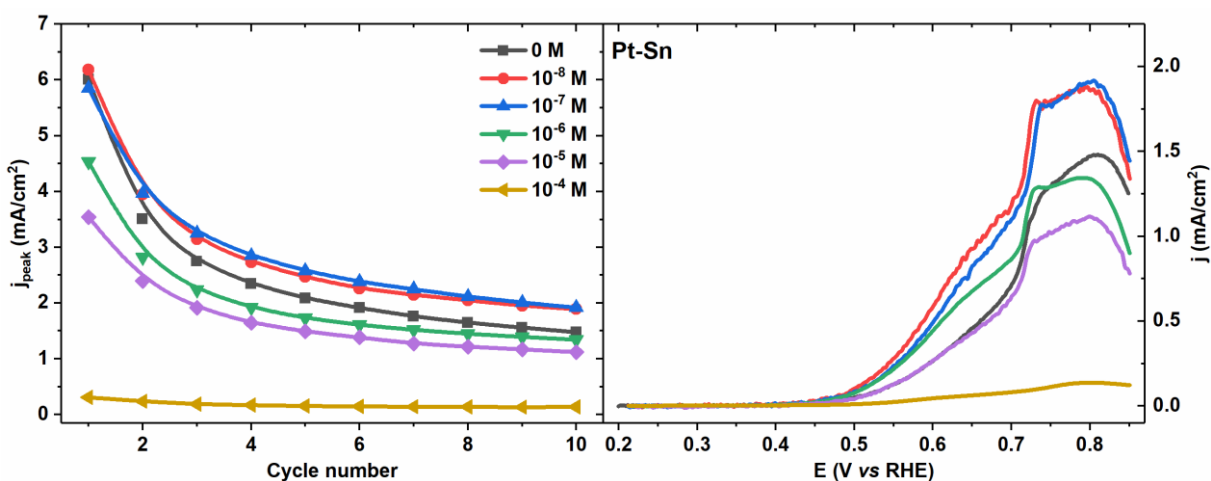


Figure S2: Evolution of j_{peak} with cycle number (left) and 10th positive scan (right) for the Pt-Sn system at various concentrations, in 0.1 M NaOH + 0.1 M glycerol at 10 mV/s.

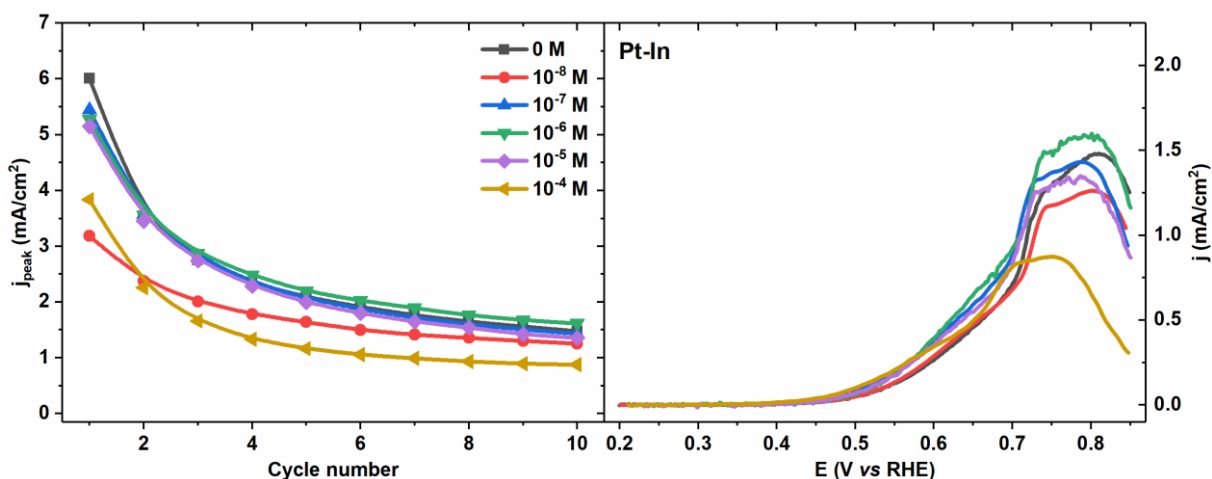


Figure S3: Evolution of j_{peak} with cycle number (left) and 10th positive scan (right) for the Pt-In system at various concentrations, in 0.1 M NaOH + 0.1 M glycerol at 10 mV/s.

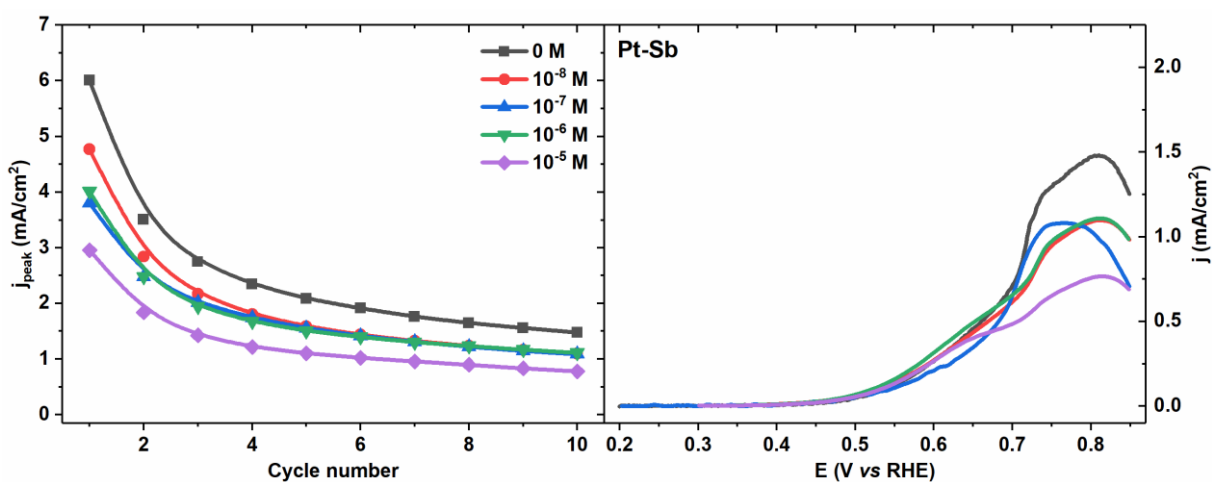


Figure S4: Evolution of j_{peak} with cycle number (left) and 10th positive scan (right) for the Pt-Sb system at various concentrations, in 0.1 M NaOH + 0.1 M glycerol at 10 mV/s.

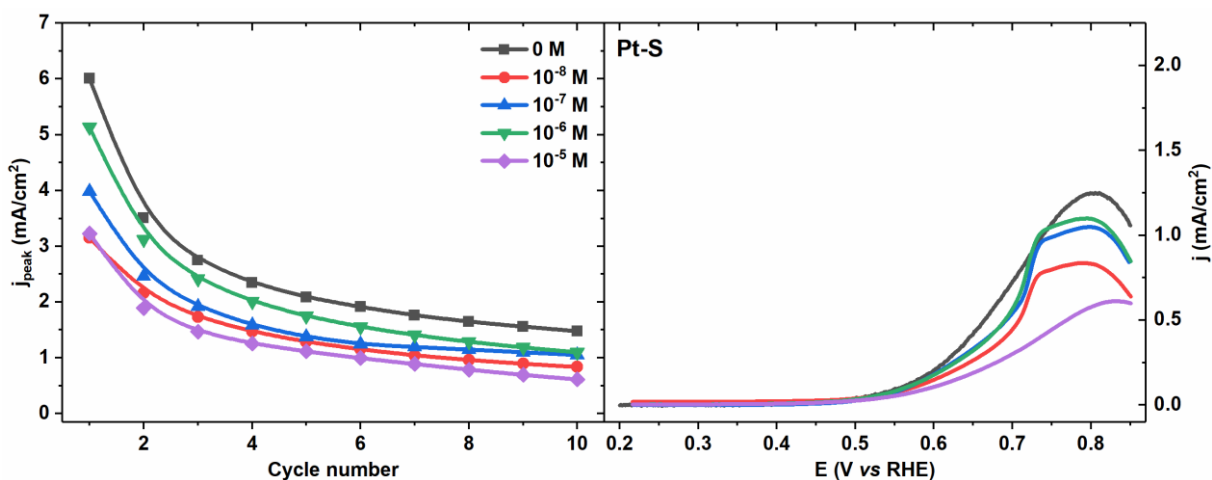


Figure S5: Evolution of j_{peak} with cycle number (left) and 10th positive scan (right) for the Pt-S system at various concentrations, in 0.1 M NaOH + 0.1 M glycerol at 10 mV/s.

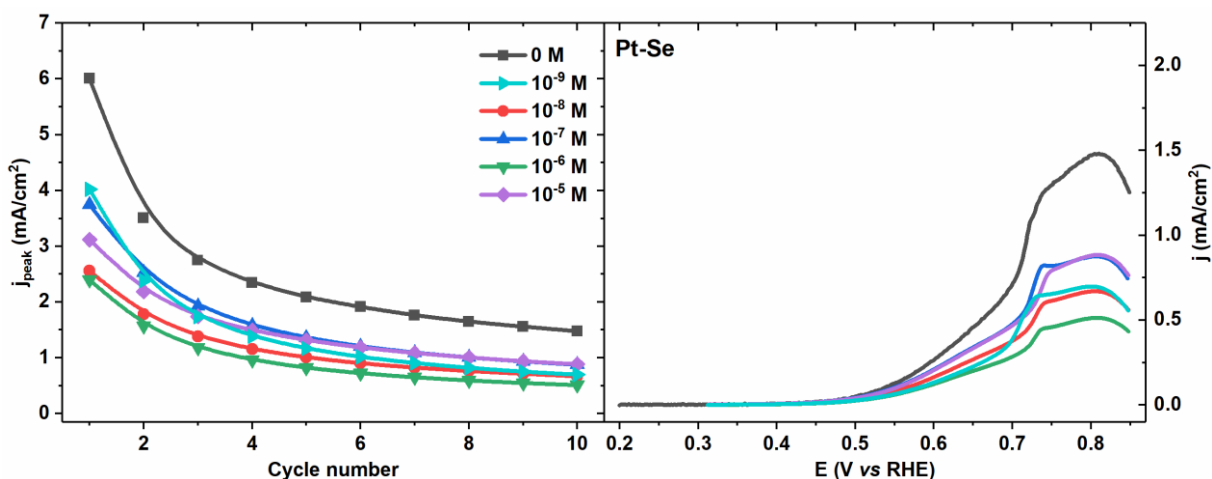


Figure S6: Evolution of j_{peak} with cycle number (left) and 10th positive scan (right) for the Pt-Se system at various concentrations, in 0.1 M NaOH + 0.1 M glycerol at 10 mV/s.

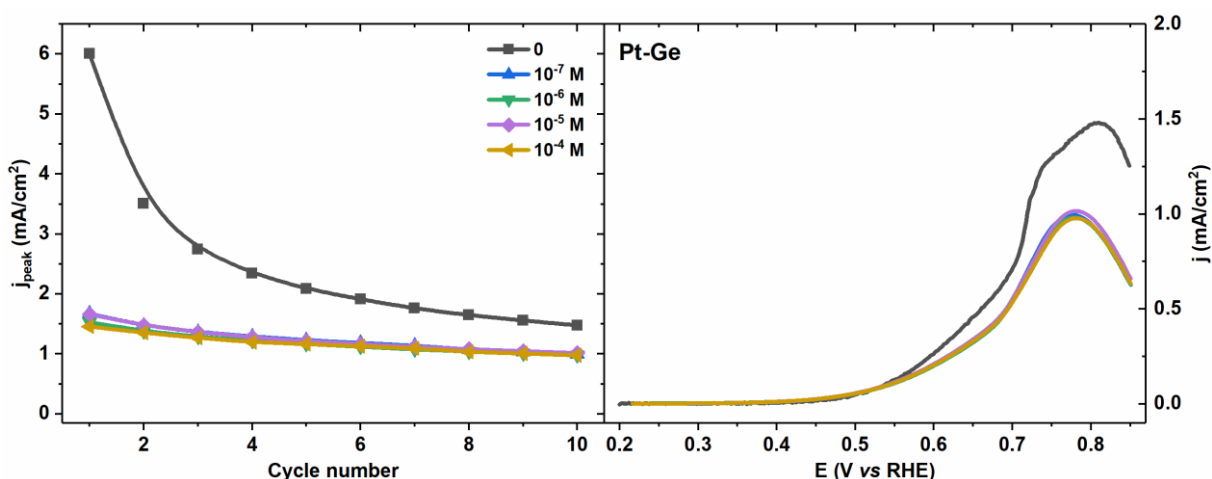


Figure S7: Evolution of j_{peak} with cycle number (left) and 10th positive scan (right) for the Pt-Ge system at various concentrations, in 0.1 M NaOH + 0.1 M glycerol at 10 mV/s.

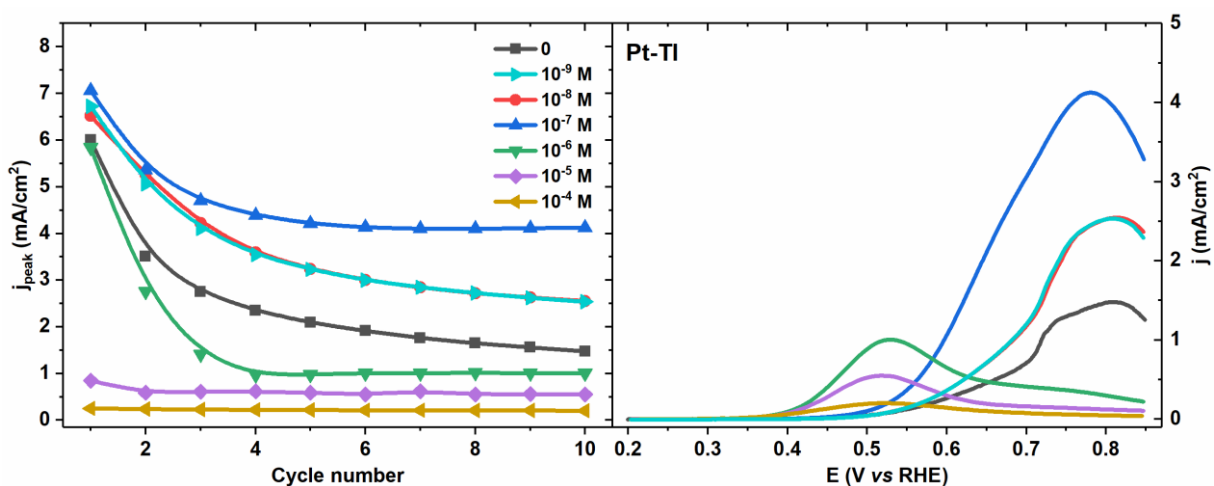


Figure S8: Evolution of j_{peak} with cycle number (left) and 10th positive scan (right) for the Pt-Tl system at various concentrations, in 0.1 M NaOH + 0.1 M glycerol at 10 mV/s.

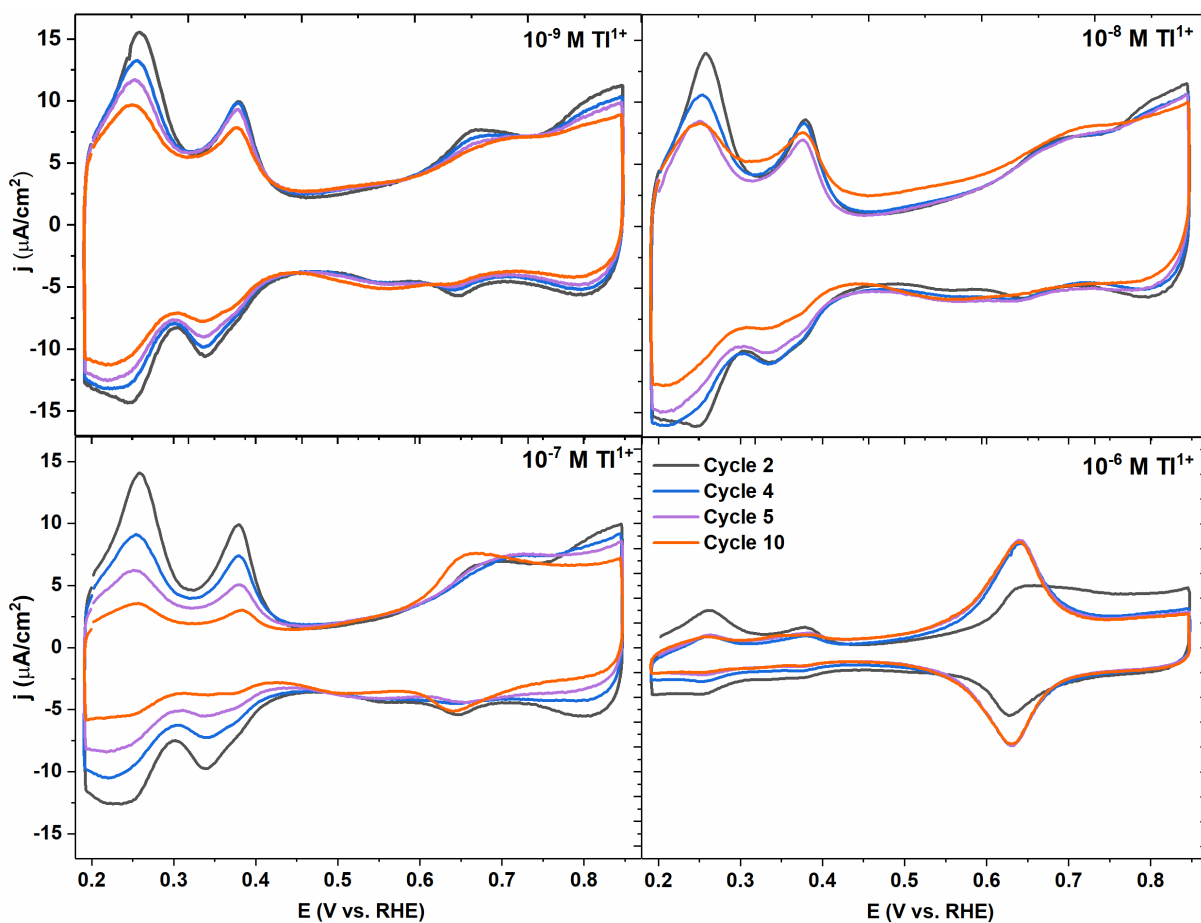


Figure S9: Cycling a Pt_p electrode in 0.1 M NaOH with different amounts of TI¹⁺ ions in solution, at 10 mV/s.

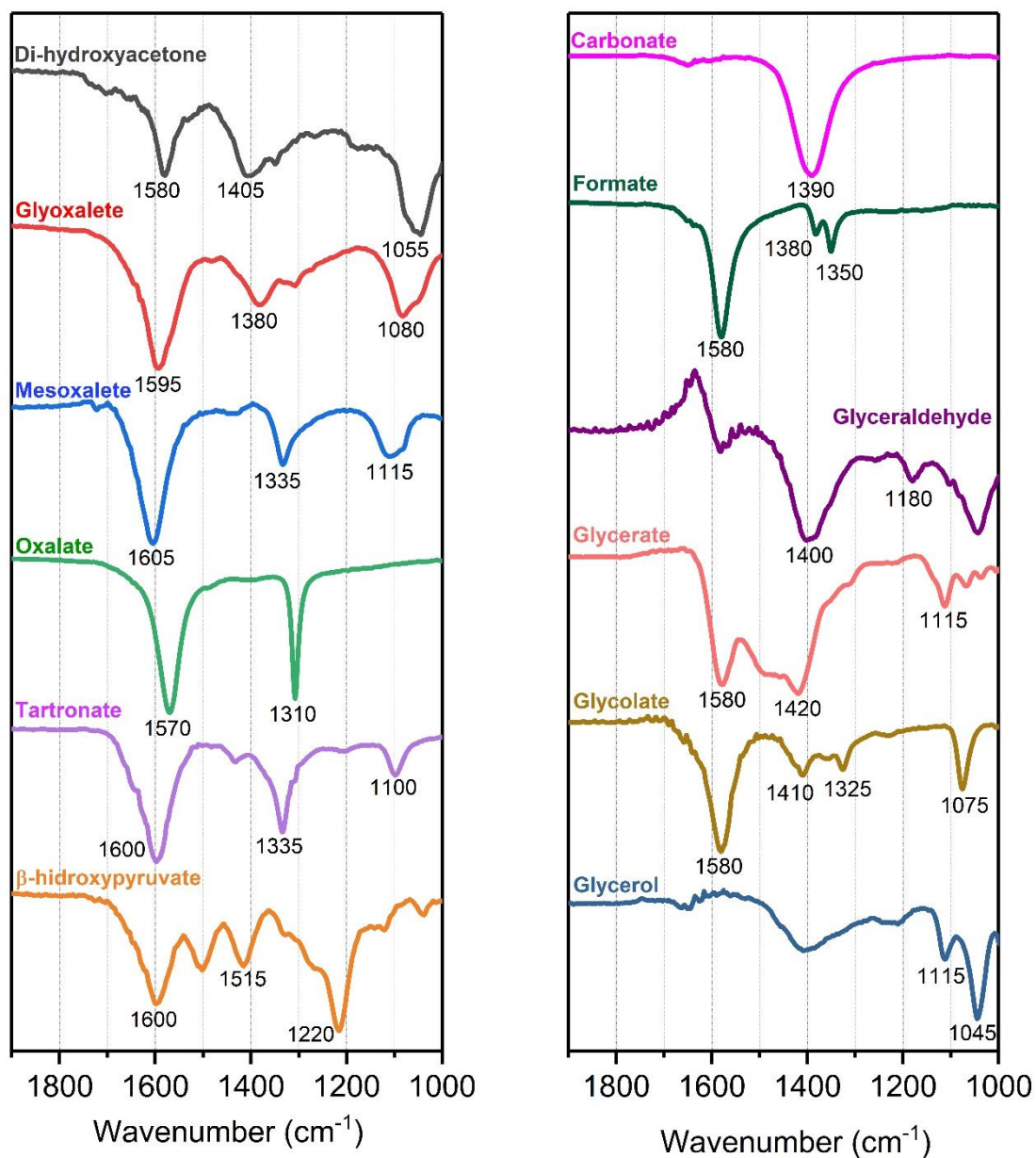


Figure S10: FTIR spectra collected of several possible oxidation products, using the attenuated total reflection configuration. Solutions were made of 0.1 M NaOH + 20 mM products. Reprinted with permission from ref.[83]. Copyright 2022 American Chemical Society.

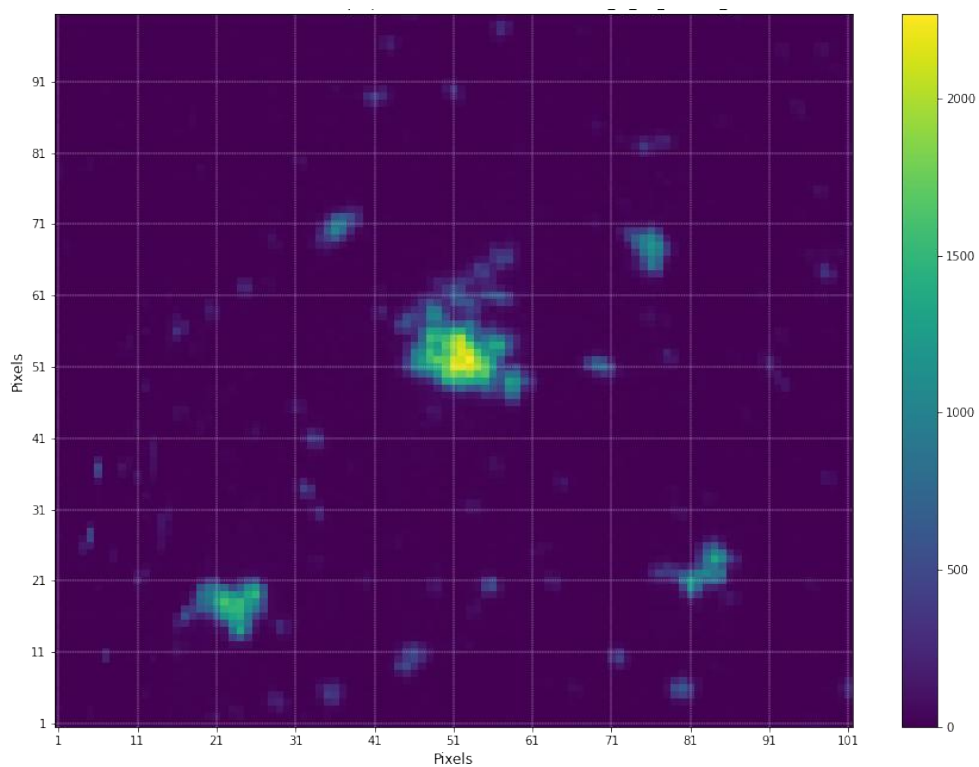


Figure S11: *in situ* XAS image of Pt_{sphere} dispersed on a glassy carbon electrode, without polarization, showing a cluster on its center. Image size is 50 x 50 μm with a step of 5 μm .

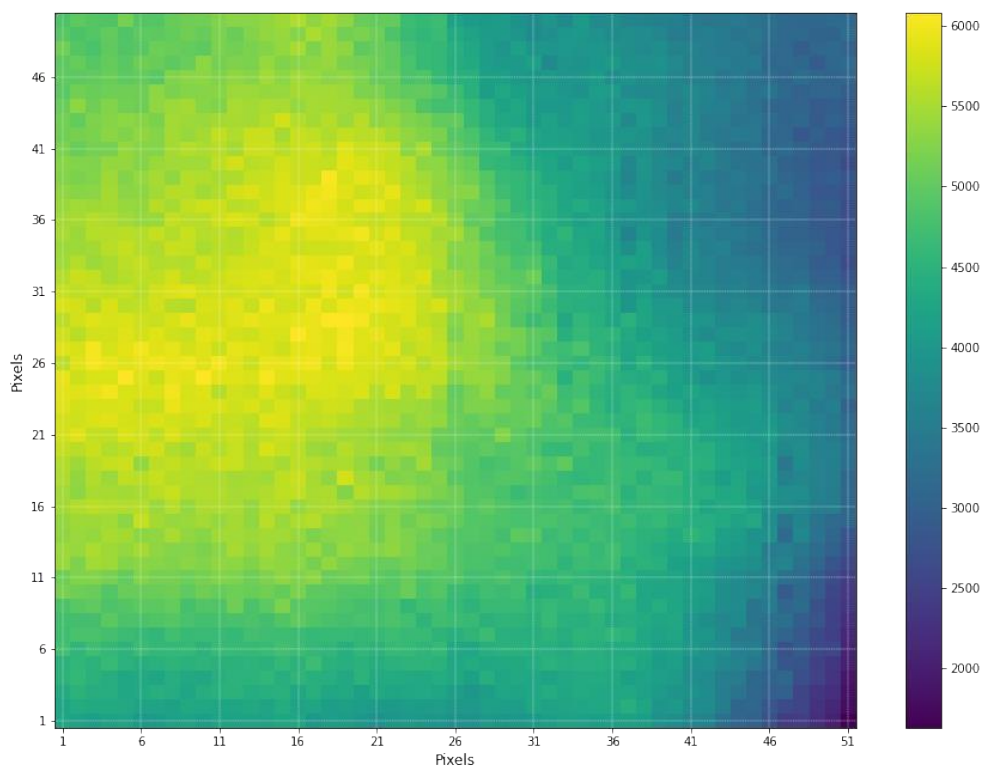


Figure S12: Zoomed image of the nanoparticle cluster located at the center of **fig. S11**, the spot in which the *in situ* XAS was collected. Image size is 2 x 2 μm with a step of 0.04 μm .

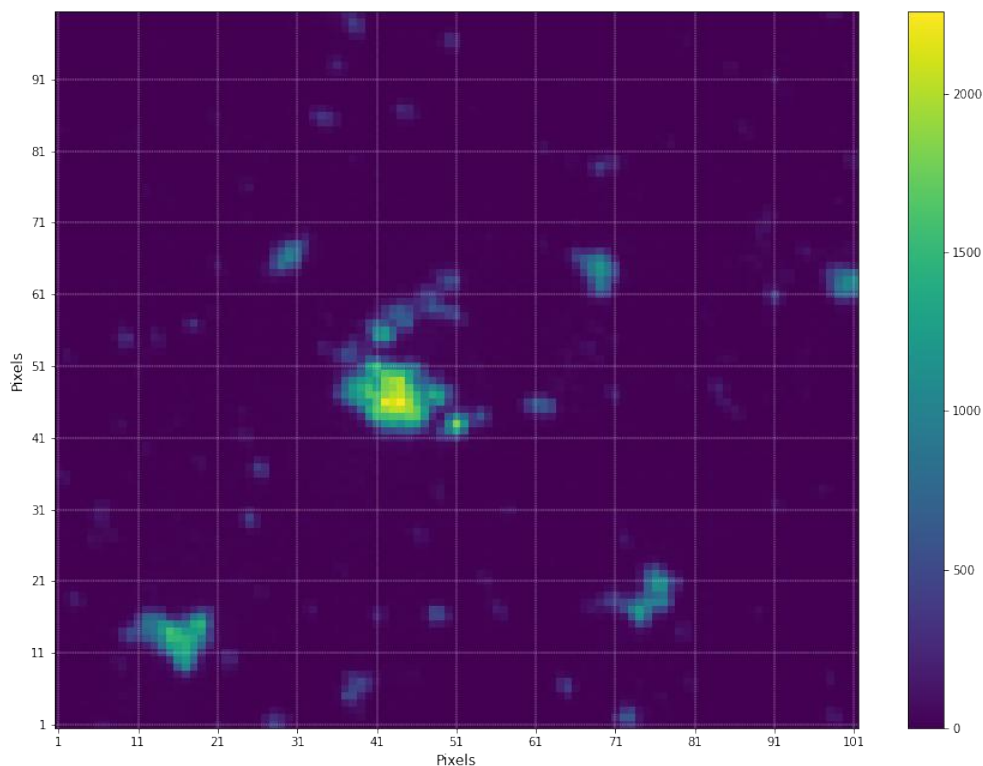


Figure S13: Image of the Pt cluster showed in **fig. S11** and **S12** after collecting the XAS spectra at + 1.20 V (vs RHE). Image size is 50 x 50 μm with a step of 5 μm .

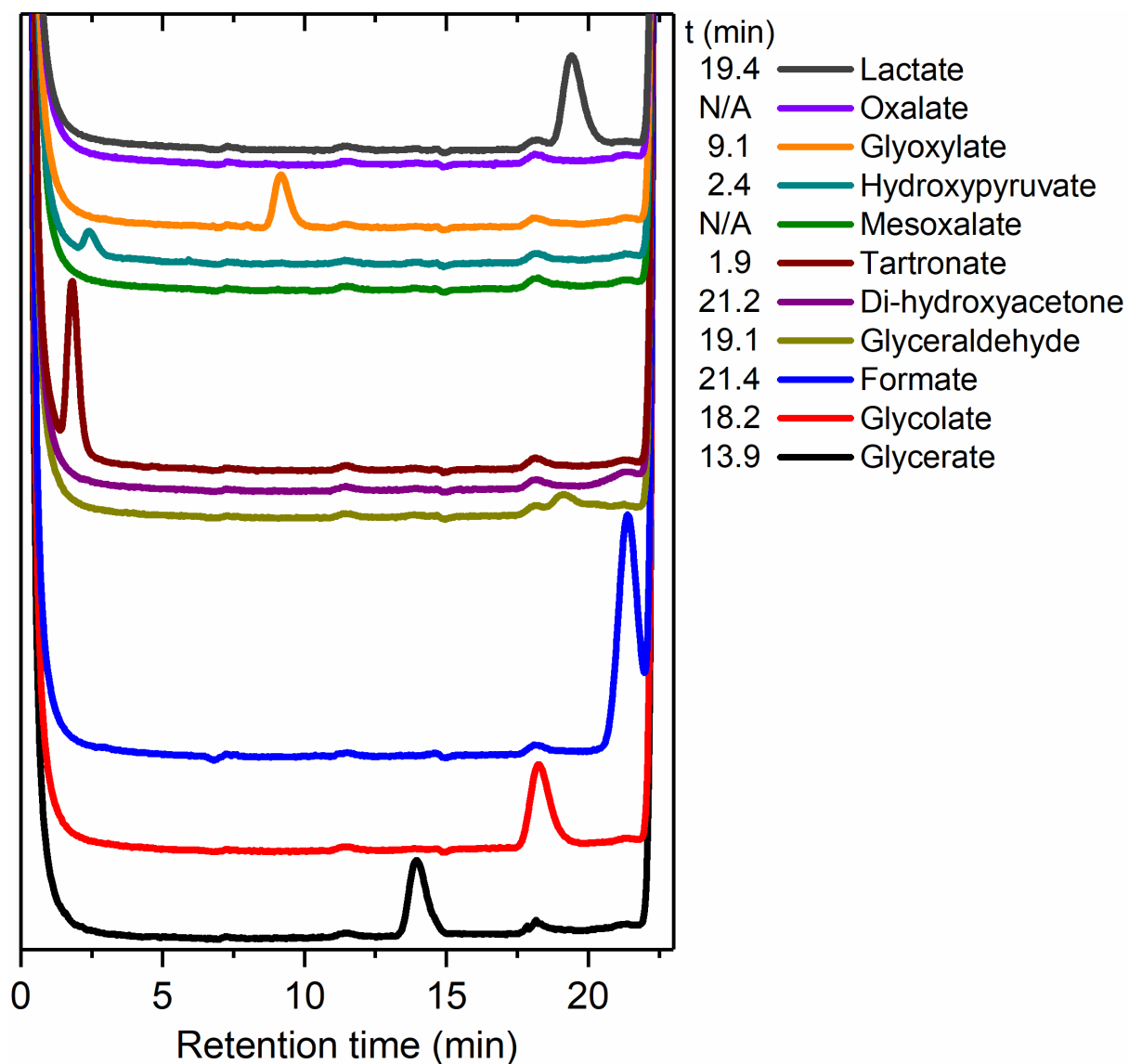


Figure S14: Chromatograms for the external standards used to identify the possible oxidation products from glycerol oxidation, using the RI detector. Each sample consists of 0.1 mM of the respective oxidation product in an acidified electrolyte solution (0.1 M NaOH + 0.1 M glycerol, with enough H₂SO₄ to drop its pH to 3.30).

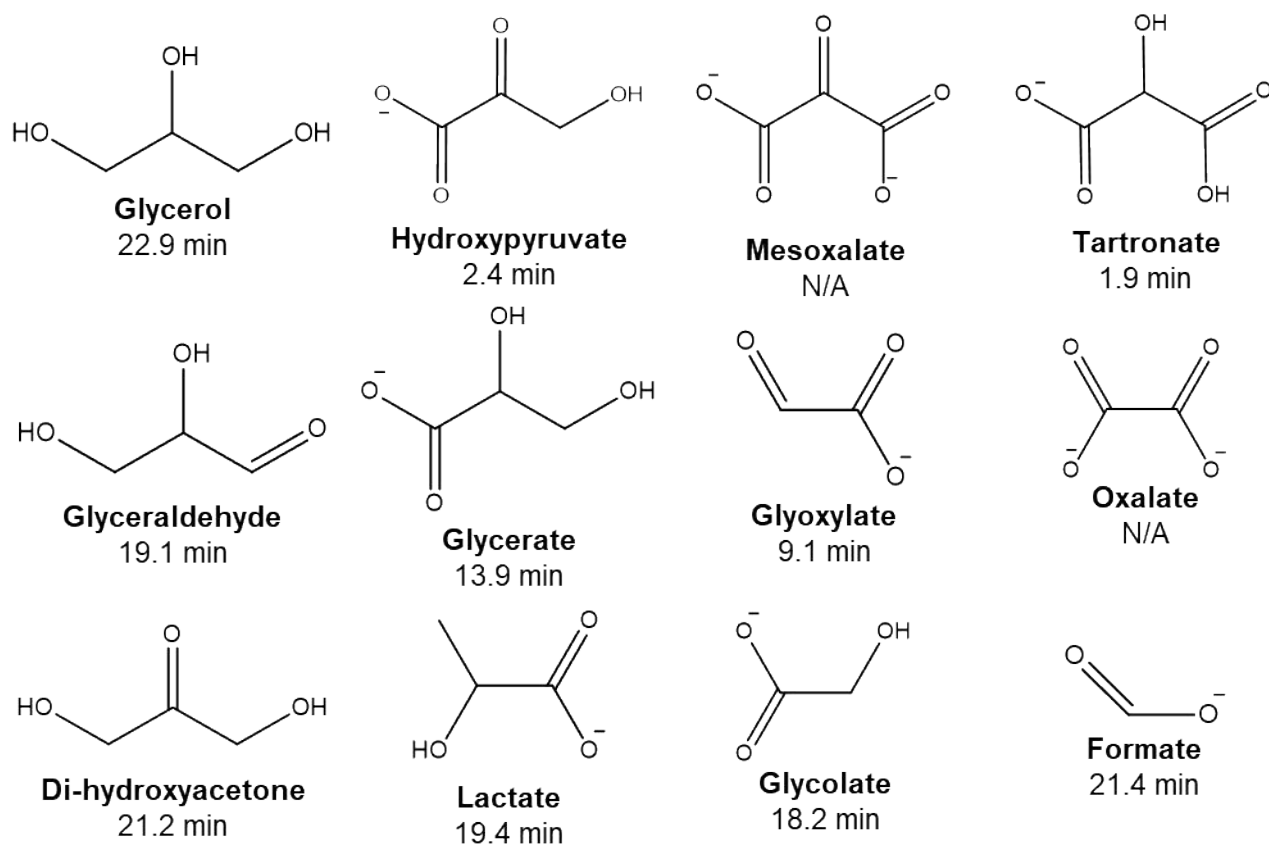


Figure S15: Chemical structure of glycerol and the molecules used in the external standards of **fig. S14**.

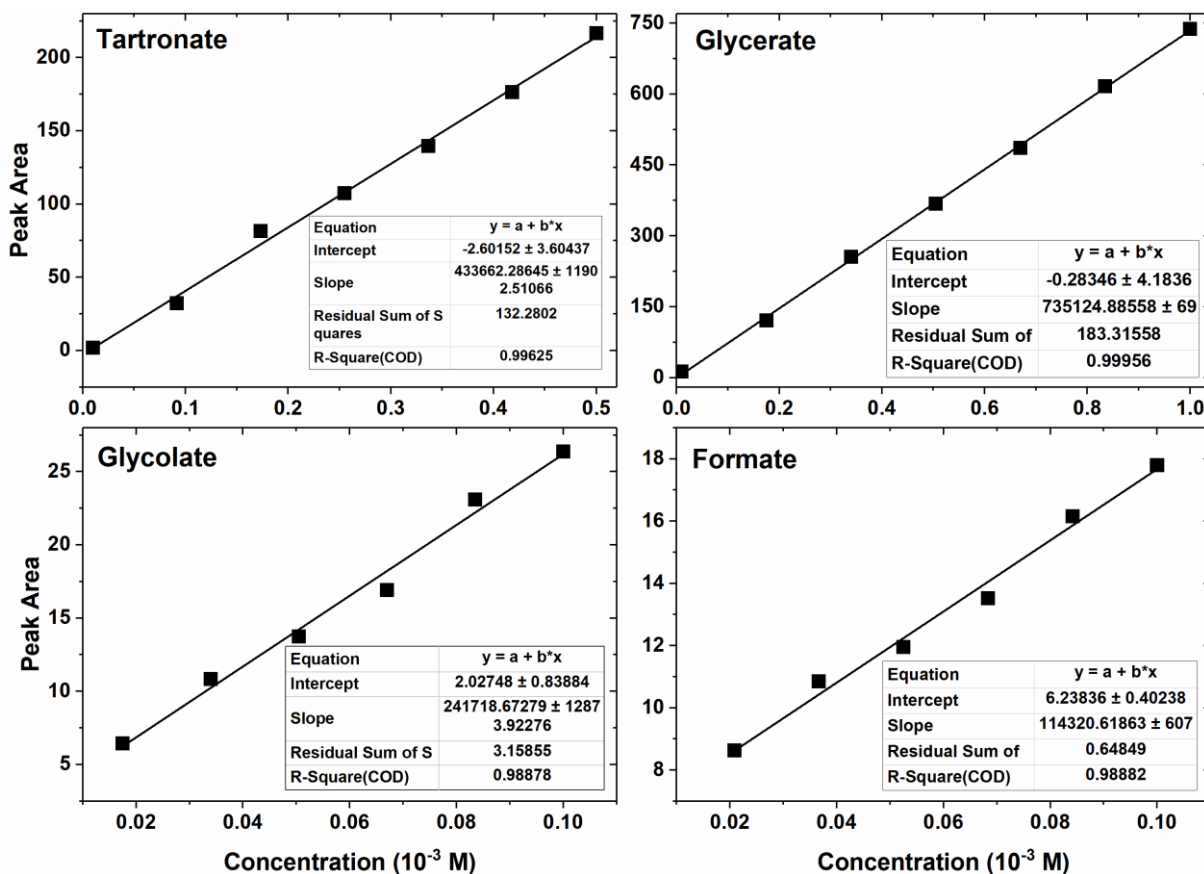


Figure S16: Calibration curves used to quantify the main observed oxidation products. Reprinted with permission from ref.[83]. Copyright 2022 American Chemical Society.

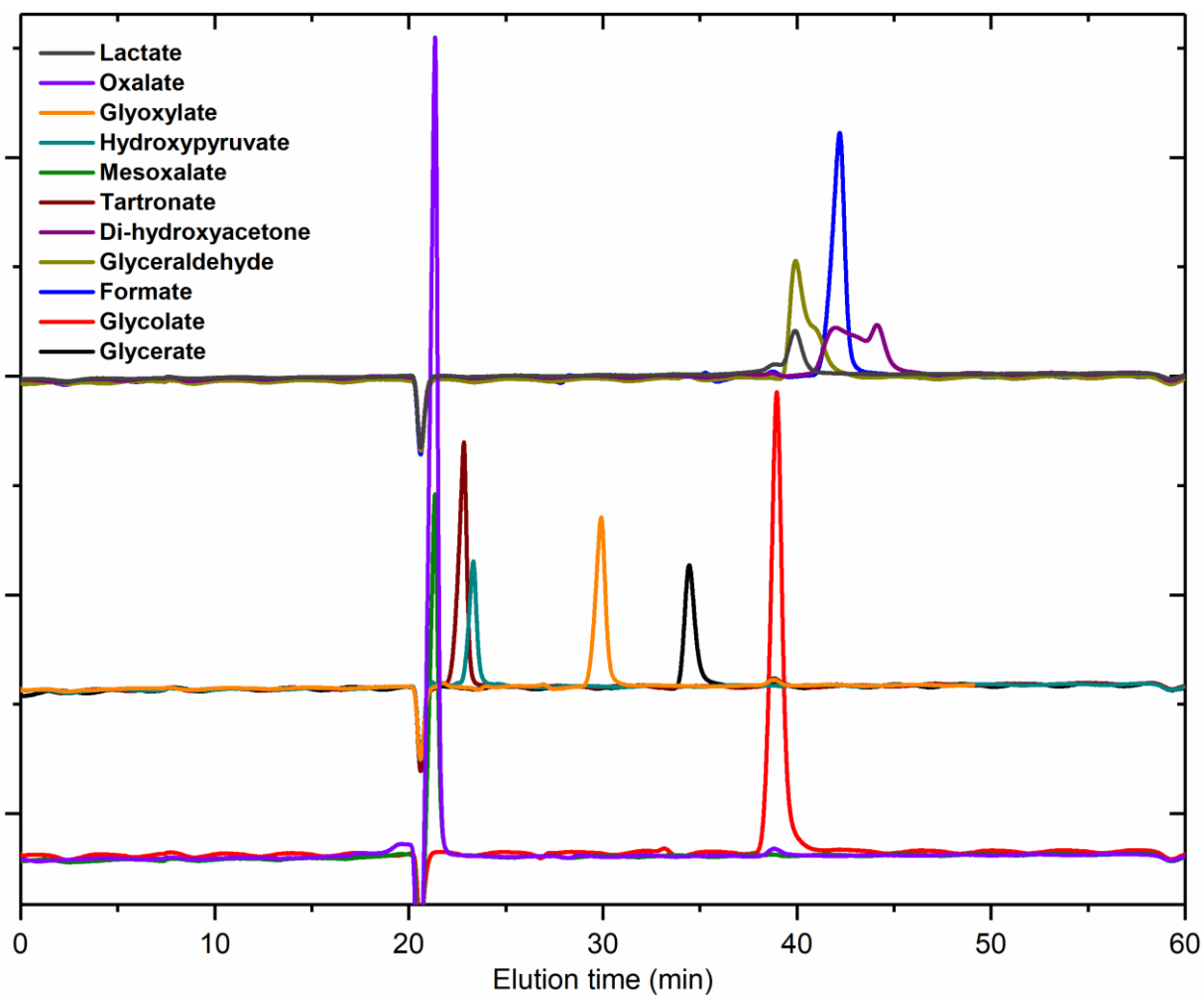


Figure S17: Elution time for the various oxidation products using our methodology. Each sample consists of the respective pure organic molecules diluted in ultrapure water.

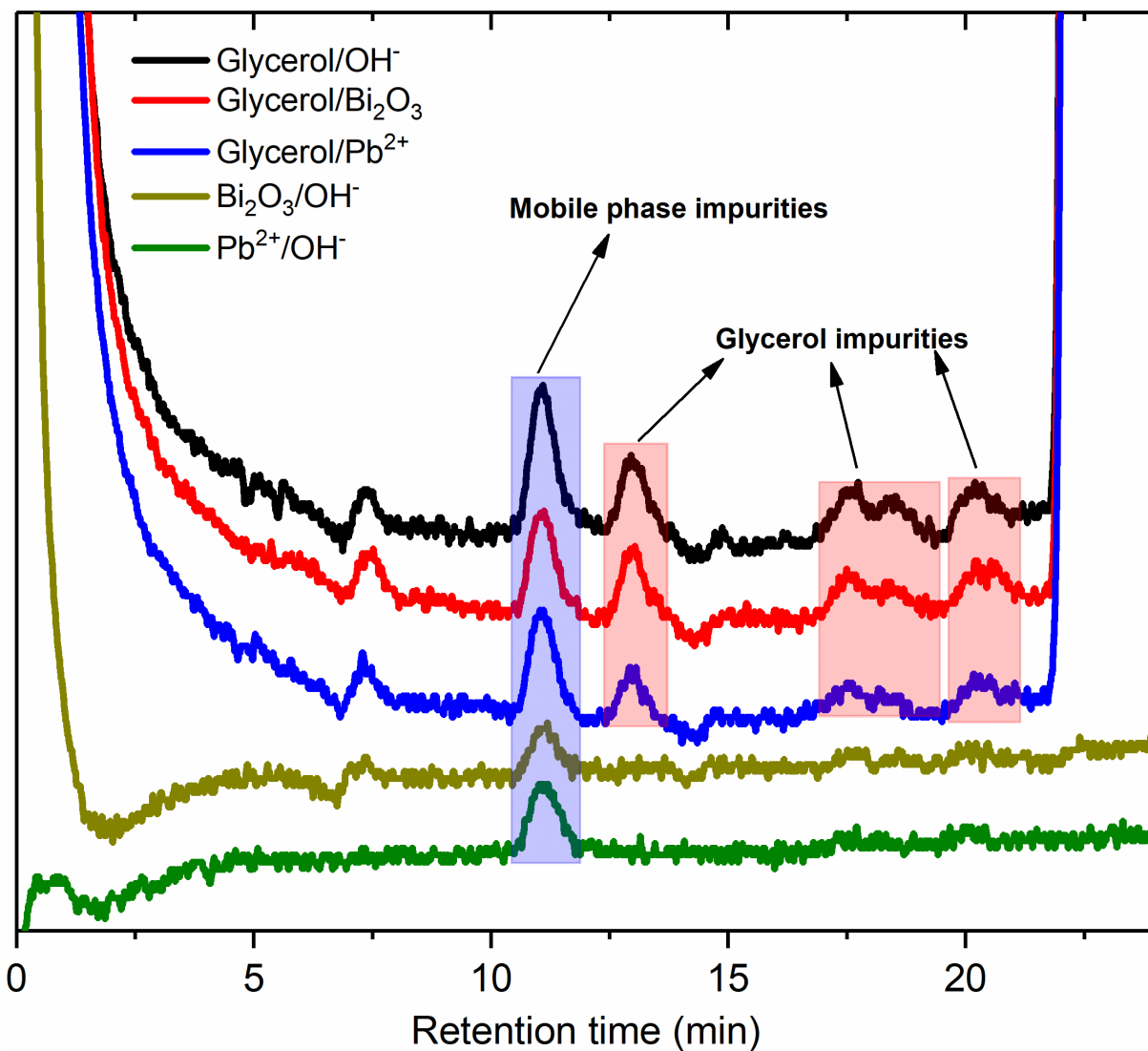


Figure S18: Chromatograms studying the presence of impurities in multiple electrolyte compositions: (black) 0.1 M NaOH + 0.1 M glycerol; (red) 0.1 M NaOH + 0.1 M glycerol + 10⁻⁵ M Bi₂O₃; (blue) 0.1 M NaOH + 0.1 M glycerol + 10⁻⁵ M Pb²⁺; (dark yellow) 0.1 M NaOH + 10⁻⁵ M Bi₂O₃; (green) 0.1 M NaOH + 10⁻⁵ M Pb²⁺.

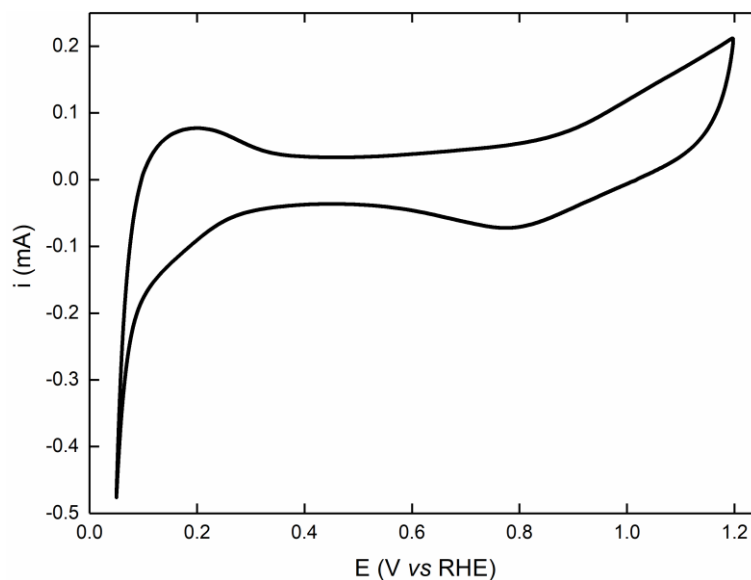


Figure S19: Blank voltammogram of the Pt/C/CP electrode in 1.0 M H₂SO₄ at 50 mV/s. Adapted from ref.[⁶⁵].

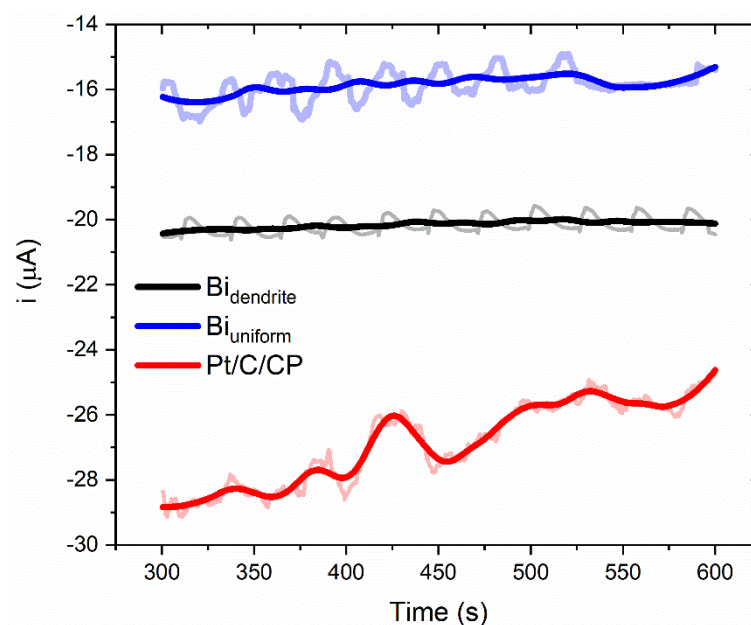


Figure S20: Chronoamperometries at potentials equal $\frac{3}{4}$ of P_{\max} of μ FCs operating with Pt/C/CP (red, $E = 0.33$ V), *in situ* Bi-Pt/C/CP (blue, $E = 0.83$ V) and *operando* Bi-Pt/C/CP (black, 0.434 V) anodes, at a flow rate of 100 μ L/min. Anolyte and catholyte were 0.1 M KOH + 0.1 M glycerol and 1.0 M H₂SO₄ + 0.5 M Na₂S₂O₈.

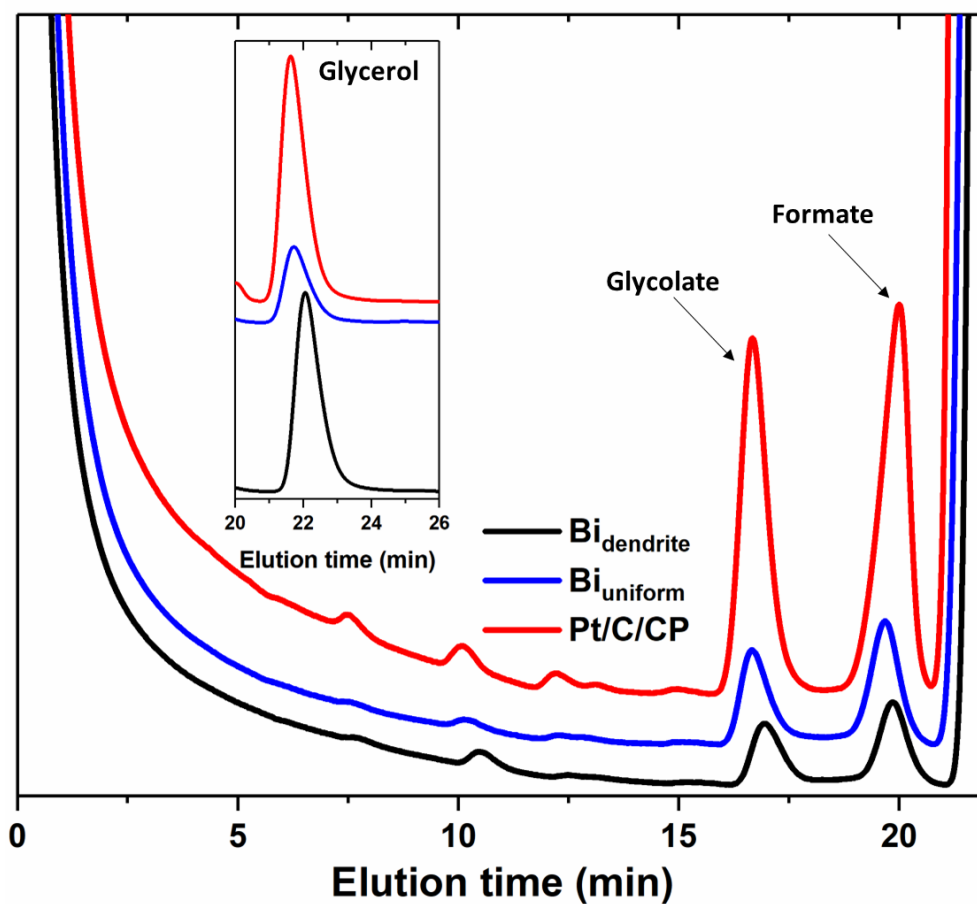


Figure S21: Chromatograms of the samples collected during chronoamperometry at $\frac{3}{4}$ of maximum power density on the μFCs shown in **fig. S22**. Using data from ref.[65].

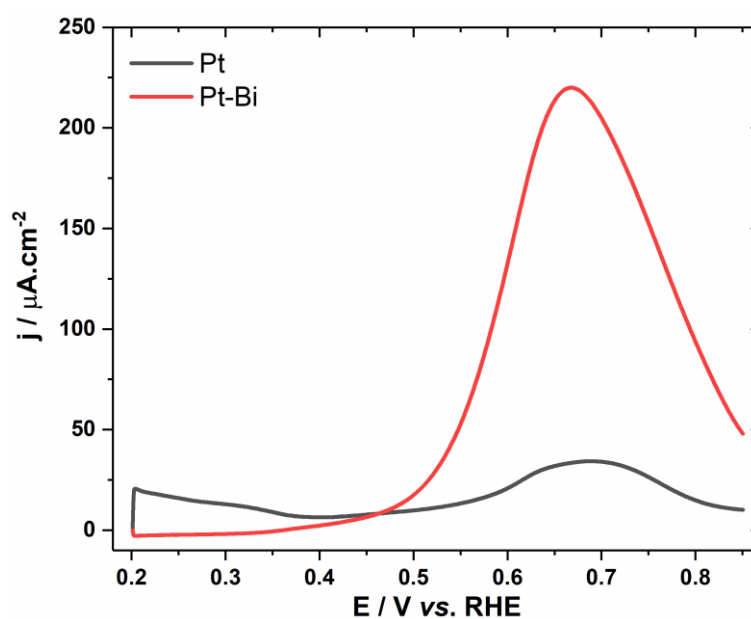


Figure S22: 1st positive-sweep of glyceric acid oxidation, in 0.1 M NaOH + 10^{-3} M glyceric acid, on a clean Pt_p electrode and after addition of 10^{-5} M Bi_2O_3 to the electrolyte. Sweep rate was 10 mV/s. Adapted from ref.[82].